

SURFACTANT PROTEIN A (SP-A) AFFECTS
PULMONARY SURFACTANT MORPHOLOGY AND
BIOPHYSICAL PROPERTIES

CENTRE FOR NEWFOUNDLAND STUDIES

**TOTAL OF 10 PAGES ONLY
MAY BE XEROXED**

(Without Author's Permission)

LYNN-ANN D. WORTHMAN



**Surfactant Protein A (SP-A) affects Pulmonary Surfactant
Morphology and Biophysical Properties.**

Lynn-Ann D. Worthman

B.Sc.(hons.) Memorial University, 1995

Submitted in partial fulfilment of the requirements for the degree of Master of Science

Department of Biochemistry

Memorial University of Newfoundland,

St. John's, Newfoundland A1B 3X9

1997



National Library
of Canada

Acquisitions and
Bibliographic Services

395 Wellington Street
Ottawa ON K1A 0N4
Canada

Bibliothèque nationale
du Canada

Acquisitions et
services bibliographiques

395, rue Wellington
Ottawa ON K1A 0N4
Canada

Your file Votre référence

Our file Notre référence

The author has granted a non-exclusive licence allowing the National Library of Canada to reproduce, loan, distribute or sell copies of this thesis in microform, paper or electronic formats.

The author retains ownership of the copyright in this thesis. Neither the thesis nor substantial extracts from it may be printed or otherwise reproduced without the author's permission.

L'auteur a accordé une licence non exclusive permettant à la Bibliothèque nationale du Canada de reproduire, prêter, distribuer ou vendre des copies de cette thèse sous la forme de microfiche/film, de reproduction sur papier ou sur format électronique.

L'auteur conserve la propriété du droit d'auteur qui protège cette thèse. Ni la thèse ni des extraits substantiels de celle-ci ne doivent être imprimés ou autrement reproduits sans son autorisation.

0-612-34241-7

Canada

ABSTRACT

Surfactant protein A (SP-A) is necessary in the formation of tubular myelin, the precursor to pulmonary surfactant (PS) films at the alveolar fluid-air interface. However, the exact role of SP-A in the physicochemical properties of PS films is not understood. Epifluorescence and electron microscopy were used to investigate the interaction of SP-A, and its structural homolog, C1q, with PS. Molecular films of PS lipid extract (PSLE) containing 1 mol% fluorescent probe (NBD-PC) were spread onto a saline subphase (145 mM NaCl, 5 mM Tris-HCl, pH 6.9) containing 0, 0.13, 0.16 or 0.20 μ g/mL SP-A as well as 0, 1.64 or 5 mM CaCl₂ in the subphase. Monolayers were compressed at a slow rate (the initial rate was 0.0089 $\text{\AA}^2/\text{molecule/second}$) and film features were recorded. No differences were noted in PSLE monolayers in the absence or presence of Ca²⁺. Circular probe-excluded (dark) domains were observed against a fluorescent green background at low surface pressures ($\pi \sim 5 \text{ mN/m}$). The domains grew in size with increasing π until $\pi \geq 25 \text{ mN/m}$, then diminishing domain size was observed. The amount of dark phase was maximized at $\pi \sim 25 \text{ mN/m}$ (at 18% of the initial film area), then decreased to $\sim 3\%$ when π reached $\sim 40 \text{ mN/m}$. The addition of 0.16 or 0.20 μ g/mL SP-A with 0 or 1.64 mM Ca²⁺ in the subphase caused a reorganization of dark domains into a loose network, and the maximum amount of dark phase was increased (25%) between $\pi 10 - 28 \text{ mN/m}$. Monolayer features in the presence of 5 mM Ca²⁺ and SP-A were not significantly different from that of PSLE monolayers alone. This effect may be

due to a self-association and aggregation of SP-A in the presence of higher concentrations of Ca^{2+} . PSLE films were spread onto a subphase containing 0.16 $\mu\text{g/mL}$ Texas-Red SP-A (TR-SP-A), a fluorescent analog of SP-A, in the presence or absence of 5 mM Ca^{2+} to determine the location of the protein in the monolayer. In the absence of Ca^{2+} , TR-SP-A associated with the reorganized dark phase lipid (probe-excluded domains). The presence of 5 mM Ca^{2+} resulted in an aggregation of TR-SP-A in the fluid phase and fluid/gel phase boundaries of the monolayer. The interaction of PSLE monolayers with C1q was investigated by adding 0.16 $\mu\text{g/mL}$ of this protein to the subphase in the presence or absence of 1.64 mM Ca^{2+} . Monolayer surface texture was reorganized in a manner similar to that when SP-A was present, but the total amount of dark phase recorded ($\sim 12\%$ at π between 15-25 mN/m) was less than that observed in PSLE films in the presence of SP-A. The effect of C1q on the surface texture of PSLE films was similar to that of SP-A, hence the oligomeric structure of these C-type lectin proteins may have some impact on PSLE film organization. This study suggests that SP-A associates with PSLE monolayers, particularly gel-phase lipid, and results in some reorganization of gel-phase lipid in surfactant monolayers.

ACKNOWLEDGMENTS

I would like to thank my co-supervisors, Dr. Kevin M.W. Keough and Dr. Philip J. Davis, for their guidance and encouragement during the course of this project. I would also like to thank Dr. David Heeley for being a member of my graduate committee. I must also thank Dr. Nathan Rich for his assistance during the times when the balance was stubborn, as well as Dr. Jesus Pérez-Gil for providing the fluorescently labelled SP-A.

I would like to thank the School of Graduate Studies for providing me funding in the form of a fellowship. I also appreciate the support given to this project by the Medical Research Council of Canada.

To the members of the Keough lab (Kaushik, Tony, Svetla, June and Evelyn), I extend my gratitude for assistance they have given me, and also for their patience during my tirades.

To the ladies of the office, thanks for all your help.

Last, but not least, I thank Brett, my mother and father, as well as my friends for their support.

TABLE OF CONTENTS

Chapter 1. INTRODUCTION

1.1 Pulmonary Surfactant	1
1.2 Pulmonary Surfactant Composition	2
1.2.1 Surfactant Lipids	2
1.2.2 Protein Component of Surfactant	4
1.3 Pulmonary Surfactant Life Cycle	9
1.4 Molecular Films	11
1.5 Epifluorescence Microscopy of Monolayers	14

Chapter 2. MATERIALS AND METHODS

2.1 Materials	17
2.2 Isolation of Pulmonary Surfactant	18
2.3 Isolation of PSLE	18
2.4 Isolation and Purification of SP-A	19
2.5 Epifluorescence Microscopy of PSLE	20
2.5.1 Compression of Spread Monolayers	21
2.5.2 Compression of Monolayers formed from spread PSLE Vesicle Suspension	21
2.5.3 Image Analysis of Monolayers	22
2.6 Alternative Method of SP-A Isolation	22
2.7 Electron Microscopy of Pulmonary Surfactant	23

Chapter 3. RESULTS

3.1 Purity of Lipids and Proteins	26
3.2 Monolayers of Pulmonary Surfactant Lipid Extract	26
3.3 Monolayer Surface Texture	29
3.4 TR-SP-A Fluorescence in PSLE Monolayers	37
3.5 Dark Domain Size Distribution and Total Dark Area in PSLE Monolayers	40
3.6 PSLE Monolayers at High Resolution	46
3.7 Spread Vesicle Suspensions of PSLE	51
3.8 The Effects of 1.64 mM Ca ²⁺	56
3.9 The Effect of C1q on PSLE Monolayers	68
3.10 The Role of SP-A in PS Morphology	85

Chapter 4. DISCUSSION

4.1 PSLE Isotherms and the Effect of SP-A	92
4.2 PSLE Surface Texture and Reorganization due to SP-A	93
4.3 SP-A Oligomeric Structure and PS Interaction	100
4.4 Conclusions and Future Directions	101
References	102

List of Figures

Figure 1. The lipid and protein components of typical mammalian pulmonary surfactant	3
Figure 2. The organization of SP-A monomers	7
Figure 3. The "life-cycle" of pulmonary surfactant	10
Figure 4. Surface pressure-area isotherms of DPPC and the resulting change of state of the phospholipid	13
Figure 5. Schematics for studying monolayers by epifluorescence microscopy	15
Figure 6. Analysis of PSLE lipid content by Thin Layer Chromatography	27
Figure 7. Analysis of SP-A purity by SDS-PAGE.	28
Figure 8. Pressure-Area Isotherms of PSLE monolayers containing 0, 0.13, 0.16, and 0.20 $\mu\text{g}/\text{mL}$ SP-A in the absence or presence of 5 mM Ca^{2+}	30
Figure 9. Monolayer surface morphology of PSLE and PSLE containing 0.13, 0.16 and 0.20 $\mu\text{g}/\text{mL}$ SP-A in the subphase	32
Figure 10. Monolayer surface morphology of PSLE and PSLE containing 0.13, 0.16, and 0.20 $\mu\text{g}/\text{mL}$ SP-A with 5 mM Ca^{2+} in the subphase.	35
Figure 11. Monolayer surface morphology of PSLE spread on subphases containing 0.16 $\mu\text{g}/\text{mL}$ TR-SP-A in the absence or presence of 5 mM Ca^{2+}	38
Figure 12. The size frequency distribution of dark domains observed at various π in monolayers of PSLE and PSLE monolayers containing 0.13, and 0.16 $\mu\text{g}/\text{mL}$ SP-A in the subphase	42
Figure 13. The size frequency distribution of dark domains observed at various π in monolayers of PSLE and PSLE monolayers containing 0.13, and 0.16 $\mu\text{g}/\text{mL}$ and 5 mM Ca^{2+} in the subphase.	44

Figure 14. The %dark area of PSLE monolayers containing 0, 0.13, 0.16, and 0.20 $\mu\text{g/mL}$ SP-A in the subphase in the absence and presence of 5 mM Ca^{2+}	47
Figure 15. Monolayer surface morphology of PSLE monolayers observed through a 50X objective lens	49
Figure 16. The frequency size distribution and the %dark phase of PSLE films observed under a 40X and 50X objective lens.	52
Figure 17. Surface morphology of PSLE vesicle films containing 1 mol% NBD-PC, 10 wt% TR-SP-A, and 5 mM Ca^{2+}	54
Figure 18. The frequency size distribution and the %phase of vesicle spread PSLE with 1 mol% NBD-PC, 10 wt% TR-SP-A and 5 mM Ca^{2+}	57
Figure 19. Pressure-Area isotherms of PSLE, PSLE + 0.16 $\mu\text{g/mL}$ SP-A, PSLE + 1.64 mM Ca^{2+} , PSLE + 0.16 $\mu\text{g/mL}$ SP-A + 1.64 mM Ca^{2+} , PSLE + 5 mM Ca^{2+} , and PSLE + 0.16 $\mu\text{g/mL}$ SP-A + 5 mM Ca^{2+}	59
Figure 20. Monolayer surface morphology of PSLE and PSLE containing 0.16 $\mu\text{g/mL}$ SP-A with 1.64 mM Ca^{2+} in the subphase.	62
Figure 21. The frequency size distribution of PSLE films containing 0, 1.64 and 5 mM Ca^{2+} in the subphase.	64
Figure 22. The frequency size distribution of PSLE films containing 0.16 $\mu\text{g/mL}$ SP-A and 0, 1.64 and 5 mM Ca^{2+} in the subphase..	66
Figure 23. The %dark phase of PSLE and PSLE containing 0.16 $\mu\text{g/mL}$ SP-A with 0, 1.64 and 5 mM Ca^{2+} , with a compilation of data shown in panel D	69
Figure 24. Pressure-Area isotherms of A) DPPC and DPPC spread on 0.16 $\mu\text{g/mL}$ C1q, as well as B) PSLE and PSLE spread on 0.16 $\mu\text{g/mL}$ C1q in the absence or presence of 1.64 mM Ca^{2+}	71
Figure 25. Monolayer surface morphology of DPPC and DPPC containing C1q subphase concentrations of 0.16 $\mu\text{g/mL}$	74

Figure 26. The frequency size distribution and %dark phase of DPPC films and DPPC containing 0.16 $\mu\text{g}/\text{mL}$ C1q in the subphase.	76
Figure 27. Monolayer surface morphology of PSLE containing 0.16 $\mu\text{g}/\text{mL}$ C1q in the absence and presence of 1.64 mM Ca^{2+}	79
Figure 28. Monolayer surface morphology of PSLE containing 0.16 $\mu\text{g}/\text{ml}$ SP-A or C1q with 1.64 mM Ca^{2+}	81
Figure 29. The frequency size distribution of PSLE films containing 0.16 $\mu\text{g}/\text{mL}$ C1q in the absence and presence of 1.64 mM Ca^{2+}	83
Figure 30. The %dark phase of A: PSLE monolayers and PSLE containing 0.16 $\mu\text{g}/\text{mL}$ C1q, B: PSLE monolayers with 1.64 mM Ca^{2+} and PSLE with 1.64 mM Ca^{2+} and 0.16 $\mu\text{g}/\text{mL}$ C1q, C: PSLE monolayers and PSLE containing 0.16 $\mu\text{g}/\text{mL}$ SP-A, D: PSLE monolayers with 1.64 mM Ca^{2+} and PSLE with 1.64 mM Ca^{2+} and 0.16 $\mu\text{g}/\text{mL}$ SP-A	86
Figure 31. Electron micrograph of rat pulmonary surfactant isolated in the presence of 5 mM Ca^{2+}	88
Figure 32. Electron micrograph of PSLE + 5 mM Ca^{2+} vesicles and vesicles of DPPC/POPG 7:3 + 5wt% SP-A + 5 wt% SP-B + 5 mM Ca^{2+}	89
Figure 33. A schematic diagram of SP-A associations in monolayers of PSLE in the presence of \leq 1.64 mM or 5 mM Ca^{2+}	99

List of Abbreviations and Symbols used

γ	Surface tension
π	Surface pressure
\AA	Angstrom
AOI	Area of interest
ARDS	Adult respiratory distress syndrome
BAM	Brewster angle microscopy
CCD	Charge coupled device
DMPC	1,2-dimyristoyl- <u>sn</u> -glycero-3-phosphocholine
DPPC	1,2-dipalmitoyl- <u>sn</u> -glycero-3-phosphocholine
G	Gaseous
HC	Hydrocarbon
LC	Liquid condensed phase
LE	Liquid expanded phase
mN/m	milliNewton per metre
NBD-PC	1-palmitoyl-2-{12-[7-nitro-2-1,3-benzodiazole-4-yl)amino]dodecanoyl} phosphocholine
PC	Phosphatidylcholine
PE	Phosphatidylethanolamine
PG	Phosphatidylglycerol
PI	Phosphatidylinositol

PL	Phospholipid
PS	Pulmonary surfactant
PSLE	Pulmonary surfactant lipid extract
RDS	Respiratory distress syndrome
SDS	Sodium dodecyl sulfate
SP-A	Surfactant protein A
SP-B	Surfactant protein B
SP-C	Surfactant protein C
SP-D	Surfactant protein D
TLC	Thin layer chromatography
TR-SP-A	Texas Red-SP-A

CHAPTER 1

INTRODUCTION

1.1 Pulmonary Surfactant

Pulmonary surfactant (PS) is a heterogeneous material found at the interface between the air and the liquid layer covering the epithelial cell lining and in the aqueous lining layer of the lung. The main function of PS is to reduce surface tension (γ) in the lung, especially at low lung volumes. This effect allows the stabilization of terminal airways by preventing alveolar collapse at low transpulmonary pressures and reduces the work involved in breathing. PS reduces the surface tension at the alveolar-air interface by forming what has conventionally been considered to be a monomolecular film on the alveolar fluid (hypophase) surface.

The reduction of surface tension at the alveolar fluid-air interface is crucial for normal lung function. Infants born prematurely lack sufficient amounts of pulmonary surfactant and Respiratory Distress Syndrome (RDS) is the consequence of this deficiency. Surfactant replacement therapy is now commonly used to reduce mortality in prematurely born infants suffering from RDS. Adults who suffer major trauma or systemic infection may acquire Adult Respiratory Distress Syndrome (ARDS) due to a loss of surfactant function (Jobe, 1993; Jobe and Ikegami, 1987).

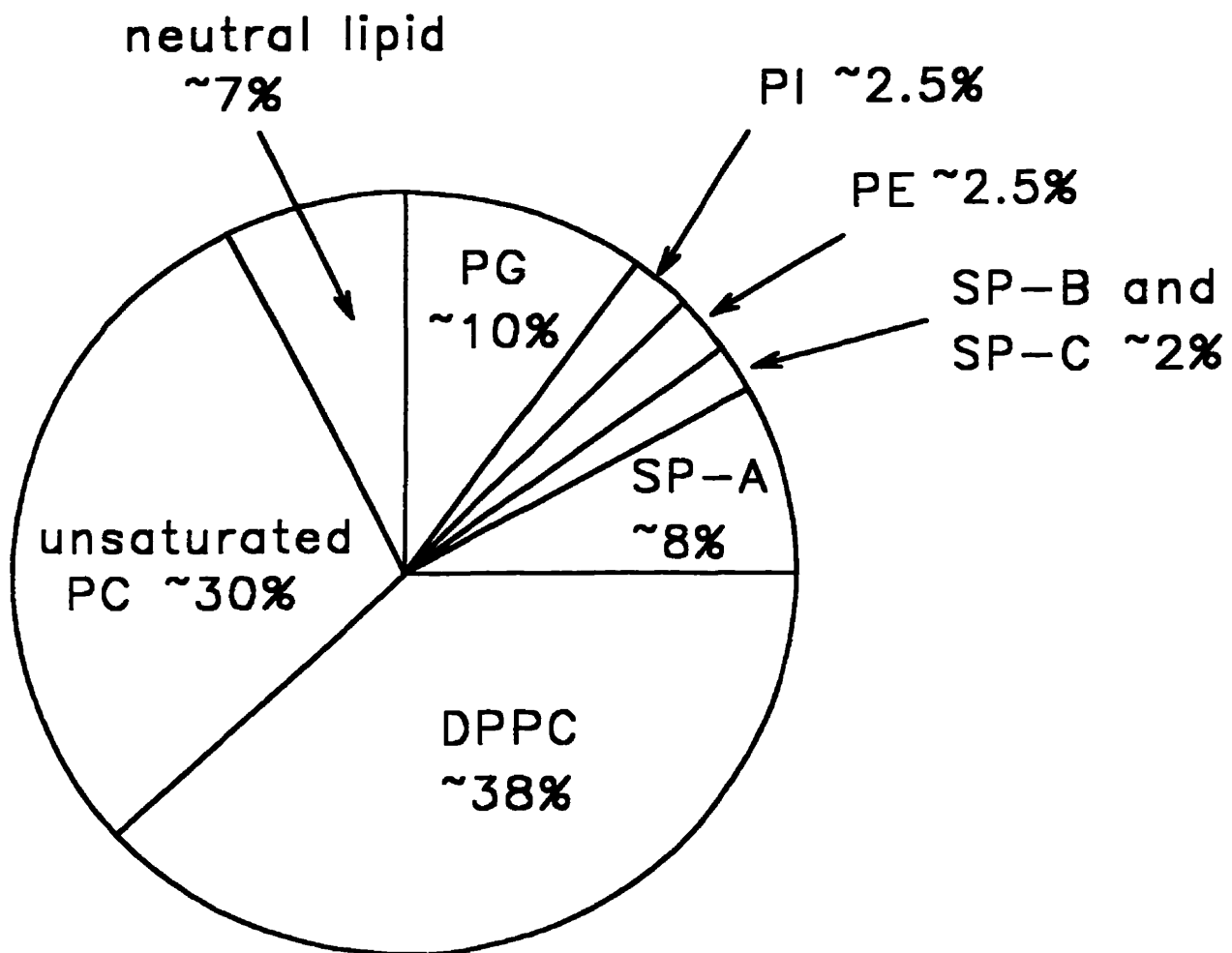
There is a continuing interest in the potential use of artificial surfactants in treatment of ARDS.

1.2 Pulmonary Surfactant Composition

Pulmonary surfactant consists of a complex mixture of lipids and proteins. Typical mammalian surfactant isolated through bronchoalveolar lavage consists of about 90% lipids and 10% protein by weight. The specific lipid and protein components of typical mammalian lung surfactant as compiled from previous data (Dobbs, 1989; Van Golde, 1988; Wright and Clements, 1987) are illustrated in figure 1. The combination of specific quantities of surfactant components may result in various morphological structures such as lamellar bodies and tubular myelin.

1.2.1 Surfactant Lipids

The major component of PS by weight is lipid (90%). Phospholipid (PL) comprises 70-80% of this lipid component. Phosphatidylcholine (PC) is the most abundant phospholipid, with dipalmitoyl phosphatidylcholine (DPPC) making up about 60% of the PC. The remainder of the PC component consists of unsaturated lipid. Phosphatidylglycerol (PG) and phosphatidylinositol (PI) are also abundant in PS, comprising 10-15% of the total phospholipid weight content. In addition, phosphatidylethanolamine (PE) comprises 2-3% of the lipid content. Small amounts of sphingomyelin (SM), lysophosphatidic acid and lysophosphatidylcholine, and neutral lipids such as cholesterol, cholesterol ester, diacylglycerol, triacylglycerol, and free fatty acids make up the final 5-10% of PS lipid content (Dobbs, 1989; Van



Weight Composition of typical mammalian pulmonary surfactant

Figure 1. The typical composition of mammalian pulmonary surfactant as compiled from previous data (Dobbs, 1989; Van Golde, 1988; Wright and Clements, 1987). The abbreviations used are: SP-A, surfactant-protein A; SP-B, surfactant-protein B; SP-C, surfactant-protein C; PC, phosphatidylcholine; DPPC, dipalmitoylphosphatidylcholine; PG, phosphatidylglycerol; PI, phosphatidylinositol; PE, phosphatidylethanolamine.

Golde, 1988; Wright and Clements, 1987).

Given the unusually high levels of DPPC and PG, the overall lipid composition of PS is significantly different from other tissues in the body. The high levels of DPPC and PG suggest a role for these lipids in PS function. DPPC is thought to be the component responsible for the stabilization of surface tension in the lung at low volumes. The amphipathic nature of phospholipids such as DPPC enables the formation of monomolecular films at the alveolar fluid-air interface. The hydrophilic polar headgroup of DPPC associates with the hypophase of the alveoli, while the saturated acyl chains of the phospholipid extend into the air. During exhalation, the reduction in area of the alveolar lining-air interface causes the saturated acyl chains of DPPC to come close together. As a result, surface tension is reduced at low lung volumes and the alveolar-air interface is stabilized (Keough, 1992; Wang et al., 1995). However, studies have shown that DPPC adsorbs very slowly to an air-fluid interface and does not readily respread at the surface after monolayer collapse. It has been suggested that anionic and unsaturated lipids, as well as surfactant proteins, aid in surfactant adsorption and resspreading at the surface (Fleming and Keough, 1988; Wang et al., 1995; Wang et al., 1996). The PG content of mammalian lung surfactant is much higher (5-10%) than those found in other tissues, yet the exact role of this lipid in PS function is not understood.

1.2.2 Protein Component of Surfactant

Pulmonary Surfactant contains approximately 10% protein by weight. There

have been four proteins isolated and characterized by their association with PS. The accepted nomenclature of the surfactant associated proteins is surfactant protein A, B, C, and D (Possmayer, 1988). Surfactant protein A (SP-A) and surfactant protein D (SP-D) are large glycoproteins that belong to the C-type (Ca^{2+} dependent) lectin superfamily. Surfactant protein B (SP-B) and surfactant protein C (SP-C) are small hydrophobic proteins that are highly soluble in organic solvents such as chloroform/methanol mixtures.

Surfactant protein A, the surfactant-associated protein of greatest component by weight (~8 wt%), was the first to be isolated and characterized. SP-A consists of monomers of about 228 amino-acids having a molecular weight of 28-36 kDa (Hawgood, 1989). Each peptide contains four distinct domains: an amino terminus containing a cysteine residue for disulfide links, a collagen-like domain consisting of Gly-X-Y repeats, a short hydrophobic neck region, and a globular carbohydrate recognition domain (CRD). The CRD region of SP-A contains an N-linked glycosylation site and varying monomeric molecular masses (28-36 kDa) is a consequence of glycosylation differences among monomeric units. Each CRD region contains one carbohydrate binding site and two high affinity Ca^{2+} binding sites. It is suspected that one Ca^{2+} site is located in the carbohydrate binding site. A triple-helix subunit is formed from peptide trimers, and six of these subunits form a large quaternary structure reminiscent of a flower bouquet totalling 18 monomeric units (King et al., 1989). The collagen-like triple helices form the stalk and the globular CRD domains are the "flowers". The overall structural organization of SP-

A (see figure 2) is very similar to that of C1q, another member of the C-type lectin superfamily and a component of the complement system (Haagsman et al., 1989; Johansson and Curstedt, 1997; Kuroki and Voelker, 1994; Voss et al., 1988). Many studies have indicated a role for SP-A in PS regulation and function. *In vitro* studies have shown that SP-A interacts with gel-phase lipids, especially DPPC, and this interaction is dependent upon the sn-2 positioned acyl chain of the phospholipid (PL) (Casals et al., 1993; Kuroki and Akino, 1991). SP-A, in the presence of Ca^{2+} is crucial in the conversion of PS lamellar bodies into tubular myelin (TM) (Benson et al., 1984; Suzuki et al., 1989; Williams et al., 1991). It has been shown that PL aggregation in the presence of Ca^{2+} is enhanced with SP-A in a reversible manner (Hawgood et al., 1985). This phenomena may be relevant to TM formation (Haagsman et al., 1990; Meybloom et al., 1997). Yet recent studies have indicated that the mechanism of SP-A-mediated lipid aggregation differs from that of PL binding (McCormack et al., 1994). It has been proposed that occupancy of the high affinity CRD Ca^{2+} binding site results in a conformational change in SP-A structure, yet SP-A self-association and aggregation may require the occupation of both Ca^{2+} binding sites (Haagsman et al., 1990). However PL aggregation, as mediated by SP-A is not related to the self-association of SP-A molecules in the presence of Ca^{2+} (Ruano et al., 1996). The secretion of PS components from type II cells and the subsequent "recycling" of these components back to the type II cell is regulated by SP-A (Dobbs et al., 1987; Kuroki et al., 1996; Ryan et al., 1989; Wright et al., 1987; Wright et al., 1989; Young et al., 1989).

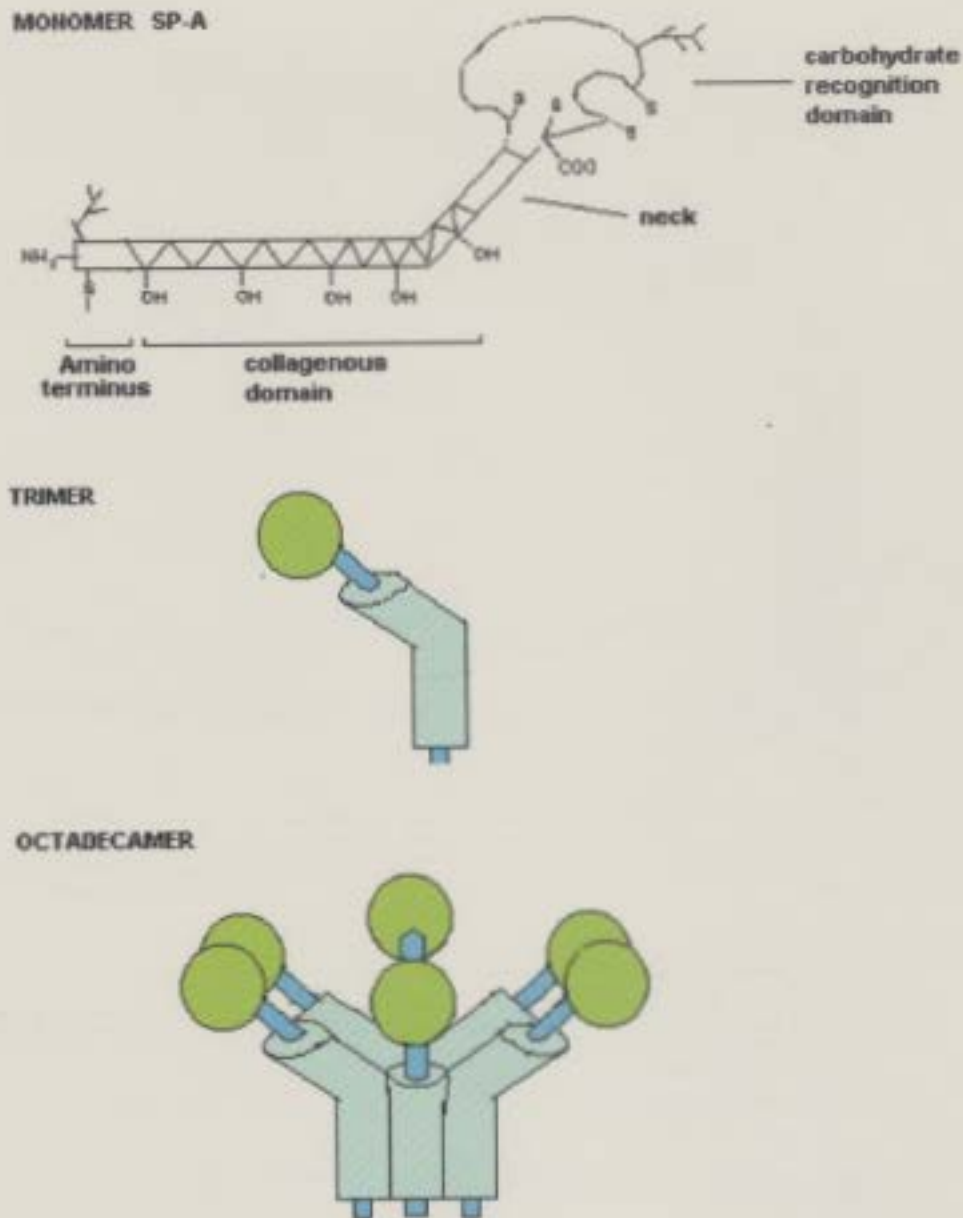


Figure 2. The organization of SP-A monomers. SP-A monomers consist of four domains: an amino terminus, a collagenous domain, a neck region, and a carbohydrate recognition domain. The collagenous domains of the monomeric units promotes the formation of triple helices (denoted trimer). The final structure of SP-A is an octadecamer that is reminiscent of a flower bouquet. [redrawn from Kuroki and Voelker,(1994), with the kind permission of author].

The role of SP-A in the physicochemical properties of PS is not fully determined. SP-A may accelerate the transfer of PS lipid to the air-hypophase interface in the presence of the hydrophobic surfactant proteins B and C (Chung et al., 1989; Schürch et al., 1992; Yu and Possmayer, 1993). The anionic nature of certain PS lipids, especially PG, does not promote mixing with acidic SP-A in spread monolayers at physiological pH, unless in the presence of Ca^{2+} (Taneva et al., 1995). Studies have indicated that SP-A and PS neutral lipids may reorganize DPPC in adsorbed PSLE films, and may also assist in the formation of a DPPC-rich reservoir below the monolayer surface (Yu and Possmayer, 1996). Others have shown that genetically altered mice lacking the SP-A protein display normal breathing (Korfhagen et al., 1996), suggesting that SP-A is not vital for respiratory function.

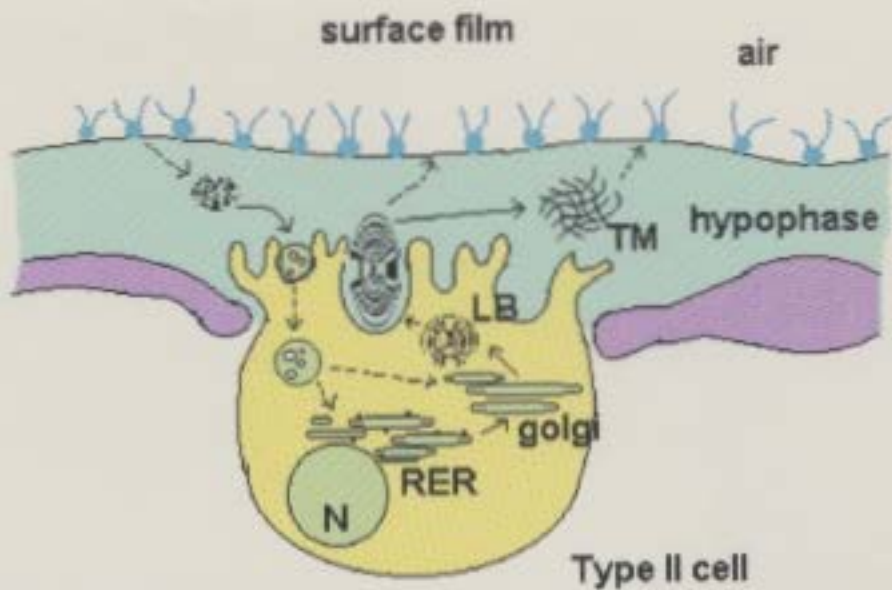
The C-type lectin superfamily of proteins, such as SP-A and C1q, are commonly involved in immune response. The structural organization of this protein class may be an important factor in the interaction of collectins with immune cells and pathogens (Wright, 1997). Others have shown that SP-A, not unlike C1q, enhanced phagocytosis by macrophages during the immune response. However, SP-A can not mimic C1q in the initiation of the classical complement cascade, nor can C1q stimulate lipid uptake by type II pneumocytes (Tenner et al., 1989).

The hydrophobic surfactant-associated proteins, SP-B and SP-C, make up about 1-2 wt% of PS composition. SP-B monomers contain 79 amino-acids having a molecular weight of 8.7 kDa. The monomer is comprised of many basic amino-

acid residues, and it is cysteine-rich. SP-B exists as a homodimer held by disulfide links and has a secondary structure of about 50% α -helices and 20% β -sheet. The many basic amino-acid residues allow for specific interactions with anionic and neutral lipid, and as a consequence SP-B may localize at the surface of lipid domains (Morrow et al., 1993). SP-C is a lipoprotein of 33-35 amino-acids and it is acylated with palmitoyl groups. The secondary structure of SP-C is 60-90% α -helical with the major portion of the helix being formed by hydrophobic amino-acids, thereby enabling this molecule to be a transmembrane protein (Beers and Fisher, 1992; Vandenbussche et al., 1992). SP-C orients itself parallel to lipid acyl chains in bilayers and the basic N-terminus of SP-C is able to interact with anionic PG (Keough, 1992; Keough et al., 1992). The PS associated hydrophobic proteins, in conjunction, have been shown to enhance PS lipid adsorption and resspreading. Yet individually, SP-B is more efficient at these tasks than SP-C (Taneva and Keough, 1994). All hydrophobic components, both lipid and protein, can be extracted from PS using chloroform/methanol solvent mixtures.

1.3 Pulmonary Surfactant Life Cycle

The "life-cycle" of PS involves a series of dynamic processing and transformation steps. The processing of surfactant materials occur in both the type II pneumocyte found in the alveolar epithelial lining and the extracellular fluid (hypophase) that bathes the epithelium. Figure 3 illustrates the PS "life-cycle" in the lung. Surfactant materials are synthesized in the endoplasmic reticulum of the type



N = nucleus

LB = lamellar body

TM = tubular myelin

RER = rough endoplasmic reticulum

Figure 3. The "life-cycle" of pulmonary surfactant. (N= nucleus; RER= rough endoplasmic reticulum; LB= lamellar body; TM= tubular myelin; SF= surface film). The figure is not drawn to scale. [redrawn from Wright and Clements, (1987), with the kind permission of author].

II cell. Surfactant lipids and proteins are processed further in the golgi complex, then secreted as lamellar bodies. The lamellar bodies are exocytized from the type II cell into the hypophase (Stratton, 1978). The SP-A content of these lamellar bodies is low (Oosterlaken-Dijksterhuis et al., 1991; Froh et al., 1990) and it is suspected that SP-A is secreted from type II cells into the hypophase by another pathway. An unusual morphological form of surfactant, known as tubular myelin (TM), occurs in the hypophase and likely results from a specific interaction between the lamellar body and SP-A in the presence of Ca^{2+} (Williams et al., 1991, Benson et al., 1984). It is widely believed that TM is the direct precursor to the monolayer form of surfactant as TM rapidly adsorbs to the hypophase-air interface. This rapid formation of the surfactant monolayer is very important to lung function. Cyclic compression and expansion of the lung may result in the exclusion of PS components from the monolayer into the hypophase, and then the components are recycled by the type II pneumocyte (Williams, 1992; Wright and Clements, 1987).

1.4 Molecular Films

Molecular or Langmuir-Blodgett film systems have been used extensively in the study of surface properties of PS. Monolayer studies provide information about two-dimensional phase behaviour of lipid-lipid and lipid-protein films. The amphipathic nature of lipid allows for the formation of a monolayer at an air-water interface and the adsorption of lipid molecules to the surface will result in a reduction in surface tension (γ). The reduction in surface tension may also be

measured as an increase in surface pressure (π) exerted by the molecules at the air-water interface (Albrecht et al., 1981). Surface pressure is defined as the surface tension of the air-water interface minus the surface tension of the air-molecule-water interface (Gaines, 1966). A decrease in the intermolecular area of each lipid molecule will result upon compression of the monolayer, and the surface pressure exerted by the film will increase as the molecules are forced into close proximity.

Information about the physical state of a monolayer can be obtained from surface pressure-area isotherms (Cadenhead et al., 1980). A change in the packing density of the phospholipid acyl chains through lateral compression will result in a change in the physical state of the monolayer (Cadenhead, 1985). Furthermore, variables such as temperature, pressure and type of lipid will effect physical status. Monolayers spread at temperatures above the phase transition temperature (T_c) of the phospholipid will exist in a gaseous (G) phase at very low π (~ 0 mN/m), and compression will result in a Gaseous (G)/Liquid Expanded (LE) phase transition. With further compression, the monolayer will remain in a LE phase until monolayer collapse. However, phospholipid monolayers spread at a temperature below the characterized T_c will experience a G/LE followed by LE/Liquid Condensed (LC) phase transition with compression. Further compression of the monolayer will result in a Solid Condensed (SC) phase due to the tight packing of the lipid molecules (Cadenhead et al., 1980)

Pressure-area isotherms of dipalmitoylphosphatidylcholine (DPPC) represent a typical example of a monolayer experiencing a change in physical states upon

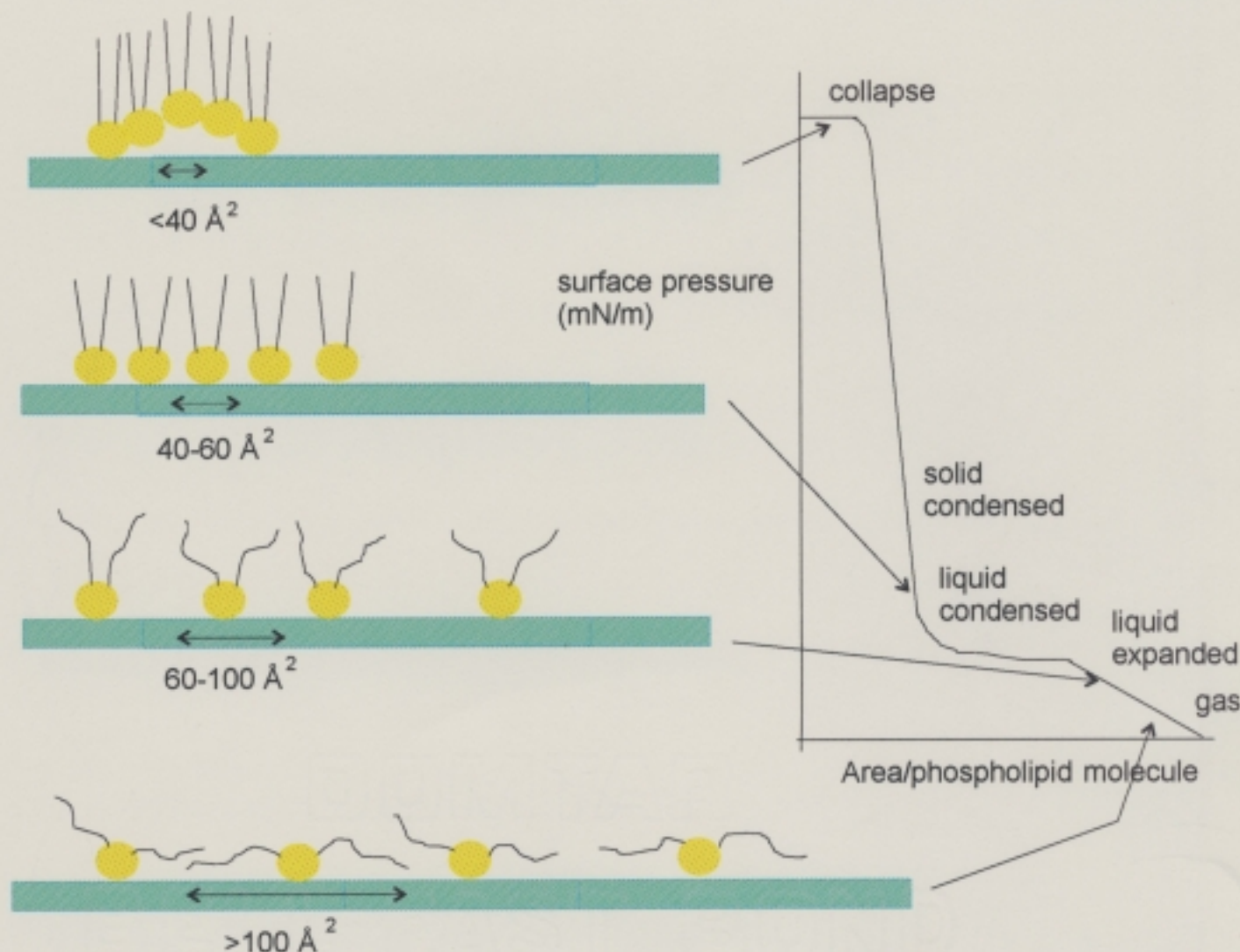


Figure 4. Surface pressure-area isotherm of DPPC and the resulting changes of state of the phospholipid. The compression of a DPPC monolayer will result in a physical change of state in the PL. The molecular area will decrease, and the PL will change from gaseous, liquid expanded, liquid condensed to solid phase as a consequence. Ultimately, the monolayer will collapse at extremely high pressures.

compression (see figure 4). The T_c of DPPC is 41 °C, therefore monolayers spread over an aqueous subphase at room temperature will undergo G/LE (~ 0 mN/m) and LE/LC (~ 7 mN/m) phase transitions. The formation of a SC phase is suspected at pressures ~ 30 mN/m and limiting molecular area of the phospholipid will result in monolayer collapse at ~ 70 mN/m. The physical and molecular interactions of DPPC are of interest to those who study lung surfactant, as it is proposed that monolayers formed at the alveolar-air interface become rich in DPPC due to the preferential "squeeze-out" of non-DPPC components during lung compression and expansion (Goerke and Gonzales, 1981; Hildebran et al., 1979).

1.5 Epifluorescence Microscopy of Monolayers

Epifluorescence microscopy of monolayers at the air-water interface has proven invaluable in the study of lipid-lipid and lipid-protein interactions (Ahlers et al., 1990; Heckl et al., 1987; Möhwald, 1990; Nag and Keough, 1993; Nag et al., 1996; Nag et al., 1997; von Tscharner and McConnell, 1981; Weis and McConnell, 1985). An epifluorescent microscopic attachment to a surface balance allows for the direct visualization of monolayer surface textures when low molar concentrations of fluorescent probe are introduced to the film (see figure 5). The fluorescent probe will preferentially partition into a particular phase in the molecular film, and as a consequence, the separation of the monolayer into G/LE and LE/LC phases may be visualized.

Specific lipids or proteins may be labelled with different fluorophores. A

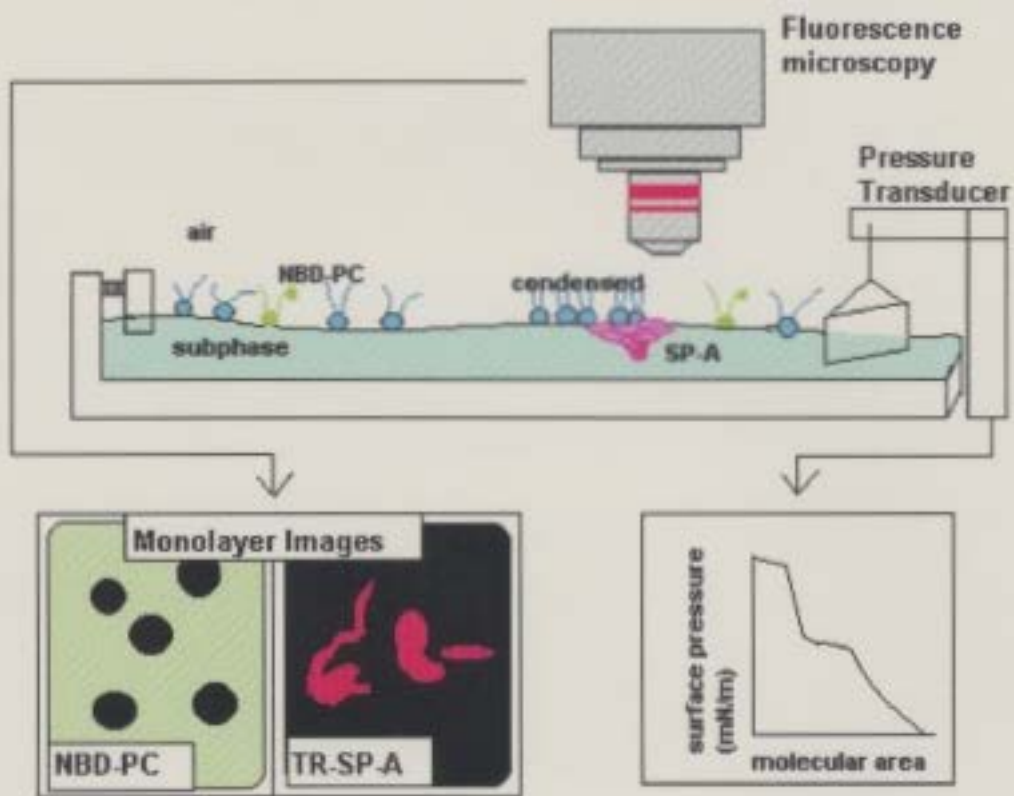


Figure 5. Schematics for studying monolayers by epifluorescence microscopy. Lipids are spread at an air-saline interface and compressed. Surface tension is measured by a platinum dipping plate and force transducer. Pressure/area isotherms are generated by measuring the change in pressure of the monolayer with decreased molecular area. Monolayers are visualized with the use of a fluorescent probe and images are recorded with a charge coupled device (CCD) camera, image intensifier and a videotape recorder.

commonly used fluorescent probe in epifluorescent studies is 1-palmitoyl-2{[(7-nitro-2-1,3-benzoxadiazole-4-yl)amino]dodecanoyl}phosphocholine (NBD-PC). Due to the bulky NBD moiety located on the end of the sn-2 PC acyl chain, the probe localizes in the disordered LE phase (von Tscharner and McConnell, 1981; Slotte and Mattjus, 1995). The labelling of protein with fluorescent moieties such as fluorescein and Texas red (TR) allows for observation of specific lipid-protein interactions (Nag et al., 1997; Ruano et al., 1997).

Objectives:

The main objective of this study was to analyze the interactions of SP-A with lipids of pulmonary surfactant. It was of interest to us in understanding the role of this protein in monolayers of PS at an alveolar fluid-air interface. We proposed that SP-A will modify the arrangement of lipids in monolayers of PSLE due to a specific interaction of SP-A with PS lipids. Monolayers of PSLE were spread onto subphase containing various concentrations of SP-A in the absence or presence of Ca^{2+} . The interaction of SP-A with PSLE monolayers may provide insight into the role of SP-A in surfactant monolayer formation and function in lung mechanics.

C1q, a protein of the complement component system, is structurally homologous to SP-A. The interaction of C1q with PSLE may shed some light on the influence of quaternary structure of SP-A and its affect on surfactant function. These studies utilized both epifluorescent and electron microscopy to study the interaction of SP-A or C1q with PS and PSLE.

CHAPTER 2

MATERIALS AND METHODS

2.1 Materials

For the purpose of epifluorescent microscopy studies, the fluorescent lipid probe, 1-palmitoyl-2-{12[(7-nitro-2,1,3-benzoxadiazole-4-yl)amino]dodecanoyl}-sn-glycero-3-phosphocholine (NBD-PC) was purchased from Avanti Polar Lipids (Pelham, AL). Chloroform and methanol were HPLC grade solvents from Fisher Scientific (Ottawa, ON). The protein C1q was purchased from Sigma Chemical Co. (St. Louis, MO). TR-SP-A was received from Dr. J. Pérez-Gil (Dept. Bioquímica, Madrid, Spain).

For transmission electron microscopy studies, glutaraldehyde and osmium tetroxide (OsO_4) were purchased from Fisher Scientific (Ottawa, ON). Embedding resin (TAAB 812 epoxide) was purchased from Marivac (Halifax, NS).

All water used in these studies was double-distilled, the second distillation being from dilute potassium permanganate. All glassware used was chromic acid washed, rinsed thoroughly, and baked at 180 °C for 8 hours prior to use.

2.2 Isolation of Pulmonary Surfactant

Pulmonary surfactant was isolated from porcine lungs by bronchoalveolar lavage and purified by centrifugation procedures (Taneva and Keough, 1994b). Fresh porcine lungs were lavaged intratracheally with 0.15 M NaCl (4 °C). The lavage was centrifuged at $800 \times g_{av}$ for 10 minutes to remove cellular debris and the resulting supernatant was centrifugated at $8000 \times g_{av}$ for 60 minutes to pellet the surfactant. The surfactant pellet was resuspended in 0.1 M NaCl, 1.64 M NaBr, 0.005 M Tris, pH 7.4 and centrifuged in a swinging bucket rotor at $81.500 \times g_{av}$ for 8 hours. The resulting floating pellicle was resuspended in 0.1 M NaCl, 0.005 M Tris, pH 7.4 and spun at $65.000 \times g_{av}$ for 2 hours to obtain the pulmonary surfactant used in this study. All centrifugation procedures were performed at 4 °C. The surfactant pellet was resuspended in no more than 10 mL 0.15 M NaCl per lung.

2.3 Isolation of PSLE

Lipids and hydrophobic surfactant proteins were extracted from pulmonary surfactant by the method of Bligh and Dyer (1959). To 0.8 volume of surfactant, 2 volumes of methanol and 1 volume of chloroform were added. The mixture was vortexed vigorously. This was followed by another volume of chloroform, and thorough vortexing. One volume of water was added, and the mixture was vortexed once more. The aqueous and organic phases were separated by centrifugation, and the bottom organic phase was removed. The aqueous phase was extracted as described previously with chloroform, then by 2:1 (vol/vol) chloroform/methanol.

The resulting organic phases, now termed pulmonary surfactant lipid extract (PSLE), were pooled.

The concentration of phosphorus in pulmonary surfactant and PSLE was obtained by a modified version of the analysis of organic phosphorus (Keough and Kariel, 1987; Bartlett, 1959). When necessary, the estimated weight of the PL in PSLE was determined by multiplying the total phosphorus concentration by 25.

2.4 Isolation and Purification of SP-A

SP-A was isolated by treatment of the surfactant suspension with 1-butanol extraction (Haagsman et al. 1987). Pulmonary surfactant (1 lung/10 mL saline) was added slowly by pipet into 500 mL of redistilled 1-butanol with stirring at room temperature and the mixture was stirred for an additional 30 minutes. The resulting white precipitate was spun down by centrifugation at 10,000 $\times g_{av}$ for 30 minutes in a swinging bucket rotor. The butanol was decanted, and the precipitate was dried under a stream of N₂ (g). The precipitate was washed twice with 20 mL of 0.02 M 1-O-n-octyl-β-D-gluco-pyranoside, 0.1 M NaCl, 0.01 M HEPES, pH 7.4. After each wash, the mixture was allowed to stand at room temperature for 30 minutes, then centrifuged at 100,000 $\times g_{av}$ for 30 minutes at 15 °C. The resulting pellet was resuspended in 2-3 mL 5 mM Tris, pH 7.4. The SP-A was dialysed against five changes of the same buffer for 48 hours at 4 °C. After dialysis, the insoluble material was removed by centrifugation in a fixed angle rotor at 100,000 $\times g_{av}$ for 30 minutes at 4 °C. The SP-A was stored in small aliquots at -20°C. The purity of SP-

A was determined by SDS-polyacrylamide gel electrophoresis (12% gels) according to the method of Laemmli (1970). Prior to electrophoresis, SP-A was reduced using 5% 2-mercaptoethanol and then heated at 100 °C in the presence of SDS. The concentration of SP-A was determined by the fluorescamine assay (Udenfriend et al., 1972) using bovine serum albumin as the standard.

2.5 Epifluorescence Microscopy of Pulmonary Surfactant Lipid Extract

Epifluorescence microscopy and Surface pressure (π)-Area measurements of solvent spread monolayers of PSLE or DPPC were performed on a surface balance whose construction and operation have been described previously (Nag et al, 1990; Nag et al., 1991). The dimensions of the teflon trough are 22 x 7.8 x 1.5 cm, and a movable teflon dam acts as a barrier to compress the monolayer. The surface tension (γ) at the air/saline interface at various areas was measured by a platinum dipping plate attached to a force transducer. Surface tension of the monolayer was converted to surface pressure (π) by the following relationship; $\gamma_0 - \gamma_m = \pi$. The decrease in surface tension of the saline (γ_0) due to the surface tension of the surface monolayer (γ_m) corresponded to an increase in surface pressure (π).

The surface balance was cleaned of all surface active contaminants by washing with chloroform:methanol (1:1 v/v), followed by methanol, and then double-distilled water. The surface balance was deemed clean when a surface pressure of 0 mN/m was obtained after a complete compression of the saline subphase surface.

2.5.1 Compression of Spread Monolayers

Monolayers of PSLE or DPPC were spread from chloroform/methanol 3:1 (v/v) onto a buffered saline subphase (145 mM NaCl, 5 mM Tris, pH 6.9) containing 0, 0.13, 0.16, or 0.20 µg/mL SP-A or 0.16µg/mL C1q. All experiments were performed in the presence or absence of Ca²⁺. The monolayer was initially compressed to a surface pressure of 10 mN/m, then expanded and allowed to stand for 1 hour. This procedure allowed for the interaction of the protein with the monolayer. By rapidly compressing the monolayer, the transition of the lipids to gel phase is initiated and it has been suggested that the creation of a LE/gel phase boundary may be needed to initiate the interaction of SP-A with the monolayer (Ruano et al., 1998). The temperature of the subphase during the monolayer studies was 21 ± 2 °C. To obtain pressure-area isotherms for the purpose of comparisons between systems, monolayers were compressed at a fast rate of 4 Å²/molecule/second for 30 increments. For the purpose of visualization of monolayer surface textures, pressure-area isotherms were obtained by compressing monolayers at a slow rate of 0.0089 Å²/molecule/second for 30 increments. Accompanying monolayer surface textures were observed through a 40 or 50 x objective lens, and images were videorecorded for one minute after each incremental compression.

2.5.2 Compression of Monolayers formed from spread PSLE Vesicle Suspensions

A vesicle suspension of PSLE (100 µL, 0.750 mg phospholipid/mL) + 1

mol% NBD-PC + 10 wt% TR-SP-A was prepared. PSLE + 1 mol% NBD-PC was dried under N₂ (g) and evacuated overnight. Buffer containing 145 mM NaCl, 5 mM Ca²⁺, 5 mM Tris (pH 6.9) was added to PSLE and the mixture was vortexed. TR-SP-A was added to the mixture to yield a final concentration of 10 wt%, and the vesicle suspension was incubated for 30 minutes at 37 °C. The vesicle suspension was spread onto a buffered saline subphase using a Hamilton syringe. The monolayer was initially compressed to a surface pressure of 10 mN/m, then expanded and allowed to stand for 1 hour. After equilibration, the monolayer was compressed at a slow rate and images were recorded after each incremental compression.

2.5.3 Image Analysis of Monolayers

Image analysis was performed using JAVA 1.3 software (Jandel Scientific, Corte Madera, CA). Ten random images were framegrabbed from videotape and the number and size of dark domains for each image was determined from a set area of interest (AOI). The AOI encompassed about 80% of the television screen size and was held constant for each analysis. The percentage (%dark) of the monolayer which excluded the probe in the images was calculated. The effect of SP-A or Clq on monolayers of PSLE was assessed by their perturbation of the sizes and relative amounts of dark phase.

2.6 Alternative Method of SP-A Isolation

SP-A was isolated from rat lung lavage by manipulating the Ca^{2+} dependent interaction of SP-A with surfactant lipid (Suwabe et al., 1996). PS was isolated from rat via intratracheal lavage using a balanced salt containing of 133 mM NaCl, 2.6 mM hydrogen phosphate, 5 mM KCl, 10 mM HEPES and 1 mg/mL glucose (pH 7.4). Ca^{2+} was added to the lavage to yield a final concentration of 1 mM and the lavage was stored at -20 °C overnight. PS was washed 5 times with the aforementioned buffer + 1 mM Ca^{2+} by repetitive homogenization followed by centrifugation at 100,000 x g_{av}. PS was resuspended in 1 mL of the balanced salt solution containing 2 mM ethylene glycol-bis(β-aminoethyl ether) N,N,N',N'-tetraacetic acid (EGTA), 1 mM Mg^{2+} and the suspension was incubated at 37 °C for 30 minutes. The solution was centrifuged at 100,000 x g_{av} and the supernatant was removed and the PS was resuspended in the same buffer, incubated, and spun as previously mentioned. This procedure was repeated a total of three times, and the supernatants containing SP-A were pooled. The PS pellet [which was reduced in SP-A (PS-SP-A)] was resuspended in the balanced salt solution. SP-A, PS, and PS-SP-A were analyzed for purity by a SDS PAGE as described earlier and the morphological characteristics of PS and PS -SP-A were determined by electron microscopy (see section 2.7).

2.7 Electron Microscopy of Pulmonary Surfactant

Aqueous dispersions of PSLE were reconstituted using a detergent method

previously described by Williams et al. (1991). PSLE or DPPC/POPG (7:3) + 5 wt% SP-B (1 mg PL) was dried under a stream of N₂ (g). The dried lipid/protein mixtures were resuspended in 1 mL of 100 mM 1-O-n-octyl-β-D-glucopyranoside, 2 mM Tris, pH 7.4 to yield a final concentration of 1 mg PL/mL. The suspension was incubated for 60 minutes at 40 °C, then diluted with 10 mL of 145 mM NaCl, 1 mM ethylenediaminetetraacetic acid (EDTA), 10 mM Tris, pH 7.4. The PSLE suspension was dialysed for 48 hours at 4 °C against five changes of the aforementioned buffer. After dialysis, the PSLE samples were concentrated by centrifugation at 50,000 x g_{av} in a fixed angle rotor for 30 minutes at 4 °C. The resulting pellet was resuspended in 0.5 mL buffer (145 mM NaCl, 1 mM EDTA, 10 mM Tris, pH 7.4) and the phosphorus content of the PSLE sample was determined (Keough and Kariel, 1987; Bartlett, 1959). Aqueous dispersions of PSLE, as well as PS and PS-SP-A samples (see section 2.5), (100 µg PL) were incubated at 37 °C for 12 hours. Some samples contained 10 wt% SP-A or 10 wt% Clq with 5 mM Ca²⁺. After incubation, the samples were fixed for electron microscopy.

Aqueous dispersions of PSLE were fixed with an equal volume of 4% glutaraldehyde, 2% OsO₄, 0.2 M sodium cacodylate, pH 7.4 at 4 °C. The suspensions were spun for 10 minutes in a microcentrifuge and left for 24 hours at room temperature. After fixing, the samples were re-centrifuged, and the fixing buffer was removed. The samples were stained with 5% uranyl acetate at 4 °C for 12 hours. The uranyl acetate was removed, and the PSLE pellet was dehydrated using a series of graded acetone washes (70, 80, 90, 2 x 100%) at 4 °C in less than

2 minutes. Samples were left in a small amount of absolute acetone, and an equal volume of TAAB 812 resin was added. The samples were mixed on an orbital shaker, and 10% resin was added every 15 minutes. After 2 hours, the resin/acetone mixture was removed and fresh resin was added to the samples. The samples were left on the orbital shaker overnight to aid in the infiltration of resin into the sample. The infiltrated pellet and fresh resin were placed in a mold and allowed to polymerize at 60 °C for 8 hours. Thin sections were cut from the sample block using a glass knife and an ultramicrotome. The sections were placed on copper grids and stained sequentially with 5% uranyl acetate and alkaline lead citrate for 10 and 5 minutes respectively. Sections were observed with a Zeiss Electron microscope, photographed, and printed on Kodak paper.

CHAPTER 3

RESULTS

3.1 Purity of the Lipids and Proteins

The composition and purity of pulmonary surfactant lipid extract was determined by thin layer chromatography (TLC) using a solvent system of 65:25:4 chloroform/methanol/water. The sample was visualized by spraying with H₂SO₄, followed by charring at 180 °C. Visual comparison of the PSLE sample against PL controls showed that the extract contained substantial amounts of PC and PG, as well as a small amount of lysophosphatidylcholine and palmitic acid (figure 6).

The purity of SP-A isolated by 1-butanol extraction was determined by sodium dodecyl sulfate polyacrylamide gel electrophoresis (SDS-PAGE) and compared to SP-A isolated by Dr. J. Pérez-Gil (Spain). Under reducing conditions and using a 12% polyacrylamide separating gel, monomeric bands having molecular weights between 28-36 kDa were observed after silver staining (see figure 7). The lower molecular weight bands may be SP-A that had been deglycosylated. Very small amounts of two bands of higher molecular weight were also observed.

3.2 Monolayers of pulmonary surfactant lipid extract

Pressure-Area Isotherms of PSLE spread over subphases containing 0, 0.13, 0.16 and 0.20 µg/mL SP-A in the absence (panel A) or presence of 5 mM Ca²⁺

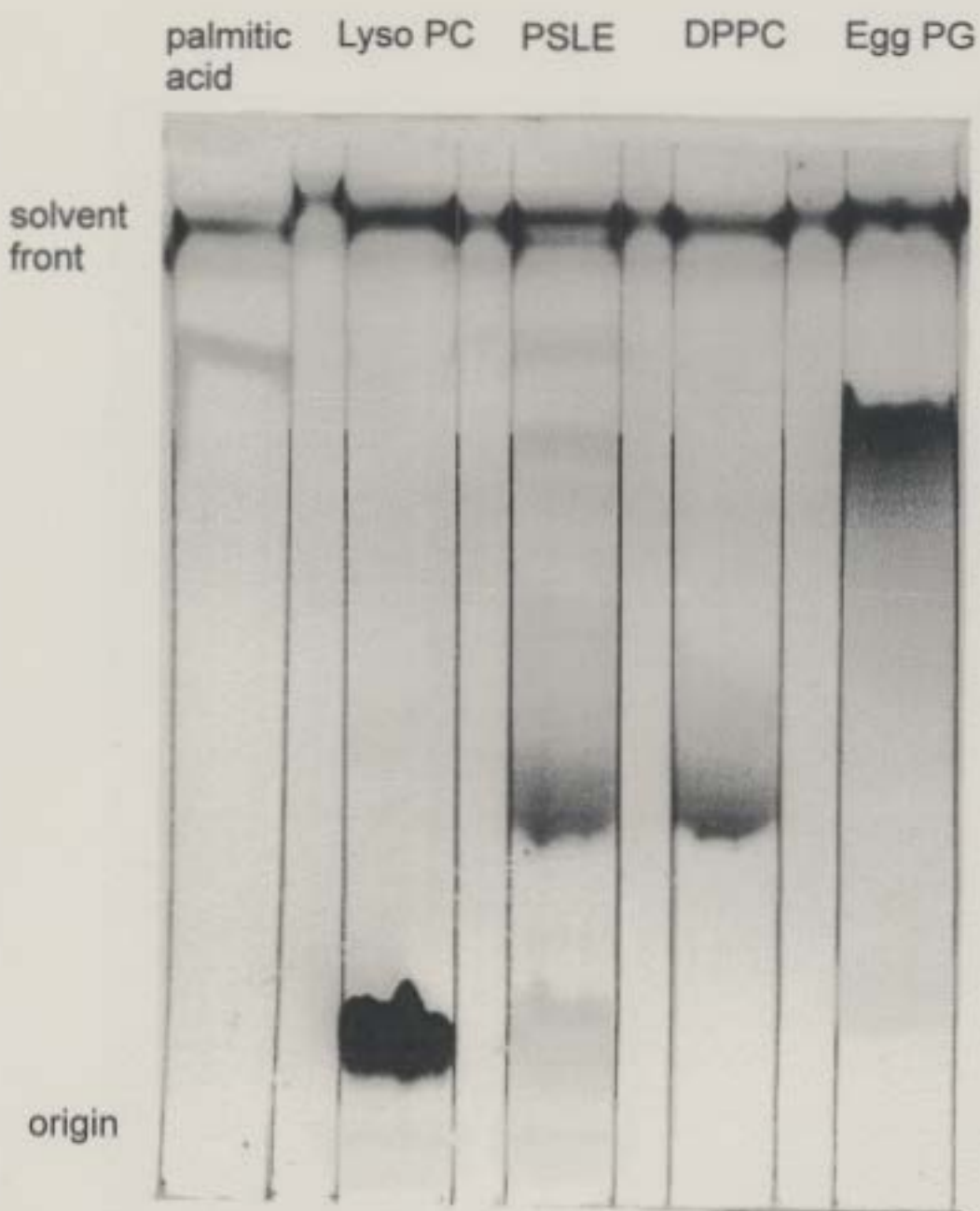


Figure 6. Analysis of PSLE lipid content by Thin Layer Chromatography. Sample lanes (A-E) contained 10 μ g phosphorus. A solvent system of 65:25:4 chloroform/methanol/ water was used and the plate was sprayed with H_2SO_4 , then charred at 180 °C. A: Palmitic acid, B: Lysophosphatidylcholine, C: PSLE, D: DPPC, E: Egg PG.

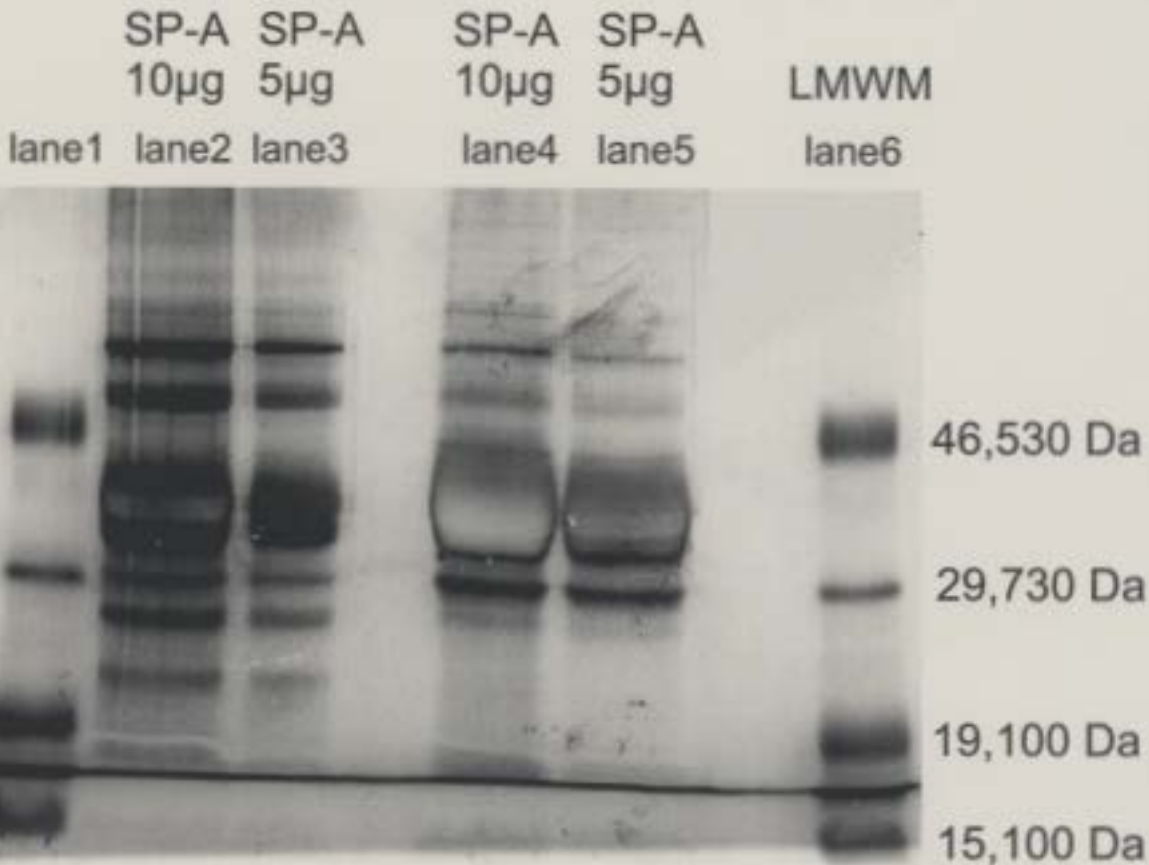


Figure 7. Analysis of SP-A purity by SDS-PAGE. SP-A isolation by 1-butanol extraction was analyzed on a 12% reducing gel. Lanes 2 and 3 contain 10 and 5 μ g of protein respectively that had been previously isolated by Dr. J. Pérez-Gil, and lanes 4 and 5 contain 10 and 5 μ g of protein recently isolated for the purpose of this study. Lanes 1 and 6 were loaded with low molecular weight markers (LMWM). The gel was stained with Daiichi silver stain.

(panel B) are shown in figure 8. The monolayers were compressed rapidly to ~ 10 mN/m, expanded to 0 mN/m, then allowed to equilibrate for one hour. After this period, the monolayers were compressed at a fast rate ($4 \text{ \AA}^2/\text{molecule /second}$). Monolayers of PSLE lift-off at ~ $90 \text{ \AA}^2/\text{molecule PL}$ and the surface pressure (π) of the monolayer increased with compression. At π of 45 mN/m, the isotherm inflected to the left, then rose sharply to 70 mN/m with further compression. Isotherms of PSLE spread on subphases containing various concentrations of SP-A differed than PSLE films in the absence of SP-A. The presence of SP-A in the subphase shifted the isothermal lift-off of PSLE monolayers to the right ($110 \text{ \AA}^2/\text{phospholipid molecule}$). With incremental compression, the isotherms of PSLE in the presence of SP-A shifted toward the normal PSLE isotherm and at $\pi \sim 45 \text{ mN/m}$ adopted a π -area profile similar to that of PSLE in the absence of protein. The presence of 5 mM Ca^{2+} (panel B) did not significantly affect PSLE monolayer behaviour.

3.3 Monolayer Surface Texture

PSLE monolayer surface morphology could be observed with the addition of 1 mol% NBD-PC. The following data are representatives of more than one experiment performed during this study. Monolayer images of PSLE, and PSLE on subphases containing 0.13, 0.16 or 0.20 $\mu\text{g/mL}$ SP-A at selected π are shown in figure 9. The monolayers were compressed rapidly to ~ 10 mN/m, expanded to 0 mN/m, then allowed to equilibrate for one hour. After this period, the PSLE films were compressed at a slow rate ($0.0089 \text{ \AA}^2/\text{molecule/second}$) which resulted in

Figure 8. Pressure-Area Isotherms of PSLE monolayers spread over subphases containing 0 (\circ), 0.13 (\bullet), 0.16 (∇), and 0.20 $\mu\text{g/mL}$ SP-A (\blacktriangledown) in the absence (A) or presence of 5 mM Ca^{2+} (B). The monolayers were compressed in steps at an initial rate of 4 $\text{\AA}^2/\text{molecule/second}$ on a subphase of 145 mM NaCl, 5 mM Tris (pH 6.9). The temperature of the subphase was $21 \pm 2^\circ\text{C}$.

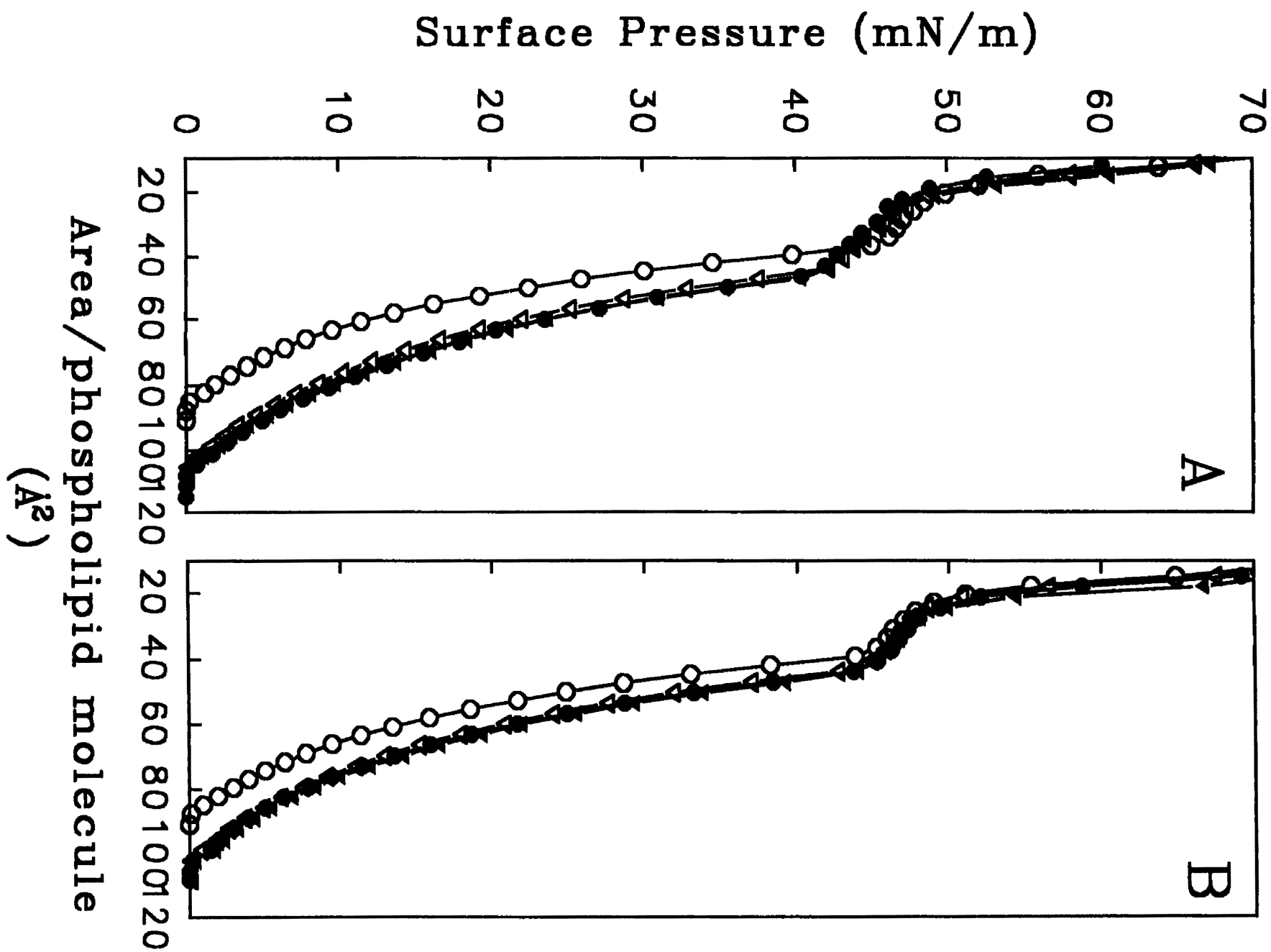
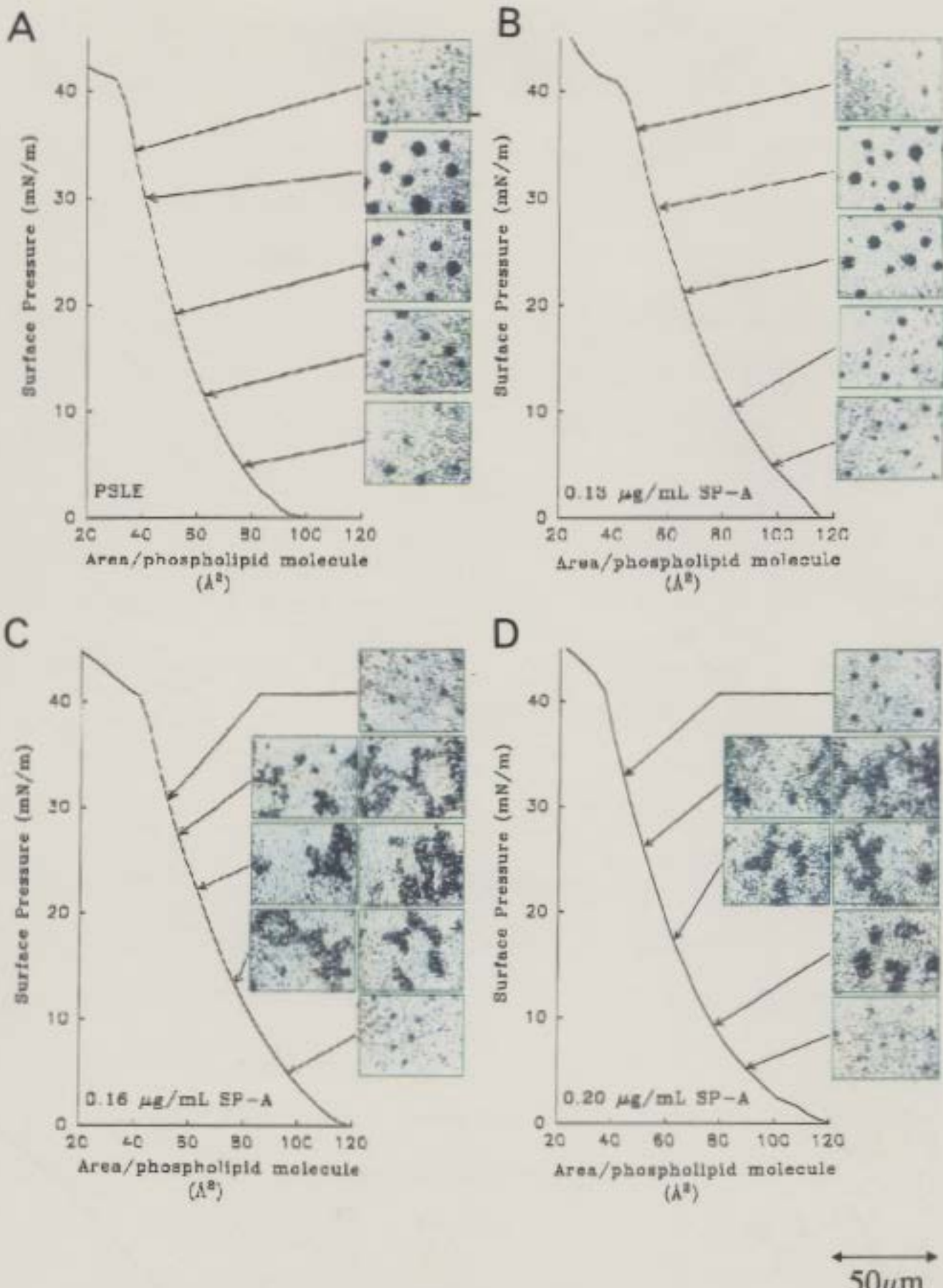


Figure 9. Monolayer surface morphology of PSLE (panel A) and PSLE spread on subphases containing 0.13 (B), 0.16 (C), and 0.20 $\mu\text{g/mL}$ SP-A (D) in the absence of Ca^{2+} . Monolayer images are accompanied by corresponding isotherms and surface pressures. The green background indicates the phase containing the fluorescent probe NBD-PC. The images were collected using a black and white CCD camera and are shown in false color to convey the impression given during direct observation. The scale bar is 50 μm .

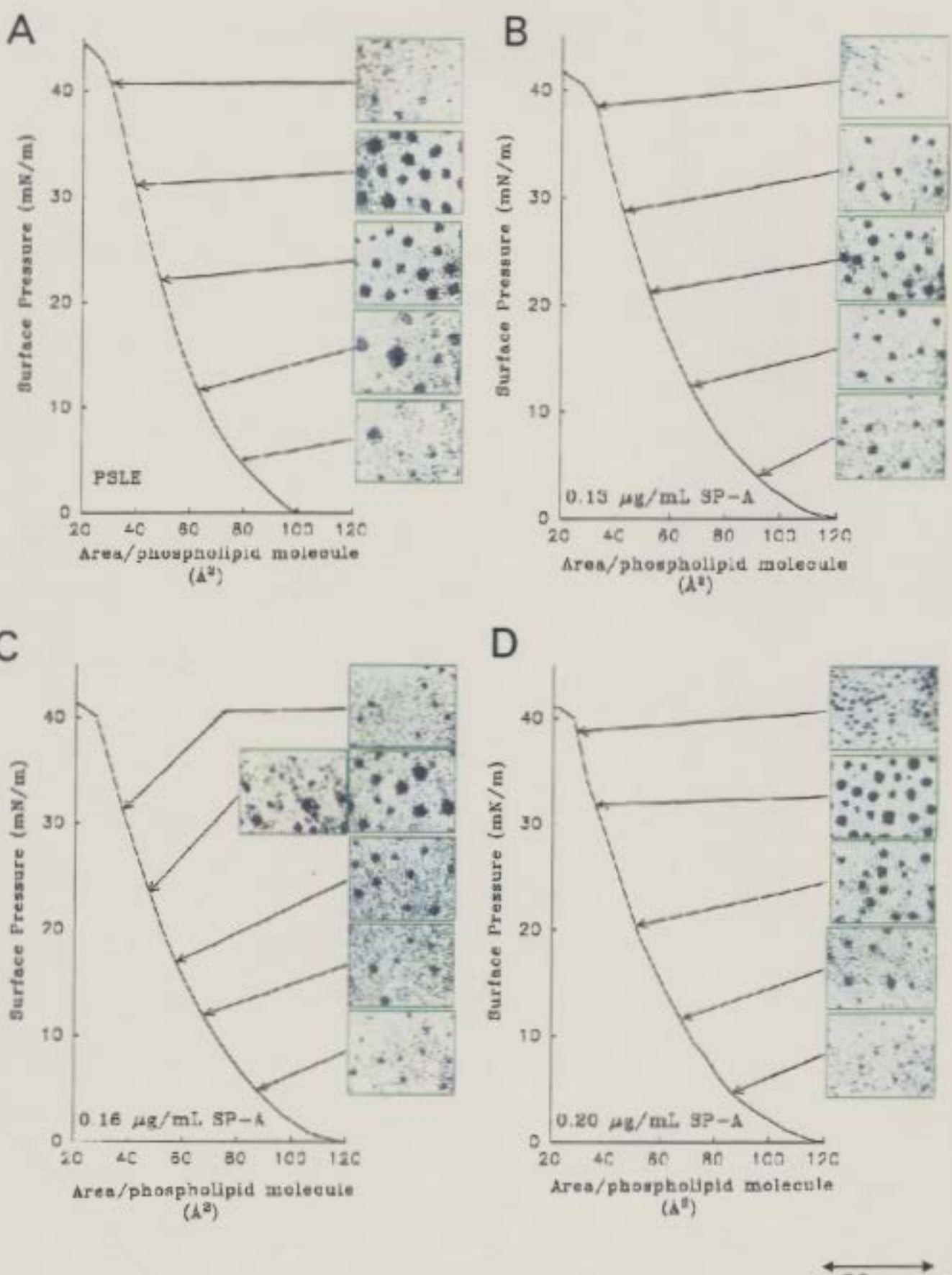


monolayer collapse at about 45 mN/m. Panel A reviews the images observed in spread monolayers of PSLE at various π . Circular, probe-excluded (dark) domains were observed amidst a fluorescent green background at low π (5 mN/m) despite the absence of a traditional liquid expanded (LE)/liquid condensed (LC) phase transition as seen in monolayers of pure lipid such as DPPC. With increased π , the dark domains were larger and seemed to come closer together. This trend continued until π of \sim 25 mN/m, then a decrease in domain size was observed. The appearance of dark domains in monolayers of PSLE have been reported previously (Discher et al., 1996; Nag et al., 1998). The addition of 0.13 $\mu\text{g/mL}$ SP-A (panel B) in the subphase had a minimal effect on PSLE monolayer surface texture. Dark domains were observed at low π , and grew in size with increased π . Once again, π beyond 25 mN/m resulted in a decrease in the domain size.

The presence of 0.16 and 0.20 $\mu\text{g/mL}$ SP-A in the subphase had a dramatic effect on the appearance of PSLE monolayer surface texture (see figure 9, panel C, D). Dark domains organized into a loose "network" at a π of \sim 10 mN/m. Areas of the film contained highly aggregated dark domains, while adjacent areas were highly fluorescent. With increased π , the "network" was not as intensely dark and the nucleation of tiny dark domains was observed. At $\pi \sim$ 27 mN/m, the network disappeared, leaving the tiny dark domains amidst a fluorescent background.

Monolayer images of PSLE and PSLE on subphases containing 0.13, 0.16 and 0.20 $\mu\text{g/mL}$ SP-A in the presence of 5 mM Ca^{2+} are shown in figure 10. The presence of 5 mM Ca^{2+} did not have a significant effect on PSLE monolayer surface

Figure 10. Monolayer surface morphology of PSLE (panel A) and PSLE spread on subphases containing 0.13 (B), 0.16 (C), and 0.20 $\mu\text{g/mL}$ SP-A (D) with 5 mM Ca^{2+} . Monolayer images are accompanied with corresponding isotherms and surface pressures. The green background indicates the phase containing the fluorescent probe NBD-PC. The images were collected using a black and white CCD camera and are shown in false color to convey the impression given during direct observation. The scale bar is 50 μm .

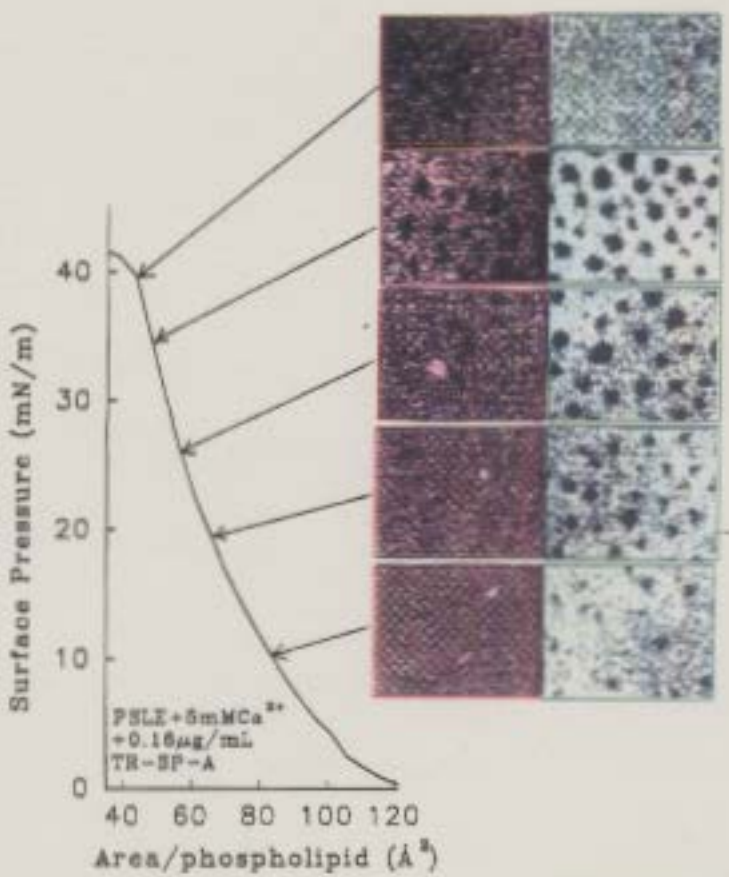
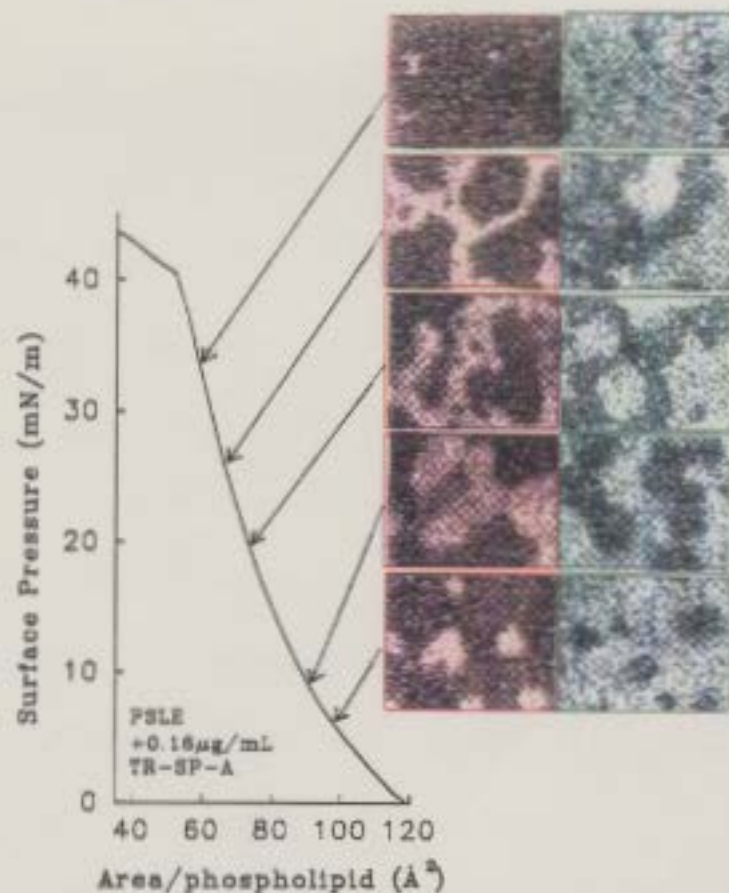


textures. The nucleation of dark domains was observed at low π (5 mN/m) and the domains grew in size until $\pi \sim 25$ mN/m. Beyond this π the visible amount of dark phase was decreased. When various concentrations of SP-A were added to the 5 mM Ca^{2+} subphase, the appearance and behaviour of the PSLE monolayer was not dramatically different from films in the absence of SP-A (panel B-D), but the size of the dark domains was smaller than those observed in the absence of the protein.

3.4 TR-SP-A Fluorescence in PSLE Monolayers

PSLE monolayers were spread onto a buffered saline subphase containing 0.16 $\mu\text{g/mL}$ TR-SP-A in the absence or presence of 5 mM Ca^{2+} . The monolayers were compressed rapidly to ~ 10 mN/m, expanded to 0 mN/m, then allowed to equilibrate for one hour. After this period, the monolayers were compressed at a slow rate ($0.0089 \text{ \AA}^2/\text{molecule/second}$) and images were collected (figure 11). The upper figure reviews the images observed in spread monolayers of PSLE on subphases containing 0.16 $\mu\text{g/mL}$ TR-SP-A in the absence of Ca^{2+} at various π using NBD-PC (right panel) or TR-SP-A (left panel) fluorescence. At π of about 10 mN/m, the images observed using NBD-PC fluorescence showed the appearance of a loosely organized "network" of dark regions amidst a fluorescent background. These images were not unlike those observed using unlabelled SP-A. The "network" was no longer detectable at π beyond 30 mN/m. TR-SP-A fluorescence was observed at the monolayer surface by switching light filters. It was interesting to note that fluorescent domains were observed amidst a dark background. The images observed with the

Figure 11. Monolayer surface morphology of PSLE spread on subphases containing $0.16 \mu\text{g/mL}$ TR-SP-A in the absence (top) or presence of 5 mM Ca^{2+} (bottom). Monolayer images are accompanied by corresponding isotherms and surface pressures. The green background (right panel) indicates phase containing the fluorescent probe NBD-PC and the red background (left panel) indicates phase containing the fluorescently labelled SP-A. The images were collected using a black and white CCD camera and are shown in false color to convey the impression given during direct observation. The scale bar is $50 \mu\text{m}$.



↔ 50 µm

aide of TR-SP-A fluorescence were reversed to those observed with NBD-PC fluorescence. Organized "networks" of fluorescent domains were observed with compression until $\pi \geq 30$ mN/m, when only tiny aggregates of TR-SP-A fluorescence were observed randomly at the film surface. While our equipment did not allow us to obtain data fast enough to record superimposable images, when the filters were switched it could be observed by eye that the red areas from TR-SP-A fluorescence corresponded to the dark areas using NBD-PC.

Images obtained from PSLE monolayers spread onto a subphase containing 0.16 $\mu\text{g/mL}$ TR-SP-A and 5 mM Ca^{2+} did not show a reorganization of dark domains as viewed through NBD-PC fluorescence (lower figure 11, right panel). The domains were circular, and they grew in size with further compression until π of 35 mN/m were reached. Beyond this π , there was a decrease in the detectable size and number of dark domains. TR-SP-A fluorescence (left panel) was minimal at lower π (≤ 10 mN/m). Tiny aggregates of fluorescently labelled protein were observed amidst a dark background. Increasing π allowed for the visualization of dark domains (25-35 mN/m), but the red fluorescence of the background was not intense. At π beyond 35 mN/m, these dark domains were not detectable, and TR-SP-A fluorescence was seen randomly as tiny aggregates.

3.5 Dark Domain Size Distribution and Total Dark Area in PSLE Monolayers

The size frequency distributions of dark domains of PSLE films containing various concentrations of SP-A at various π are shown in figure 12. The number and

size of dark domains for a particular π were counted for each of the 10 frames recorded. The size distribution of PSLE (panel A) at low π (9.2 mN/m) showed predominantly small dark domains. With increased π , the amount and size of the domains increased. This trend continued until $\pi \sim 25$ mN/m. At 36 mN/m, the monolayer contained mostly small domains ($\leq 10 \mu\text{m}^2$). The presence of 0.13 $\mu\text{g/mL}$ SP-A (panel B) in the monolayer subphase did not substantially affect dark domain size distribution. PSLE monolayers containing 0.16 (panel C) showed large domains of 100-600 μm^2 at π between 9-29 mN/m, and the spectrum and size of the smaller domains was broad. At π beyond 30 mN/m, a large number of small ($\leq 10 \mu\text{m}^2$) were observed in all monolayers.

Dark domain size distribution in PSLE monolayers in the presence of 5 mM Ca^{2+} and various concentration of SP-A are shown in figure 13. PSLE monolayers (panel A) in the presence of 5 mM Ca^{2+} displayed a similar frequency distribution pattern as that of PSLE. With increased π , the size and amount of dark domains increased, and $\pi \geq 30$ mN/m resulted in an increase in the number of small domains. The presence of various concentrations of SP-A in the subphase (0.13 $\mu\text{g/mL}$; panel B, 0.16 $\mu\text{g/mL}$; panel C), as well as 5 mM Ca^{2+} appeared to decrease the size of the dark domains. The number of small domains ($\leq 10 \mu\text{m}^2$) was increased, and there were fewer large domains ($\geq 100 \mu\text{m}^2$).

The amount of dark area in PSLE monolayers containing various concentrations of SP-A in the absence (top panel) and presence (bottom panel) of 5 mM Ca^{2+} is shown in figure 14. The amount of dark area in monolayers of PSLE

Figure 12. The size frequency distribution of dark domains observed at various π in monolayers of PSLE (A) and PSLE monolayers spread on subphases containing 0.13 (B), and 0.16 $\mu\text{g/mL}$ SP-A (C) and in the absence of Ca^{2+} . At a particular π , the average number and size of dark domains was determined for each of the 10 frames. Areas $< 3 \mu\text{m}^2$ were not included in the data. The surface pressure is indicated for each distribution shown. Error bars indicate \pm one standard deviation for 10 frames analyzed at each π .

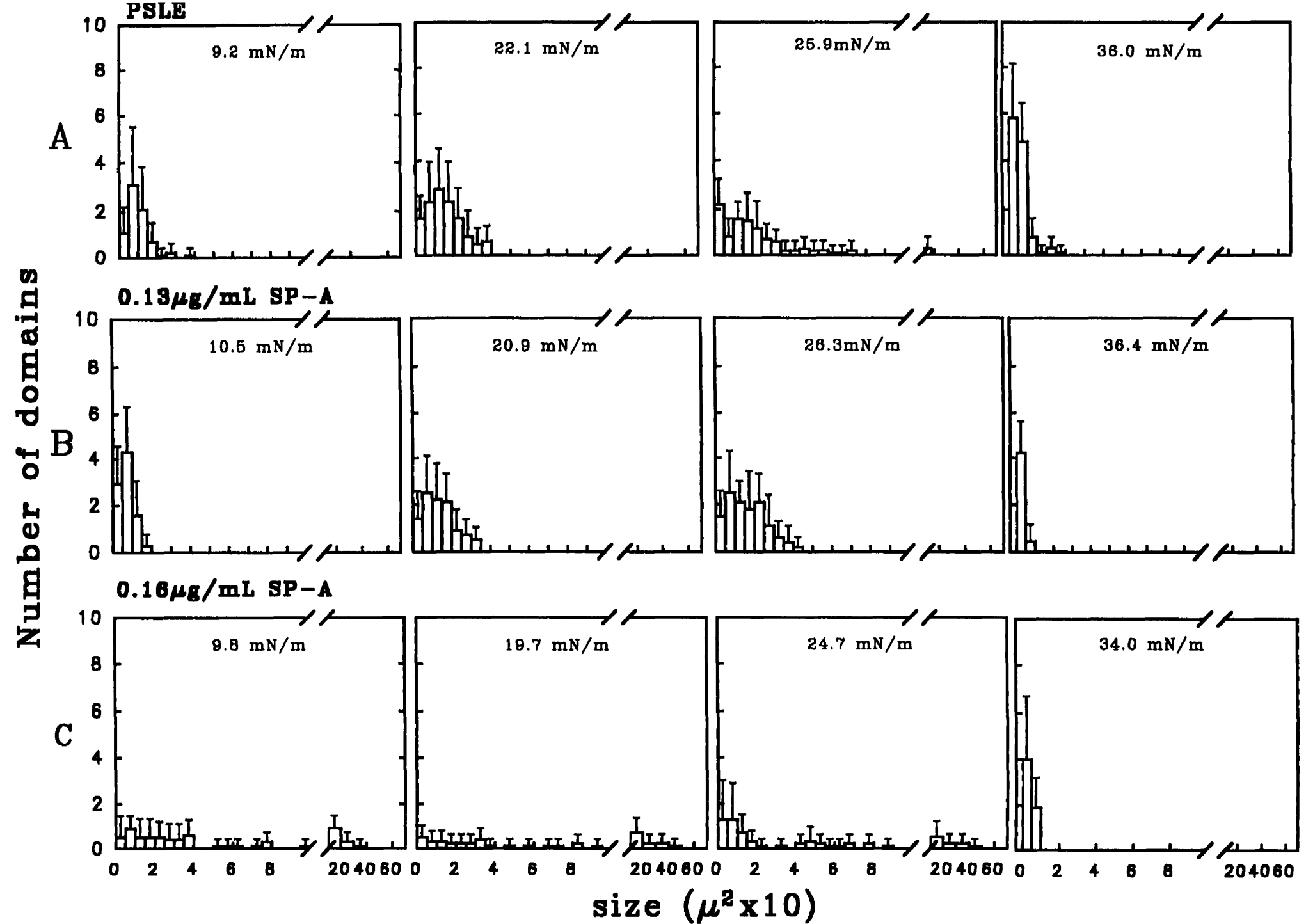
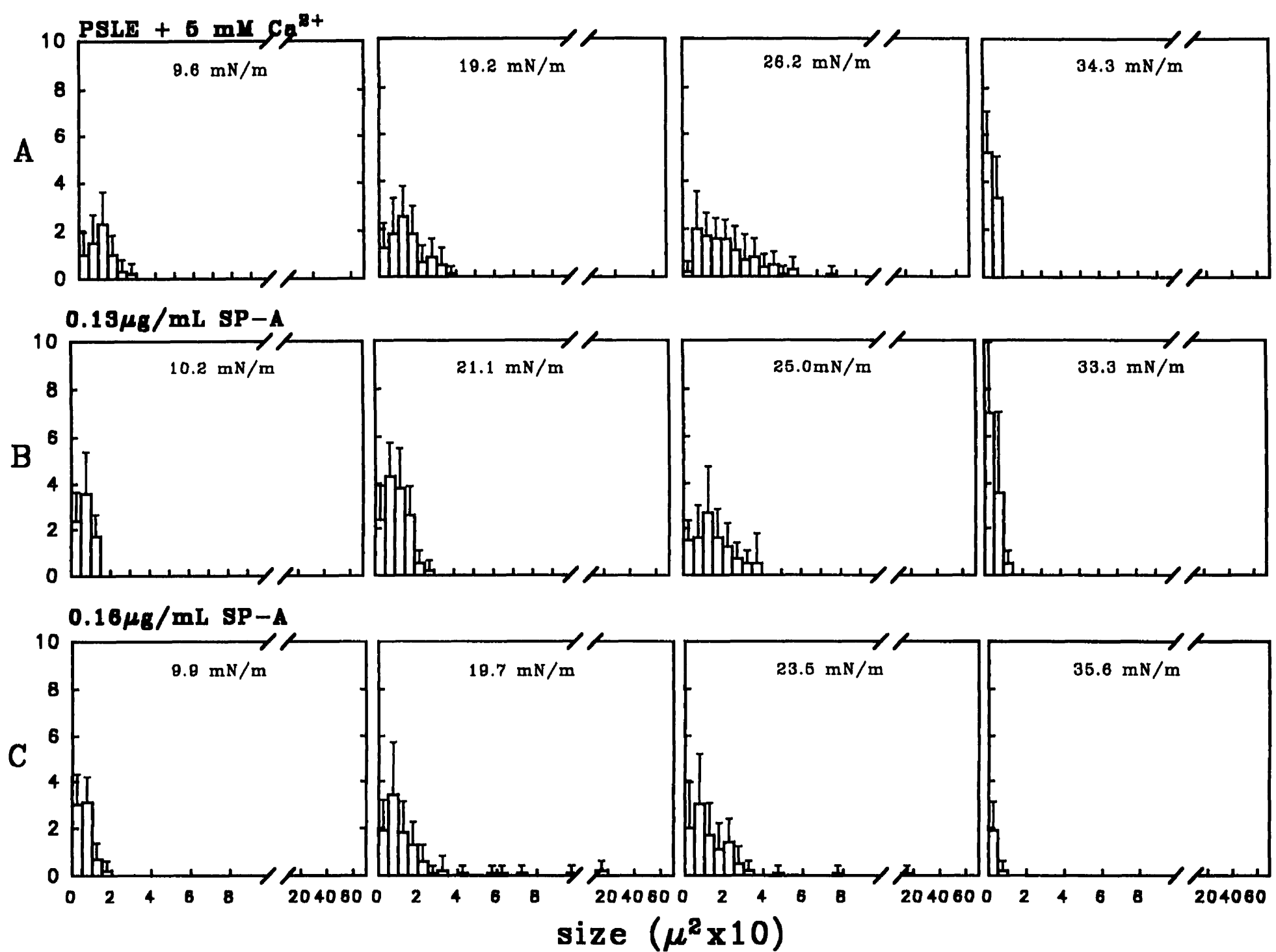


Figure 13. The size frequency distribution of dark domains observed at various π in monolayers of PSLE (A) and PSLE monolayers containing 0.13 (B), and 0.16 $\mu\text{g/mL}$ SP-A (C) and 5 mM Ca^{2+} in the subphase. At a particular π , the average number and size of dark domains was determined for each of the 10 frames. Areas $< 3 \mu\text{m}^2$ were not included in the data. The surface pressure is indicated for each distribution shown. Error bars indicate \pm one standard deviation for 10 frames analyzed at each π .

Number of domains



increased with increased π . The %dark area reached 18% at ~ 25 mN/m, but beyond this π the amount of dark area gradually decreased (2% at 40 mN/m). Similar amounts of condensation in PSLE monolayers have been reported (Discher et al., 1996; Nag et al., 1998). The presence of 0.13 $\mu\text{g/mL}$ SP-A in the subphase did not have a substantial effect on the amount of dark area observed in PSLE monolayers. Subphase concentrations of 0.16 and 0.20 $\mu\text{g/mL}$ SP-A increased the amount of dark phase to 25% at $\pi \sim 10$ mN/m, and the amount remained constant till ~ 27 mN/m. Beyond this π , the amount of dark phase decreased to $\sim 2\%$.

The presence of 5 mM Ca^{2+} in the subphase (bottom panel) did not substantially alter the amount of dark area observed on the surface of PSLE monolayers. Yet, subphase concentrations of 0.13 and 0.16 $\mu\text{g/mL}$ SP-A appeared to decrease the amount of dark area observed. Limited data was available for the effect of 0.20 $\mu\text{g/mL}$ SP-A on monolayers of PSLE in the presence of 5 mM Ca^{2+} , thus it was not reported.

3.6 PSLE Monolayers at High Resolution

PSLE monolayer spread on buffered subphase was observed using a 50x objective lens as compared to the 40 x objective lens used in the previous experiments. PSLE monolayer surface textures at various π are shown in figure 15. The higher objective lens allowed for increased resolution, and smaller domains could be observed at each π .

Figure 16 compares the size distribution (A) and the %dark phase (B) of PSLE

Figure 14. The %dark area of PSLE monolayers spread on subphases containing 0 (○), 0.13 (●), 0.16 (▽), and 0.20 $\mu\text{g/mL}$ (▼) SP-A in the subphase in the absence (A) and presence (B) of 5 mM Ca^{2+} . Error bars indicate \pm one standard deviation for 10 frames analyzed at each π . Error bars not visualized are within the size limits of the symbol.

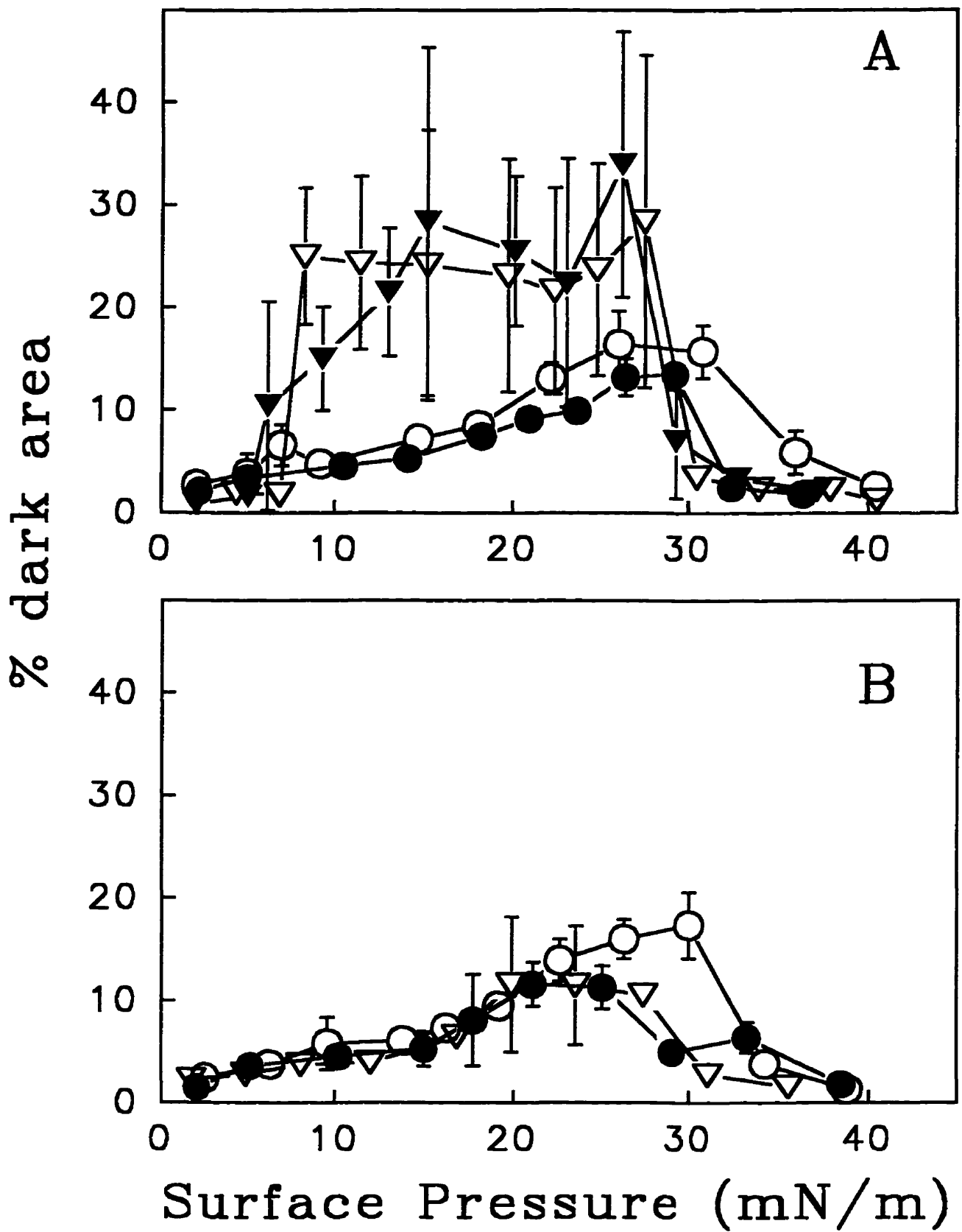
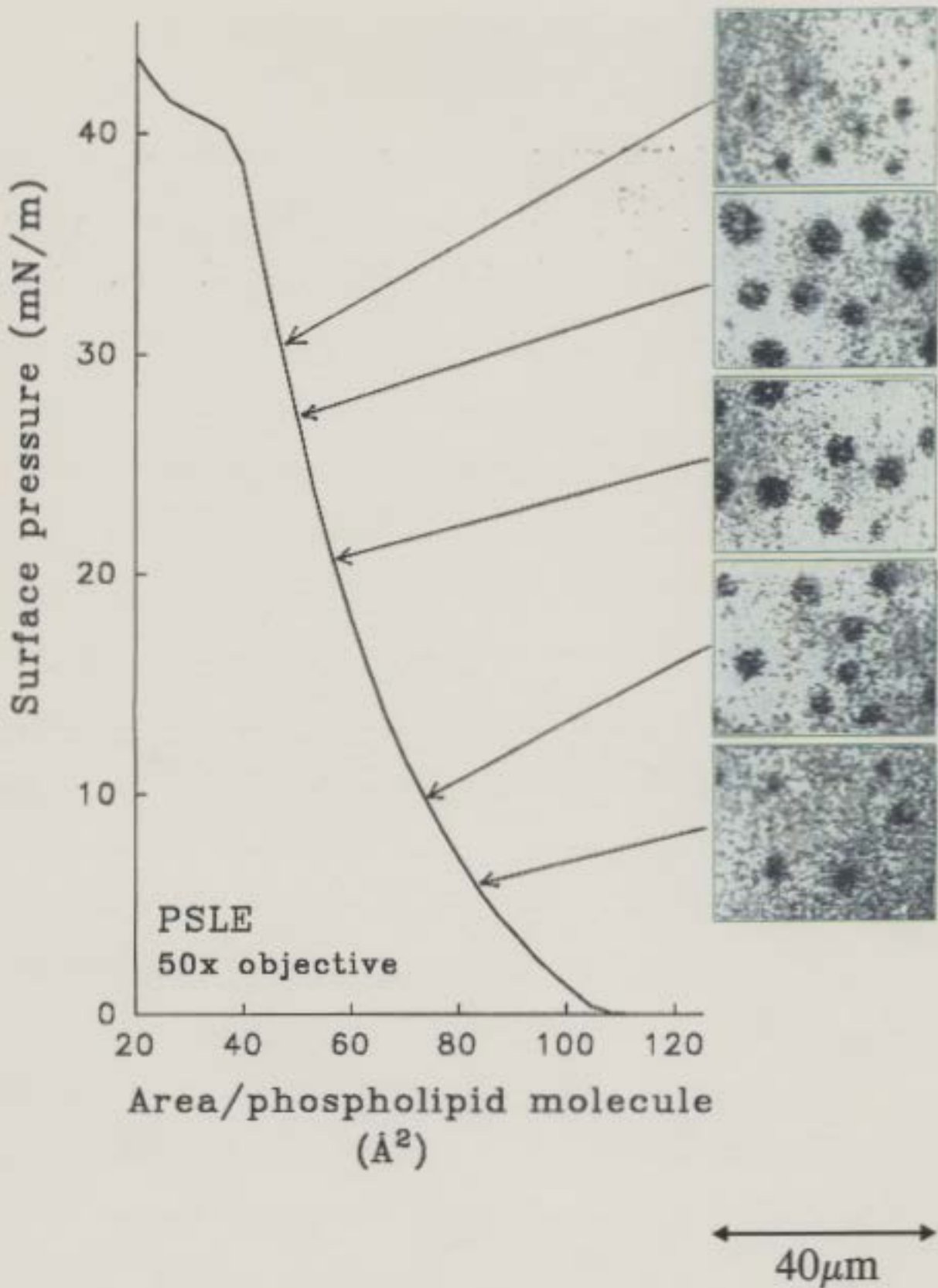


Figure 15. Monolayer surface morphology of PSLE monolayers spread over saline subphase and in the absence of Ca^{2+} observed through a 50X objective lens. Images were recorded at various π and the corresponding isotherm is shown. The images were collected using a black and white CCD camera and are shown in false color to convey the impression given during direct observation. The scale bar is 40 μm .



monolayers observed through a 40x and 50x objective lens. The number of small domains ($\leq 5 \mu\text{m}^2$) observed under the 50x objective was greater than that of the 40x objective lens. As to be expected, the number and size of the larger domains were very similar with both objectives. The %dark area observed under the 50x objective was slightly greater than PSLE monolayers observed under the 40x objective lens. But the increased number of visualized small domains ($\leq 5 \mu\text{m}^2$) did not contribute significantly to the total area of dark phase when compared to PSLE monolayers observed under the 40X objective.

3.7 Spread Vesicle Suspensions of PSLE

A vesicle suspension of PSLE containing 1 mol% NBD-PC, 10 wt% TR-SP-A and 5 mM Ca^{2+} was spread on a buffered saline subphase dropwise from a hamilton syringe. The monolayer was compressed rapidly to $\sim 10 \text{ mN/m}$, expanded to 0 mN/m, then allowed to equilibrate for one hour. After this period, the monolayer was compressed at a slow rate (0.0089 $\text{\AA}^2/\text{molecule/second}$) and images were collected. Images of PSLE monolayer and the TR-SP-A probe were visualized by switching light filters (see figure 17). At low π , tiny dark domains were visualized under the filter that allowed the passage of green light (right panel). These domains grew in size and appeared to aggregate with increased π . At π beyond 30 mN/m, the size of the dark domains seemed to decrease, yet aggregates of tiny dark areas were still visualized. The TR-SP-A, as viewed by the filter that allowed the passage of red light (right panel) aggregated in the fluid phase and fluid/gel phase boundaries of the

Figure 16. The frequency size distribution (A) and the %dark area (B) of PSLE films spread over saline subphase and in the absence of Ca^{2+} observed under a 40X (○) and 50X (●) objective lens. At a particular π , the average number and size of dark domains was determined for each of the 10 frames. The surface pressure is indicated for each distribution shown. Areas $< 3 \mu\text{m}^2$ were not included in the data. Error bars indicate \pm one standard deviation for 10 frames analyzed at each π . Error bars not visualized are within the size limits of the symbol.

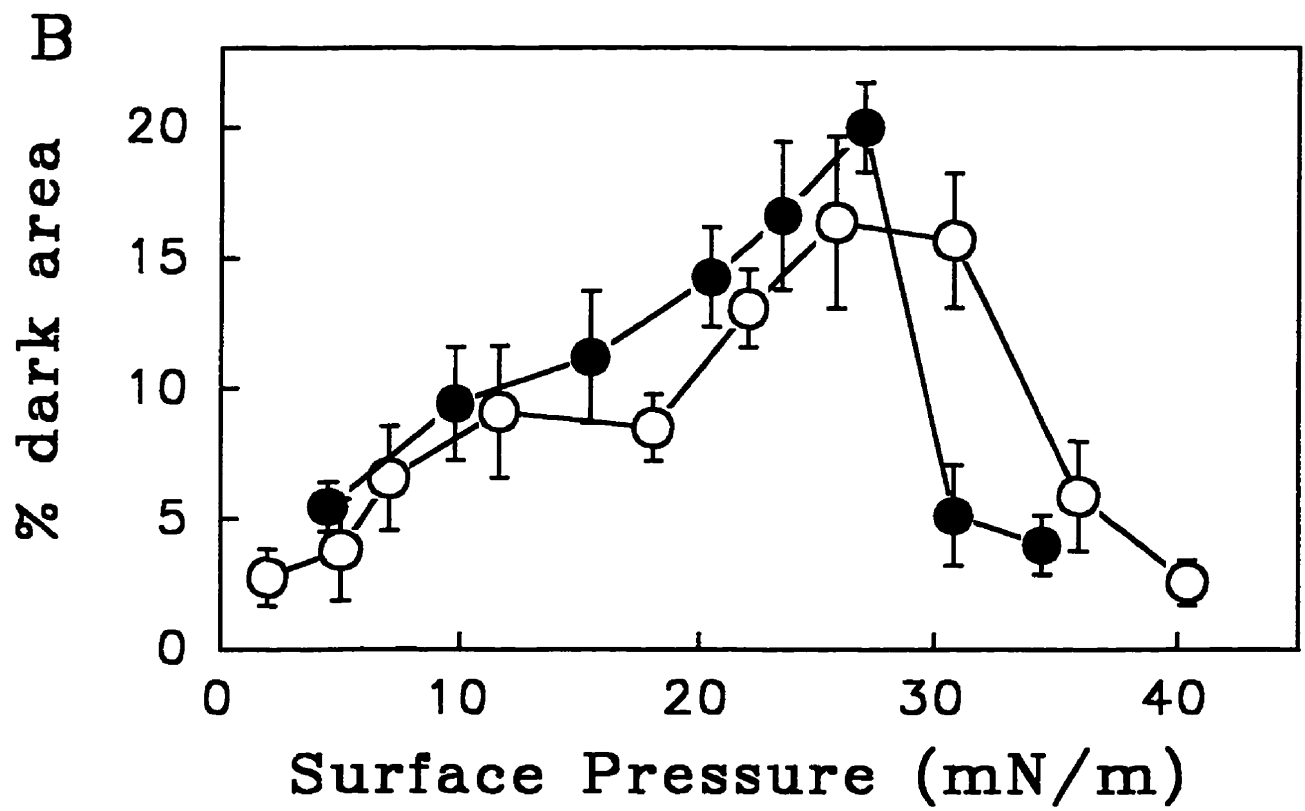
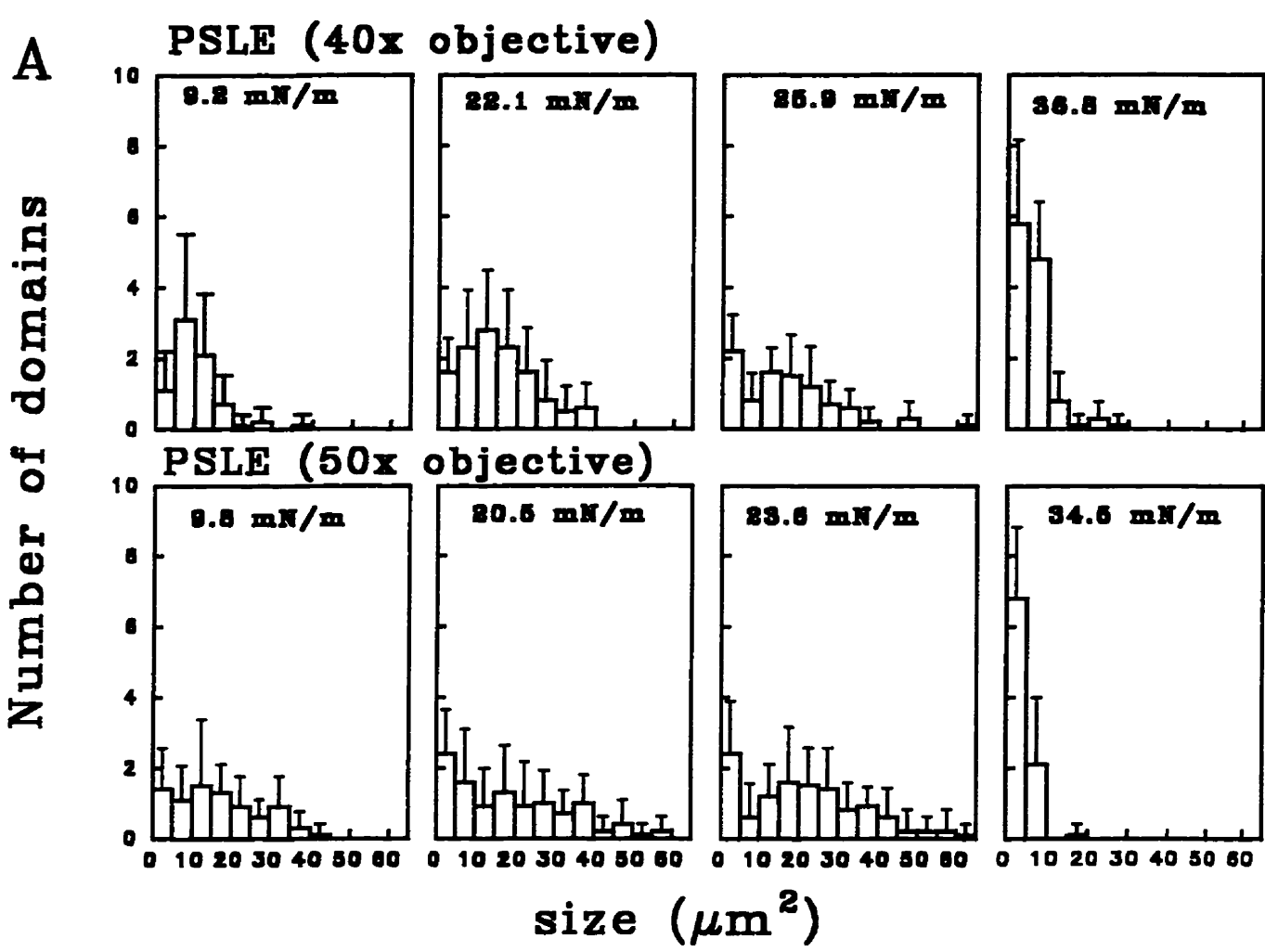
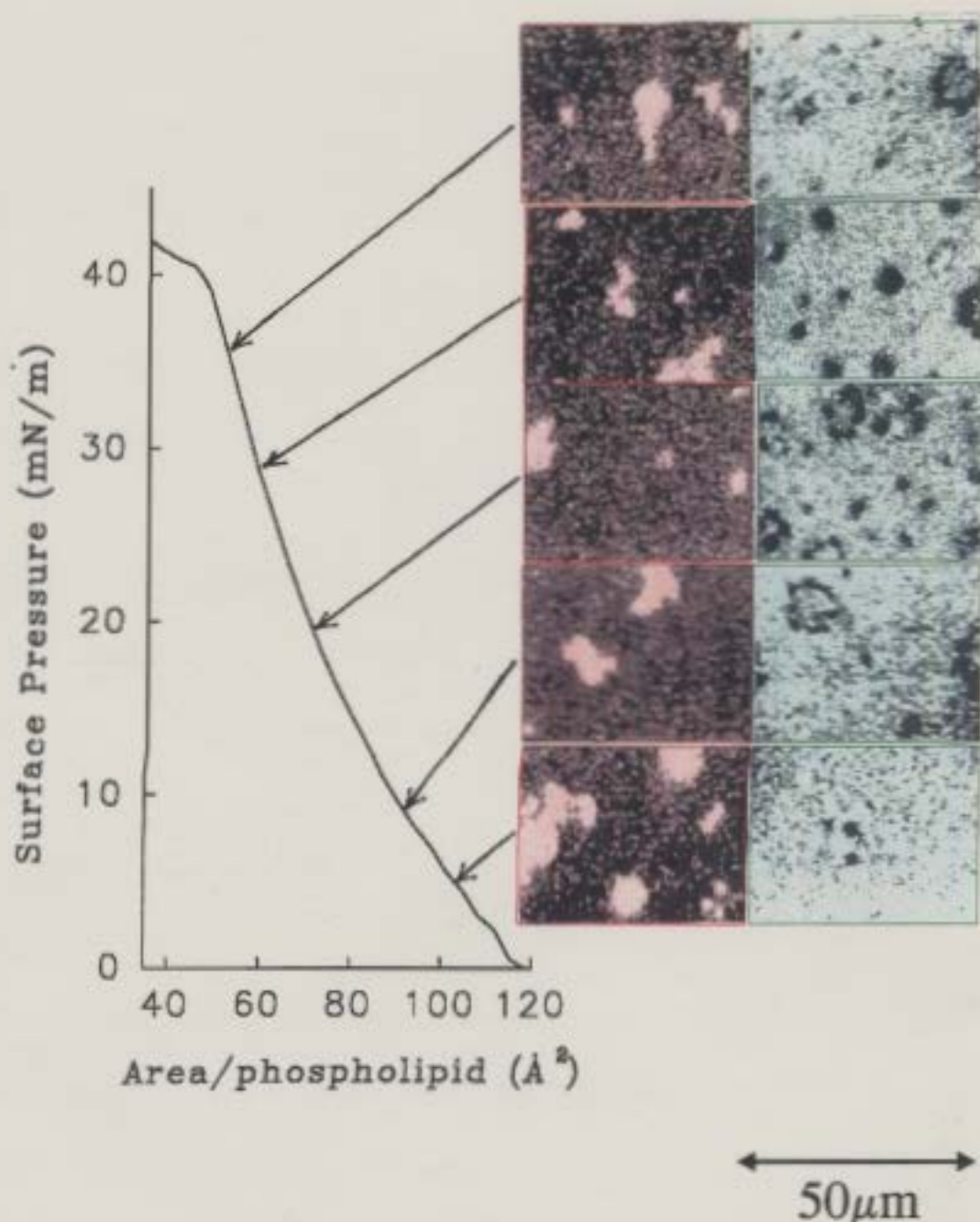


Figure 17. Surface morphology of PSLE vesicle films containing 1 mol% NBD-PC, 10 wt% TR-SP-A, and 5 mM Ca^{2+} . A vesicle suspension (0.750 mg PL/mL) was spread onto the subphase from a hamilton syringe and the adsorbed film was compressed. The right panel shows NBD-PC probe fluorescence and the left panel shows TR-SP-A probe fluorescence. The images were collected using a black and white CCD camera and are shown in false color to convey the impression given during direct observation. The images are accompanied by their corresponding isotherm. The scale bar is 50 μm .

Lipid Extract + 5mM Ca^{2+}
+ 10wt% TR-SP-A



PSLE monolayer. Increasing π did not affect the appearance of the TR-SP-A distribution.

The frequency size distribution (top) and % phase (bottom; dark domains or TR-SP-A aggregates) of films spread from PSLE vesicles containing 1 mol% NBD-PC, 10 wt% TR-SP-A and 5 mM Ca²⁺ are shown in figure 18. The dark domains (top panel, A) observed with NBD-PC fluorescence were small, but numerous. The frequency of the domains at each π were similar. The size frequency of TR-SP-A aggregates (top panel, B) remained consistent with increased π .

The area occupied by dark domains and TR-SP-A aggregates in spread dispersions of PSLE are shown at the bottom of figure 18. The amount of dark area seen with NBD-PC increased with increased π . At 25 mN/m, the maximum amount of dark area was recorded at ~13%, and this amount decreased with higher π . The amount of visualized TR-SP-A remained constant at ~3% with increased π .

3.8 The Effects of 1.64 mM Ca²⁺

Isotherms of PSLE spread over subphases containing of 0, 1.64 and 5 mM Ca²⁺ plus or minus 0.16 μ g/mL SP-A in the subphase are shown in figure 19. The monolayers were compressed rapidly to ~10 mN/m, expanded to 0 mN/m, then allowed to equilibrate for one hour. After this period, the monolayers were compressed at a fast rate (4 Å²/molecule/second). The presence of Ca²⁺ at either concentration did not affect the PSLE monolayer isotherm while the presence of 0.16 μ g/mL SP-A and various concentrations of Ca²⁺ expanded the area occupied by the

Figure 18. The frequency size distribution (top) and the % phase (bottom; dark area, ○ or TR-SP-A aggregates, ●) of vesicle spread PSLE with 1 mol% NBD-PC, 10 wt% TR-SP-A and 5 mM Ca²⁺. At a particular π , the average number and size of dark domains was determined for each of the 10 frames. The surface pressure is indicated for each distribution shown. Areas < 3 μm^2 were not included in the data. Error bars indicate \pm one standard deviation for 10 frames analyzed at each π . Error bars not visualized are within the size limits of the symbol.

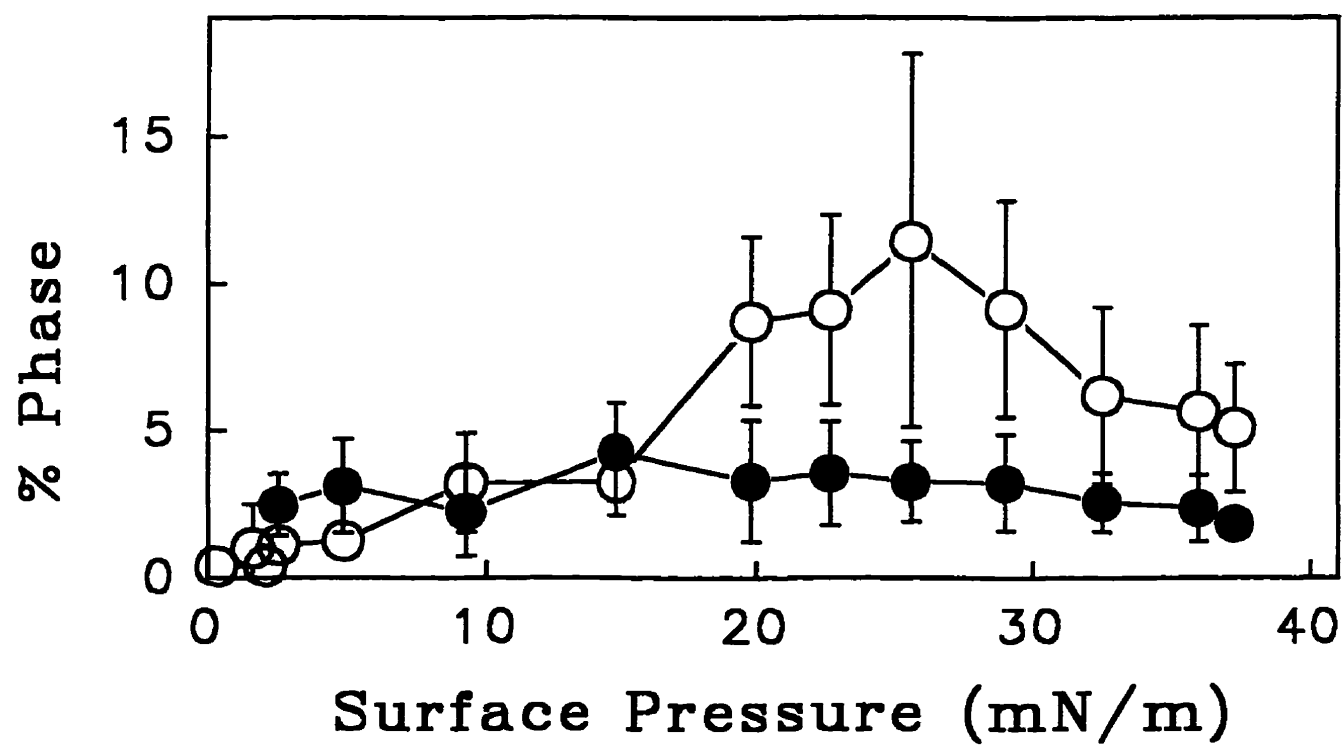
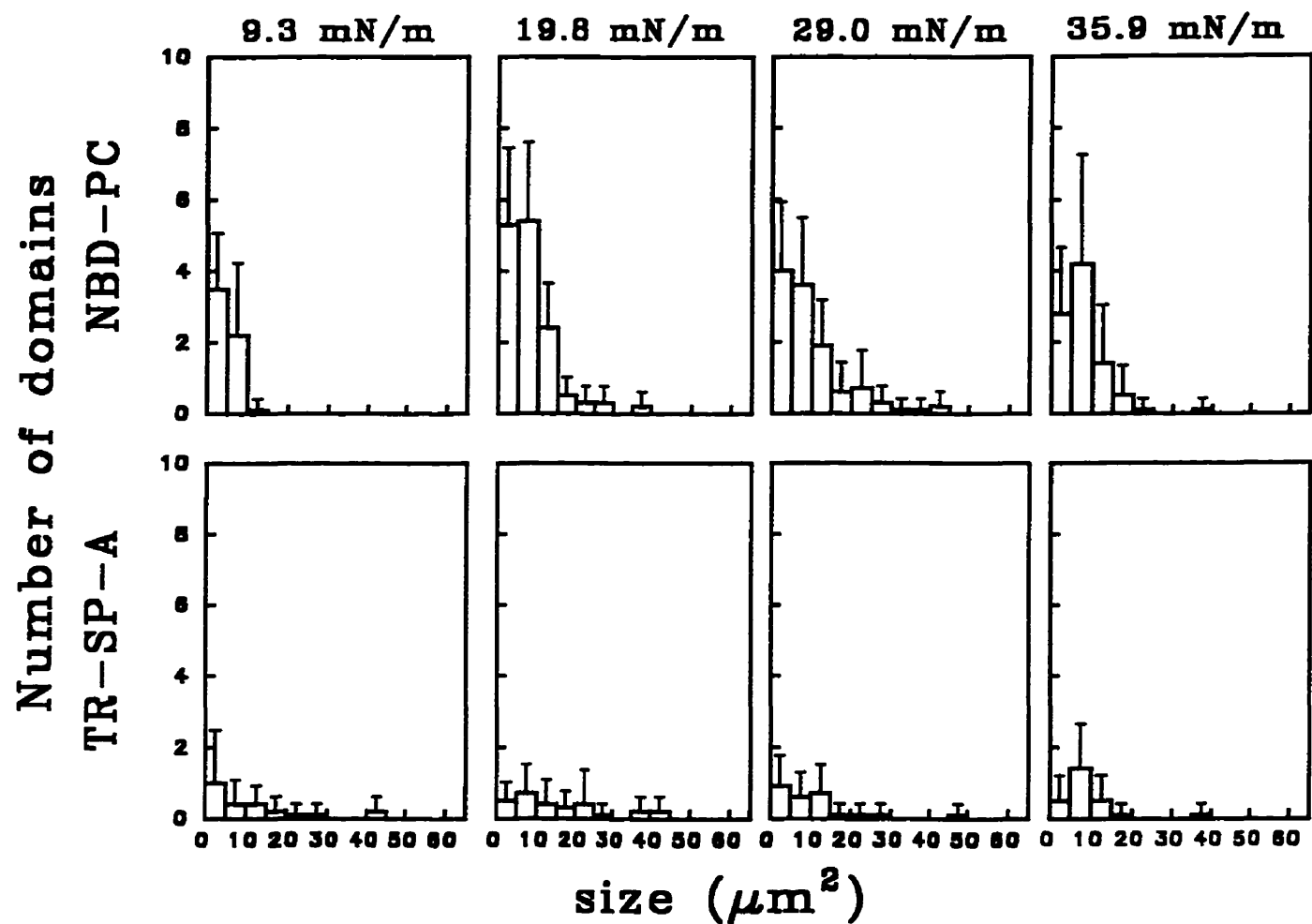
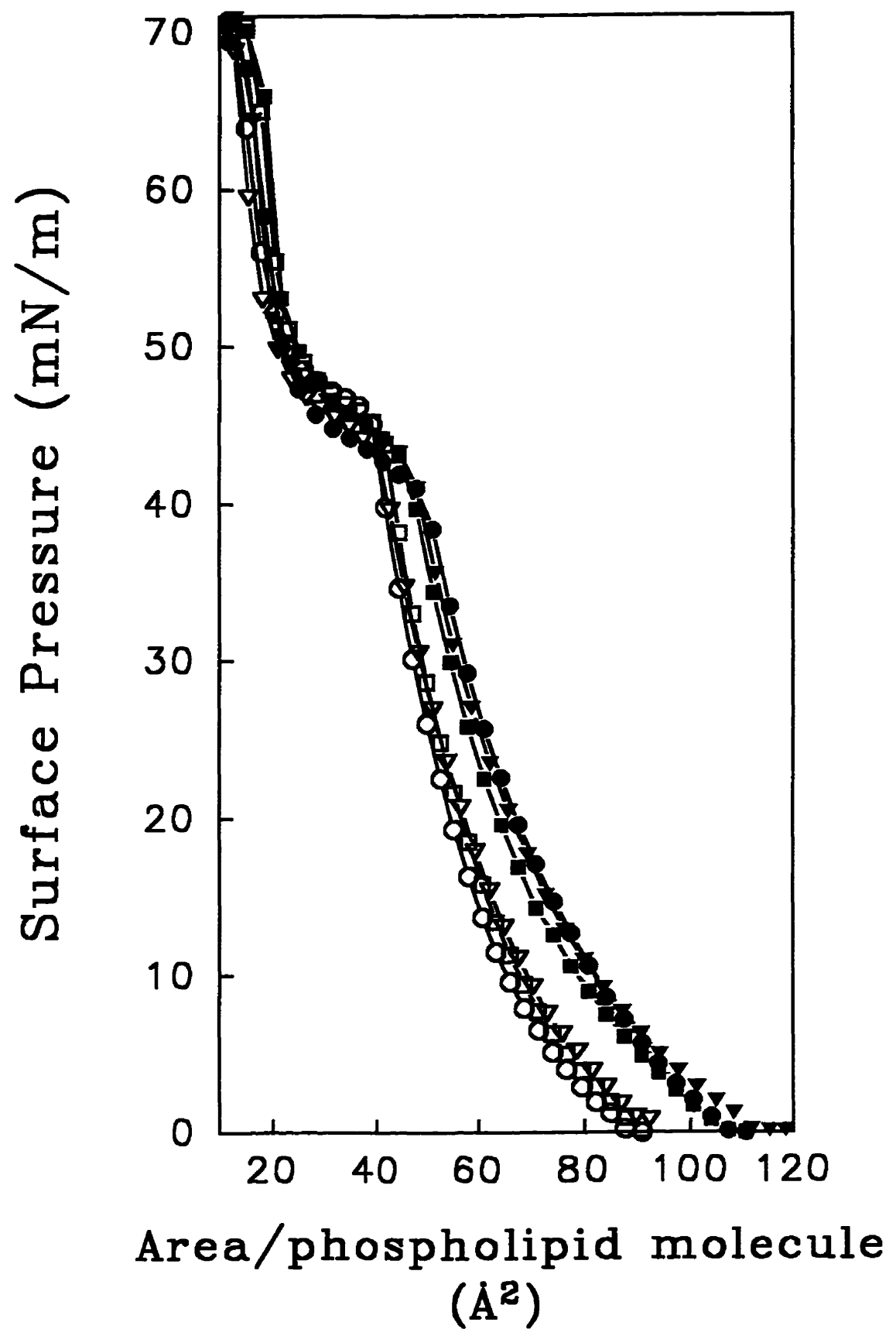


Figure 19. Pressure-Area isotherms of PSLE (○), PSLE + 0.16 μ g/mL SP-A (●), PSLE + 1.64 mM Ca²⁺ (▽), PSLE + 0.16 μ g/mL SP-A + 1.64 mM Ca²⁺ (▼), PSLE + 5 mM Ca²⁺ (□), and PSLE + 0.16 μ g/mL SP-A + 5 mM Ca²⁺ (■). The monolayers were compressed in steps at a rate of 4 $\text{\AA}^2/\text{molecule/second}$ on a subphase of 145 mM NaCl, 5 mM Tris (pH 6.9). The temperature of the subphase was 21 \pm 2 °C.



PSLE film. Isotherm profiles were similar to those previously recorded.

Monolayer surface textures of PSLE spread on subphases containing 1.64 mM Ca^{2+} plus or minus 0.16 $\mu\text{g/mL}$ SP-A are shown in figure 20. The surface texture of PSLE films in the presence of 1.64 mM Ca^{2+} (top) shared characteristics of PSLE containing either no or 5 mM Ca^{2+} . The presence of 0.16 $\mu\text{g/mL}$ SP-A and 1.64 mM Ca^{2+} in the subphase resulted in a reorganization of PSLE films. Domains aggregated into a network at $\sim 13 \text{ mN/m}$, and the organization of domains was consistent until $\pi > 20 \text{ mN/m}$. With increased π , small dark domains were observed amidst a fluorescent green background. Further compression resulted in a abrupt decrease in domain size.

The frequency size distribution of PSLE films spread on subphases containing various concentrations of Ca^{2+} are shown in figure 21. The size distribution (top) among PSLE films spread on subphases containing 0, 1.64 and 5 mM Ca^{2+} were similar. Increased π resulted in a greater number of large domains. Yet $\pi > 30 \text{ mN/m}$ caused the domain size to decrease to $< 20 \mu\text{m}^2$.

The frequency size distribution of PSLE films spread on subphases containing various concentrations of Ca^{2+} as well as 0.16 $\mu\text{g/mL}$ SP-A are shown in figure 22. The frequency size distribution of PSLE spread on a subphase containing 0.16 $\mu\text{g/mL}$ SP-A and 1.64 mM Ca^{2+} shared common traits with the other PSLE films spread over subphases containing 0 or 5 mM Ca^{2+} and 0.16 $\mu\text{g/mL}$ SP-A. At low π ($\sim 10 \text{ mN/m}$), the PSLE on 1.64 mM Ca^{2+} subphase contained numerous small domains similar to films spread on 5 mM Ca^{2+} . However π of $\sim 20 \text{ mN/m}$ resulted in a

Figure 20. Monolayer surface morphology of PSLE monolayers spread over subphases containing **1.64 mM** Ca^{2+} (top) or Ca^{2+} and **0.16 $\mu\text{g/mL}$** SP-A (bottom). The green background indicates the phase containing the fluorescent probe NBD-PC. Monolayer images are accompanied by corresponding isotherms and surface pressures. The images were collected using a black and white CCD camera and are shown in false color to convey the impression during direct observation. The scale bar is 50 μm .

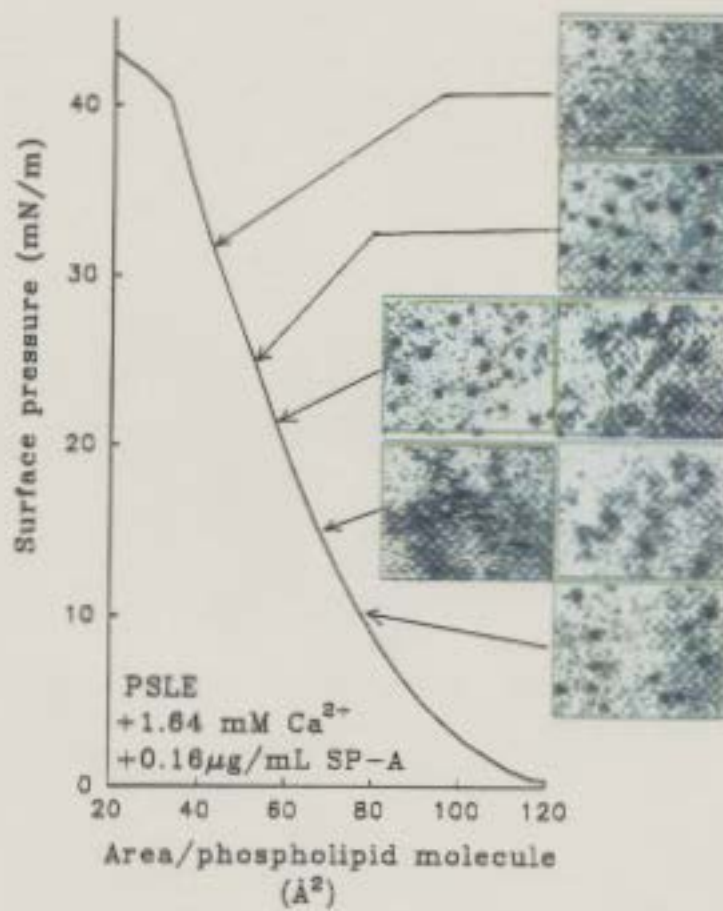
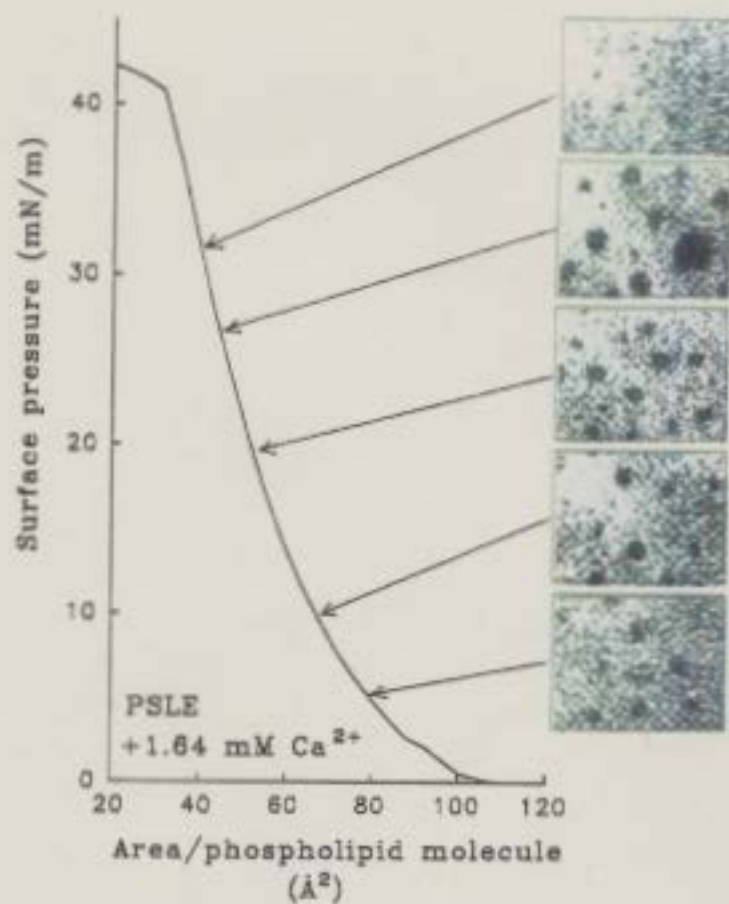


Figure 21. The frequency size distribution of PSLE films containing **0, 1.64 and 5 mM Ca²⁺** in the subphase. At a particular π , the average number and size of dark domains was determined for each of the 10 frames. The surface pressure is indicated for each distribution shown. Areas $< 3 \mu\text{m}^2$ were not included in the data. Error bars indicate \pm one standard deviation for 10 frames analyzed at each π . Error bars not visualized are within the size limits of the symbol.

Number of domains

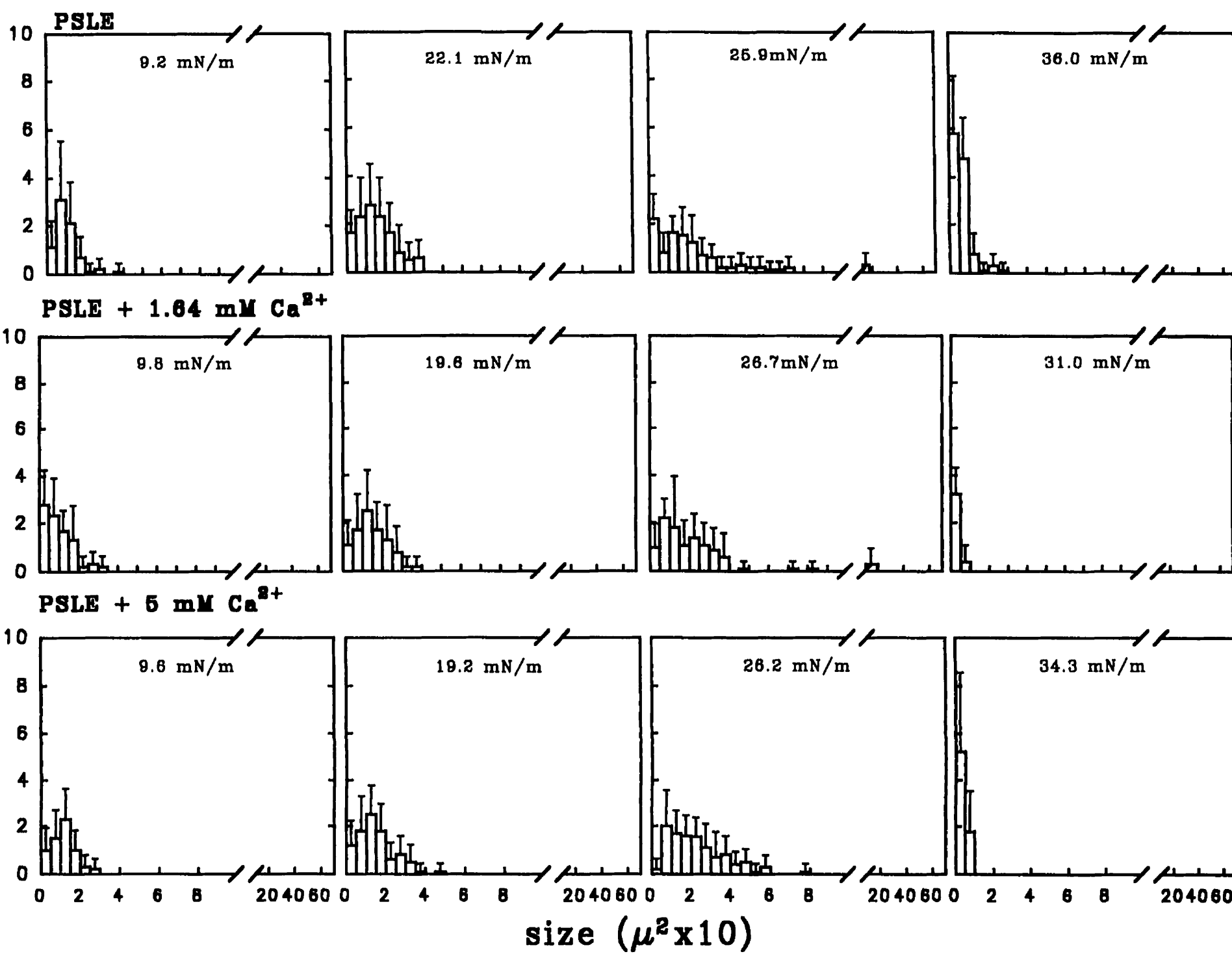
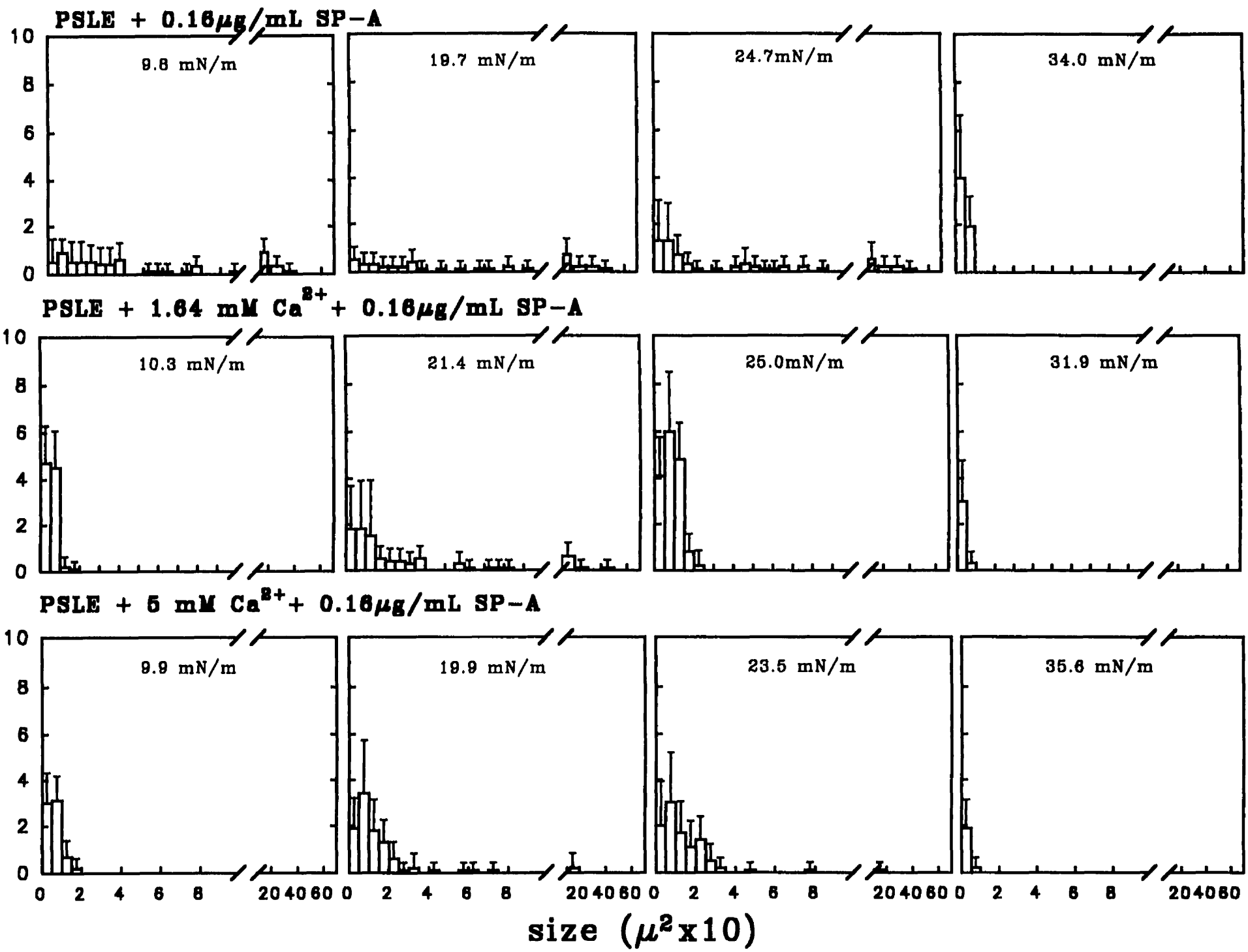


Figure 22. The frequency size distribution of PSLE films containing 0.16 $\mu\text{g/mL}$ SP-A and 0, 1.64 and 5 mM Ca^{2+} in the subphase. At a particular π , the average number and size of dark domains was determined for each of the 10 frames. The surface pressure is indicated for each distribution shown. Areas $< 3 \mu\text{m}^2$ were not included in the data. Error bars indicate \pm one standard deviation for 10 frames analyzed at each π . Error bars not visualized are within the size limits of the symbol.

Number of domains



broad size distribution of domains in a manner similar to PSLE films in the absence of Ca^{2+} , yet there was still a predominance of small domains.

The %dark area of PSLE with or without SP-A subphase concentrations of 0.16 $\mu\text{g/mL}$ in the presence of various concentrations of Ca^{2+} is summarized in figure 23. The %dark area of PSLE films containing various subphase concentrations of Ca^{2+} were very similar as well. The area of dark phase reached $\sim 18\%$ black with increased π for each of the films. The presence of 0 or 1.64 mM Ca^{2+} with 0.16 $\mu\text{g/mL}$ SP-A caused an increase in the amount of dark area in PSLE monolayers ($\sim 25\%$). But higher π was required of PSLE films spread over 1.64 mM Ca^{2+} and SP-A to reach this amount. The addition of 5 mM Ca^{2+} and 0.16 $\mu\text{g/mL}$ SP-A appeared to decrease the amount of dark area compared to PSLE films in the absence of SP-A. Panel D of figure 23 is a compilation of these results.

3.9 The Effect of C1q on PSLE Monolayers

Pressure-Area isotherms of DPPC and DPPC containing 0.16 $\mu\text{g/mL}$ C1q in the subphase are shown in figure 24 (panel A). The monolayers were compressed rapidly to $\sim 10 \text{ mN/m}$, expanded to 0 mN/m , then allowed to equilibrate for one hour. After this period, the monolayers were compressed at a fast rate (4 $\text{\AA}^2/\text{molecule/second}$). Monolayers of DPPC lift-off at $\sim 100 \text{ \AA}^2/\text{phospholipid molecule}$. The isotherm depicted an LE/LC phase transition at $\sim 7 \text{ mN/m}$, and further compression resulted in monolayer collapse at 70 mN/m . Extensive studies have been performed on monolayers of DPPC, and the results shown correlate with

Figure 23. The %dark area of PSLE (hollow symbol) and PSLE containing 0.16 $\mu\text{g/mL}$ SP-A (filled symbol) with 0 (A), 1.64 (B) and 5 mM Ca^{2+} (C), with a compilation of data shown in panel D (○ ; PSLE, ●; PSLE + 0.16 $\mu\text{g/mL}$ SP-A, ▽ ; PSLE + 1.64 mM Ca^{2+} , ▼ ; PSLE + 0.16 $\mu\text{g/mL}$ + 1.64 mM Ca^{2+} , □ ; PSLE + 5 mM Ca^{2+} , ■ ; PSLE + 0.16 $\mu\text{g/mL}$ SP-A + 5 mM Ca^{2+}). Error bars indicate \pm one standard deviation.

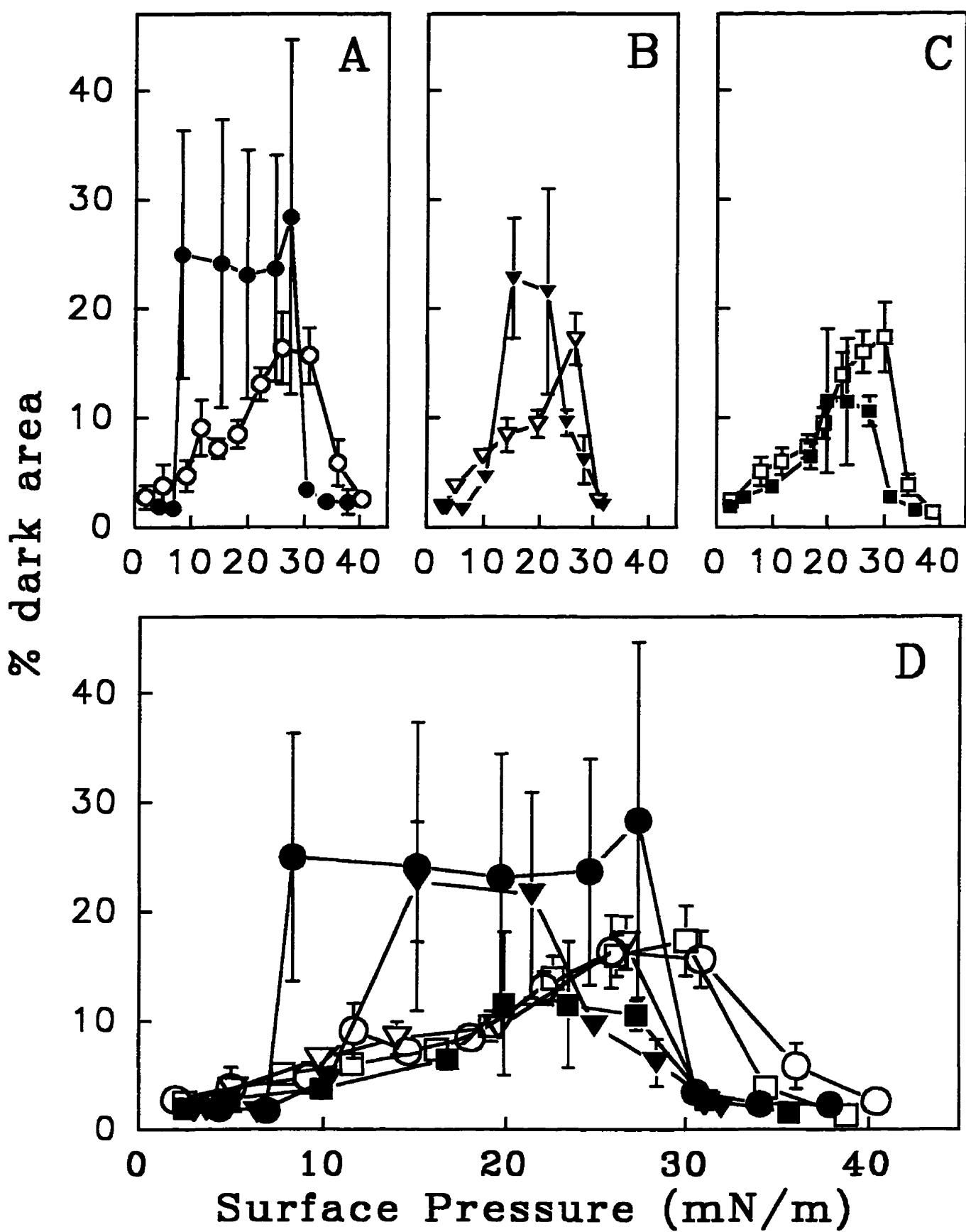
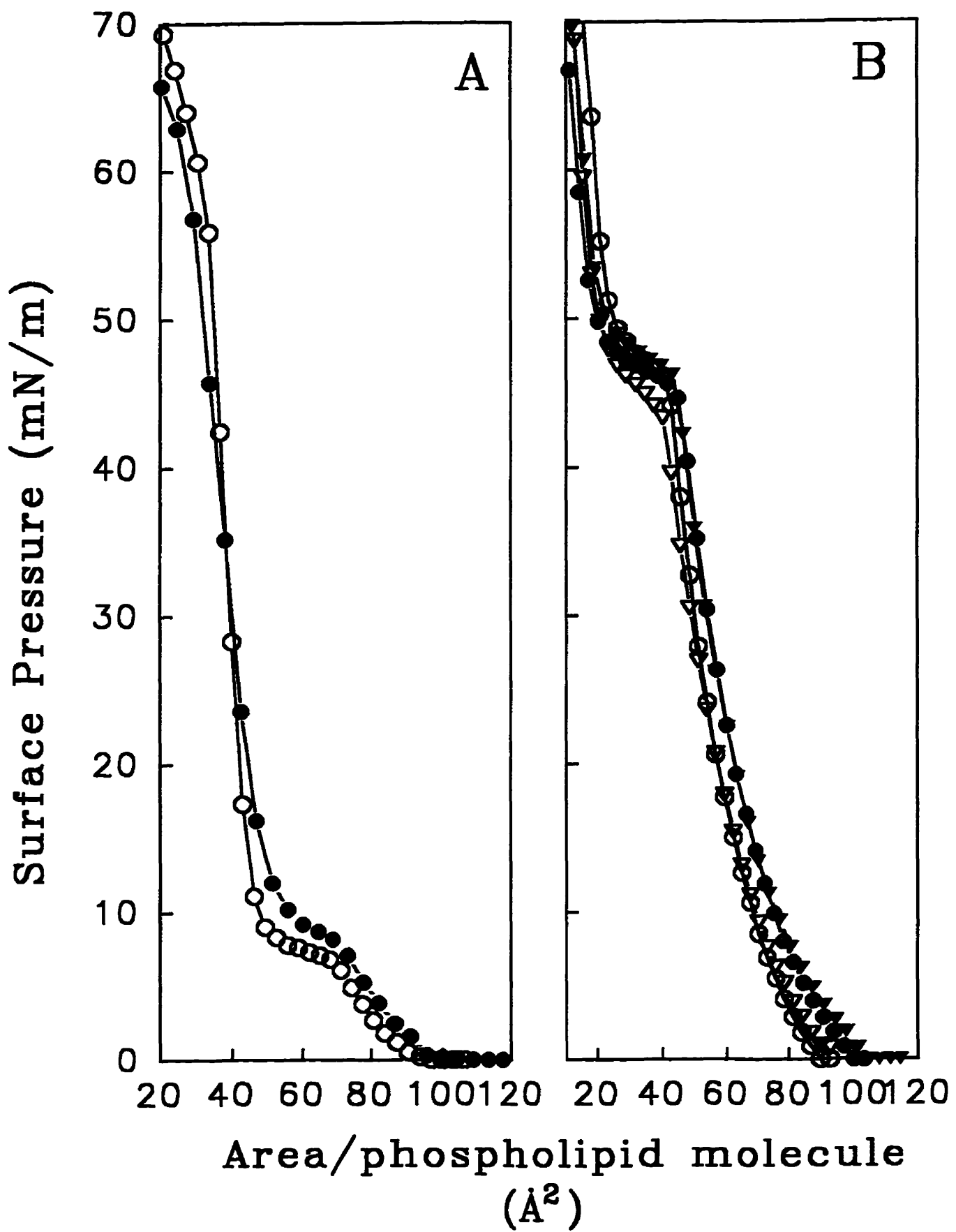


Figure 24. Pressure-Area isotherms of A) DPPC (○) and DPPC spread on a subphase containing 0.16 $\mu\text{g/mL}$ C1q (●), as well as B) PSLE (○) and PSLE on subphases containing 0.16 $\mu\text{g/mL}$ C1q (●), 1.64 mM Ca^{2+} (▽) and 0.16 $\mu\text{g/mL}$ C1q + 1.64 mM Ca^{2+} (▼). The monolayers were compressed in steps at a rate of 4 $\text{\AA}^2/\text{molecule/second}$ on a subphase of 145 mM NaCl, 5 mM Tris (pH 6.9). The subphase temperature was 21 \pm 2 °C.



others (Cadenhead et al., 1980; Lund-Katz et. al., 1988; Phillips and Chapman, 1968). The addition of C1q to the subphase did not seem to affect DPPC isothermal lift-off, but with increased π the isotherm was somewhat expanded and the LE/LC phase transition occurred at slightly higher π (~ 9 mN/m).

Pressure-Area isotherms (panel B) of PSLE, and PSLE spread over subphases containing 1.64 mM Ca^{2+} lift-off at ~ 90 Å²/phospholipid molecule, and inflect at ~ 45 mN/m. The presence of 0.16 µg/mL C1q in the subphase expanded the PSLE monolayer. Yet, increased π resulted in a leftward shift and the isotherm converged upon the PSLE isotherm.

Monolayer surface textures of DPPC films and DPPC + 0.16 µg/mL C1q are shown in figure 25. DPPC (top) at low π (< 7 mN/m) was LE phase as indicated by the homogeneous green fluorescence. At $\pi \sim 7$ mN/m, tiny nucleation points of probe-excluded LC phase appeared, and these domains grew in size with increased π . Large, kidney bean domains, characteristic of DPPC monolayers were observed at ~ 16 mN/m and these LC domains came closer together at ~ 20 mN/m (Nag et al., 1991; von Tscharner and McConnell, 1981). With the addition of C1q to the subphase, the surface film showed disorganized aggregates along side the LC domains. The shape of the kidney bean domains did not seem to be affected by the presence of C1q.

The effect of C1q on DPPC domain size distribution and %dark area is shown in figure 26. C1q did not appear to disturb DPPC domain size distribution (top). At ~ 9 mN/m, the LC domains were small and numerous, but the domains grew in size

Figure 25. Monolayer surface morphology of DPPC (top) and DPPC spread over C1q at a subphase concentration of $0.16 \mu\text{g/mL}$ (bottom). The green background indicates the phase occupied by the fluorescent probe NBD-PC. Monolayers of DPPC were compressed incrementally at a slow rate ($0.0089 \text{ \AA}^2/\text{molecule/s}$) and the images collected are accompanied with corresponding isotherms and surface pressures. The images were collected using a black and white CCD camera and are shown in false color to convey the impression given during direct observation. The scale bar is $50 \mu\text{m}$.

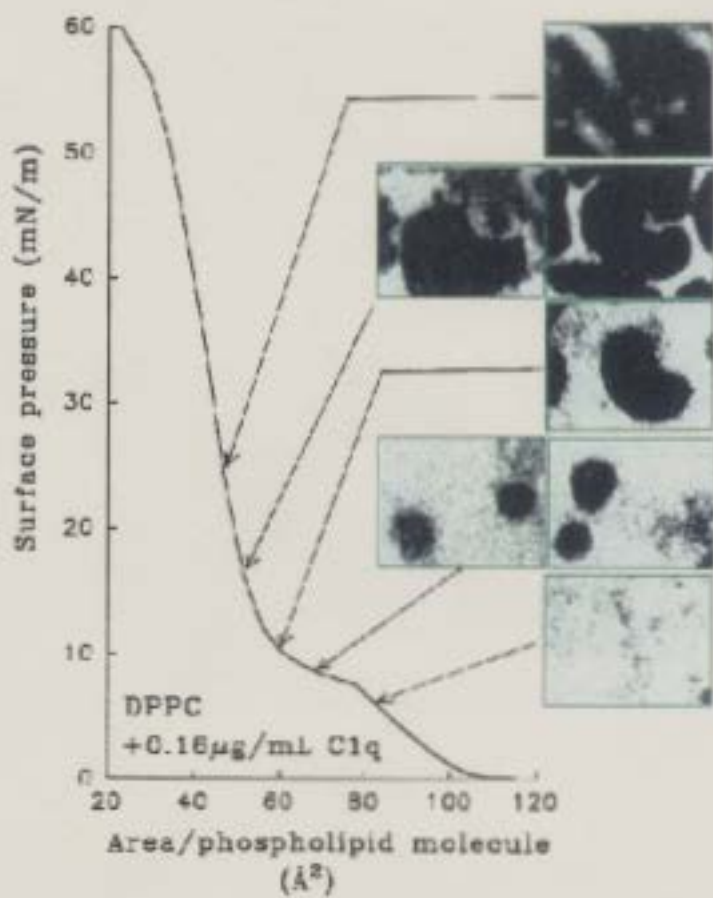
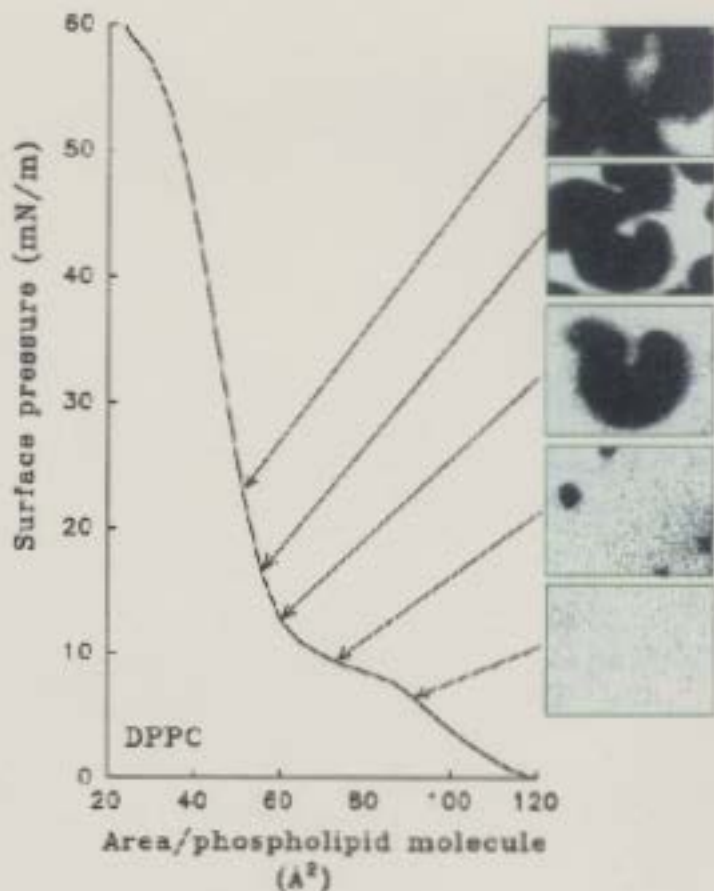
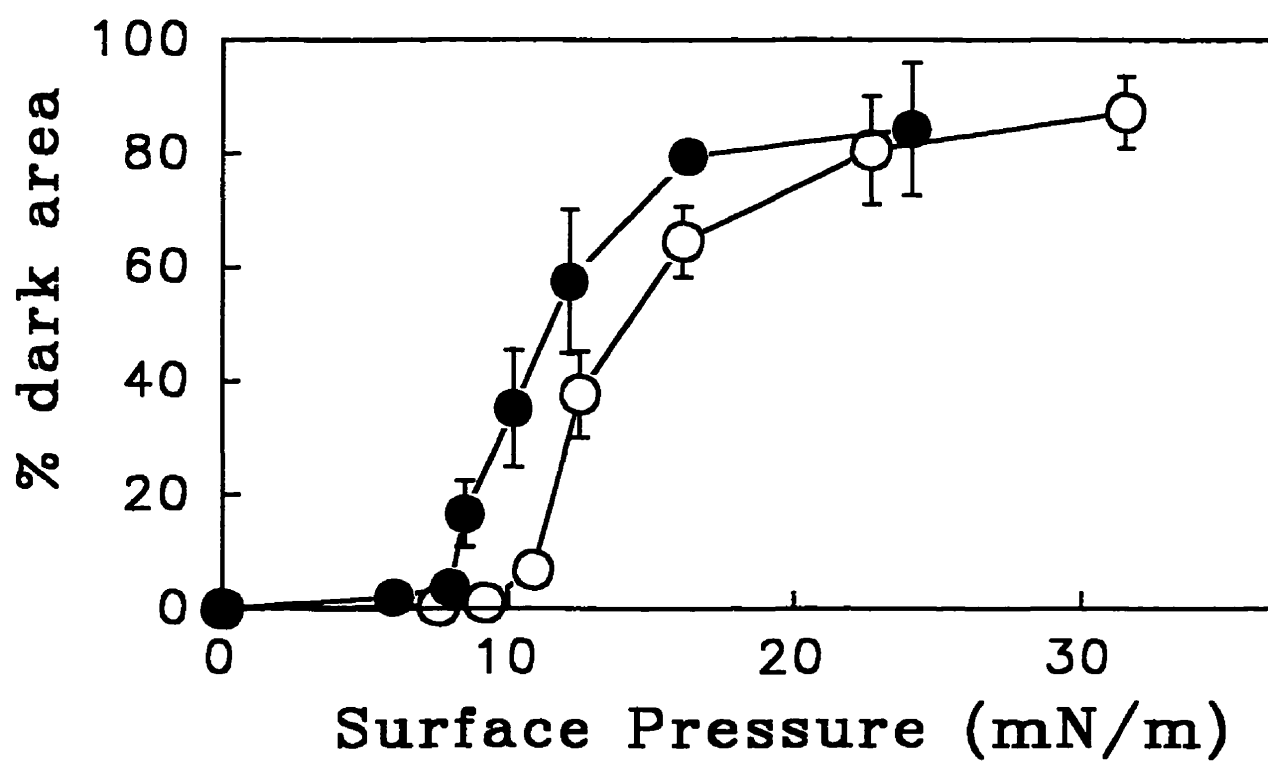
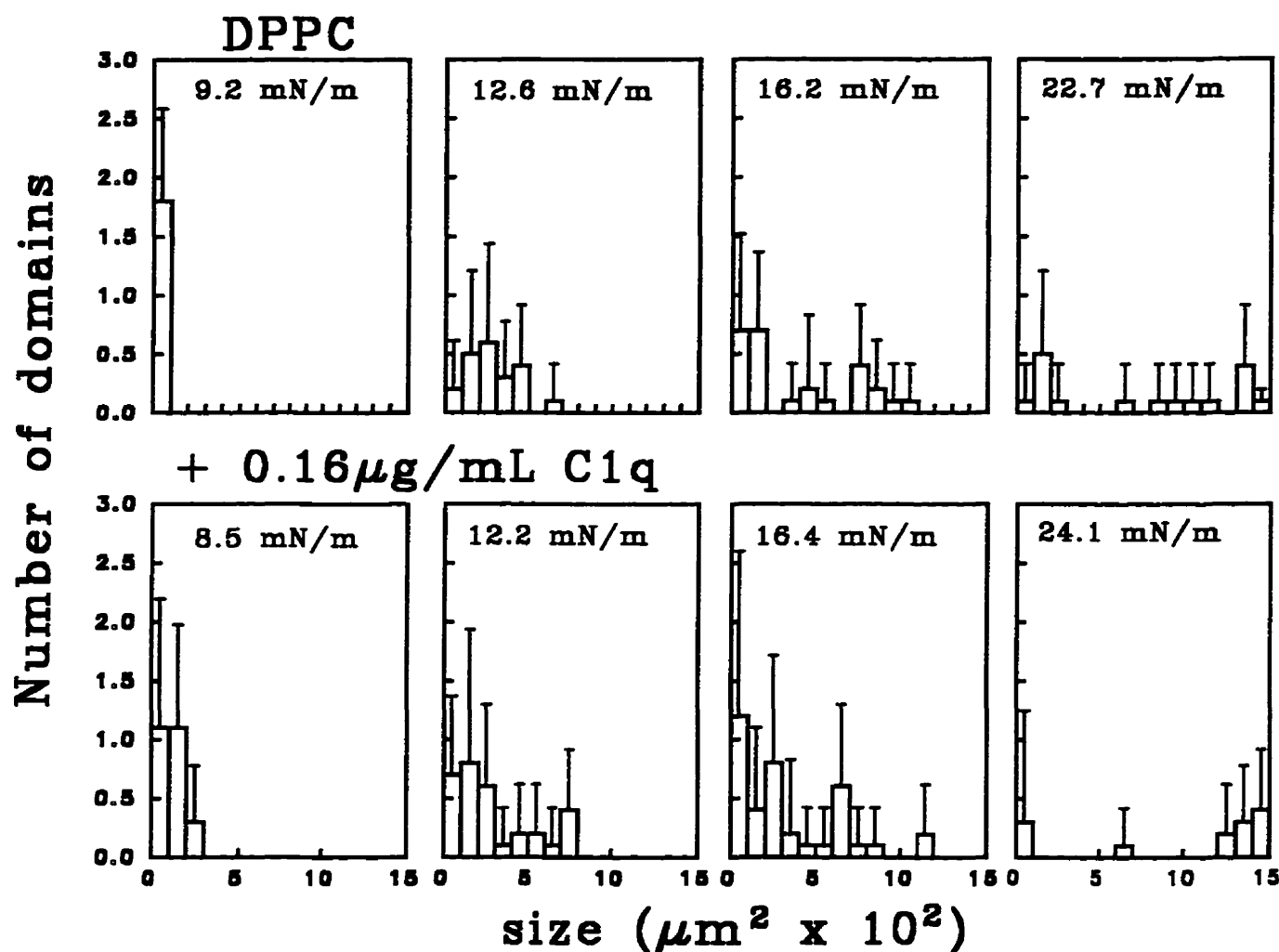


Figure 26. The frequency size distribution (top) and %dark area (bottom) of DPPC films (○) and DPPC spread over a subphase containing 0.16 $\mu\text{g/mL}$ C1q (●). At a particular π , the average number and size of dark domains was determined for each of the 10 frames. The surface pressure is indicated for each distribution shown. Areas $< 3 \mu\text{m}^2$ were not included in the data. Error bars indicate \pm one standard deviation for 10 frames analyzed at each π . Error bars not visualized are within the size limits of the symbol.



with increased π . At ~ 23 mN/m, domains were as large as $1400\text{-}1500 \mu\text{m}^2$.

Monolayers of DPPC had attained 85% dark area (see bottom, figure 26) at π of 20 mN/m in the presence or absence of C1q, but lower π was required to reach this area in the presence of C1q.

Monolayer surface textures of PSLE containing $0.16 \mu\text{g/mL}$ C1q in the subphase with or without 1.64 mM Ca^{2+} are shown in figure 27. Smaller domains were observed in PSLE monolayers in the presence of C1q (top), yet portions of the monolayer fields showed regions of aggregation not unlike PSLE in the presence of SP-A. A reorganization of dark domains into a "network" was noted in monolayer fields, however this network was not as extensive as those observed in the presence of SP-A. Increasing π to > 30 mN/m resulted in a change in the appearance of monolayer surface texture. The network was no longer observed, and tiny circular domains were visualized. The addition of 1.64 mM Ca^{2+} along with C1q (bottom), resulted in an enhancement in the observed "network". Closer examination between monolayer surface textures of PSLE in the presence of 1.64 mM Ca^{2+} with $0.16 \mu\text{g/mL}$ SP-A (top) or C1q (bottom) at ~ 20 mN/m show very similar images (figure 28).

The size frequency distribution of PSLE and $0.16 \mu\text{g/mL}$ C1q in absence (A) or presence (B) of 1.64 mM Ca^{2+} is shown in figure 29. The size distribution of domains were very similar. At ~ 10 mN/m, the domains were small, yet increased π resulted in a broader size distribution. Domains were as large as $100\text{-}200 \mu\text{m}^2$ till π of 30 mN/m. Beyond this π , domain size was reduced.

Figure 27. Monolayer surface morphology of PSLE containing $0.16 \mu\text{g/mL}$ C1q in the absence (top) and presence (bottom) of 1.64 mM Ca^{2+} . The green background indicates the phase occupied by the fluorescent probe NBD-PC. Monolayer images are accompanied with corresponding isotherms and surface pressures. The images were collected using a black and white CCD camera and are shown in false color to convey the impression given during direct observation. The scale bar is $50 \mu\text{m}$.

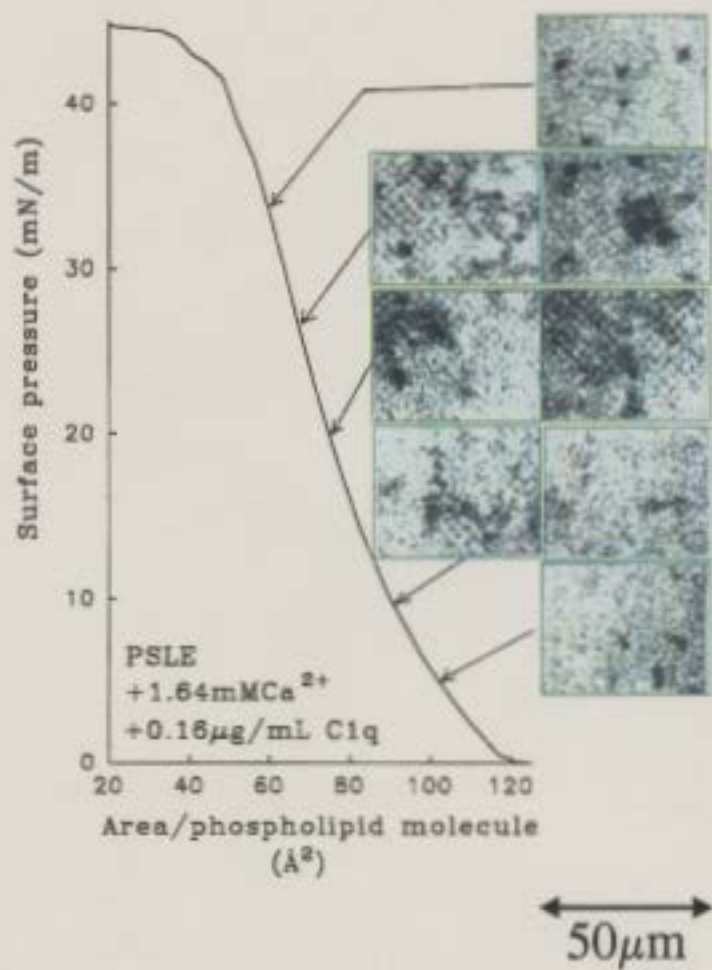
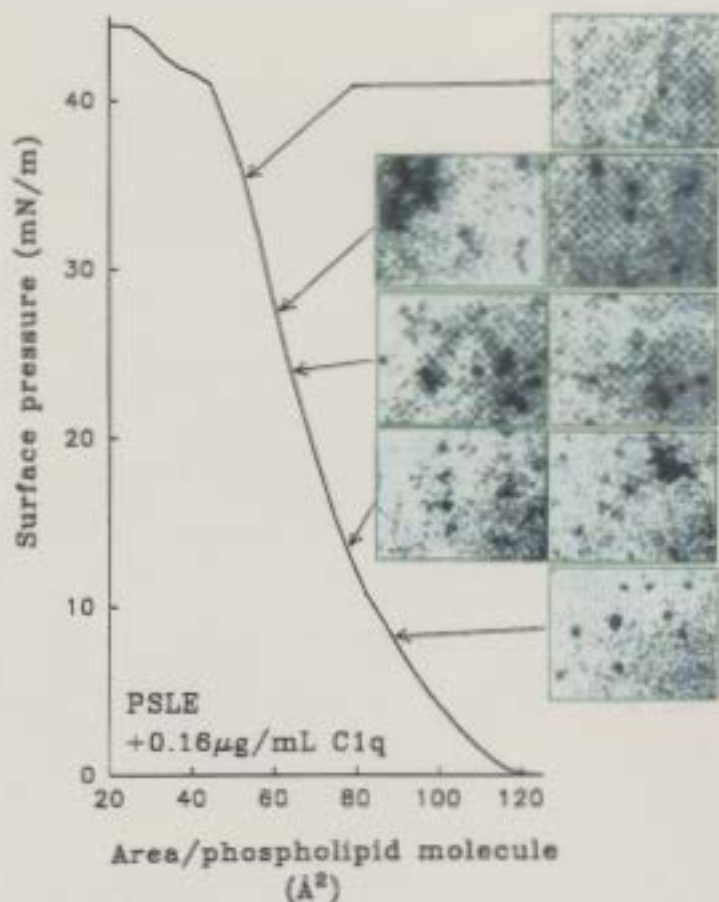
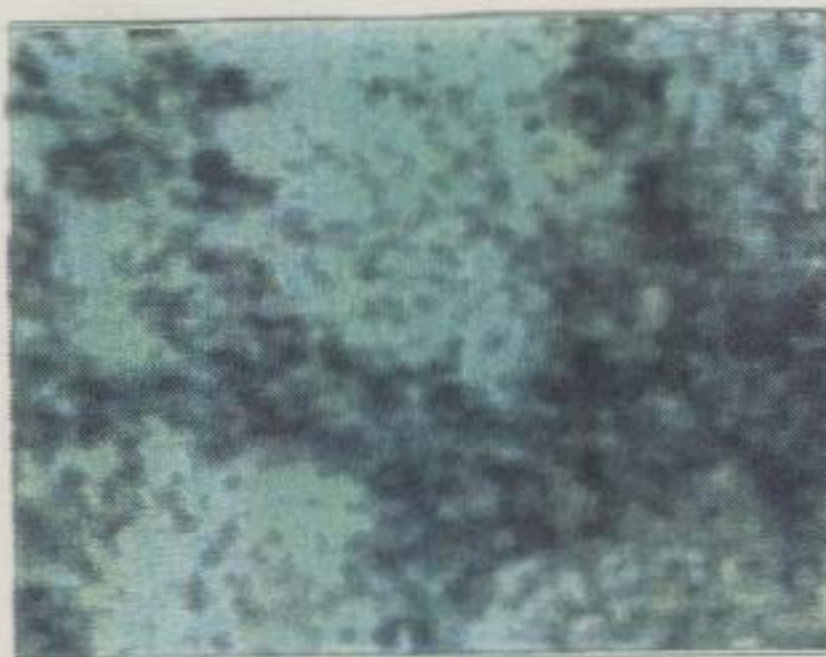


Figure 28. Monolayer surface morphology of PSLE containing $0.16 \mu\text{g/ml}$ SP-A (top) and C1q (bottom) **with 1.64 mM Ca^{2+}** . The green background indicates the phase occupied by the fluorescent probe NBD-PC. The images were collected using a black and white CCD camera and are shown in false color to convey the impression given during direct observation. The scale bar is $25 \mu\text{m}$.



PSLE + 1.64 mM Ca²⁺ + 0.16μg/mL SP-A



PSLE + 1.64 mM Ca²⁺ + 0.16μg/mL C1q

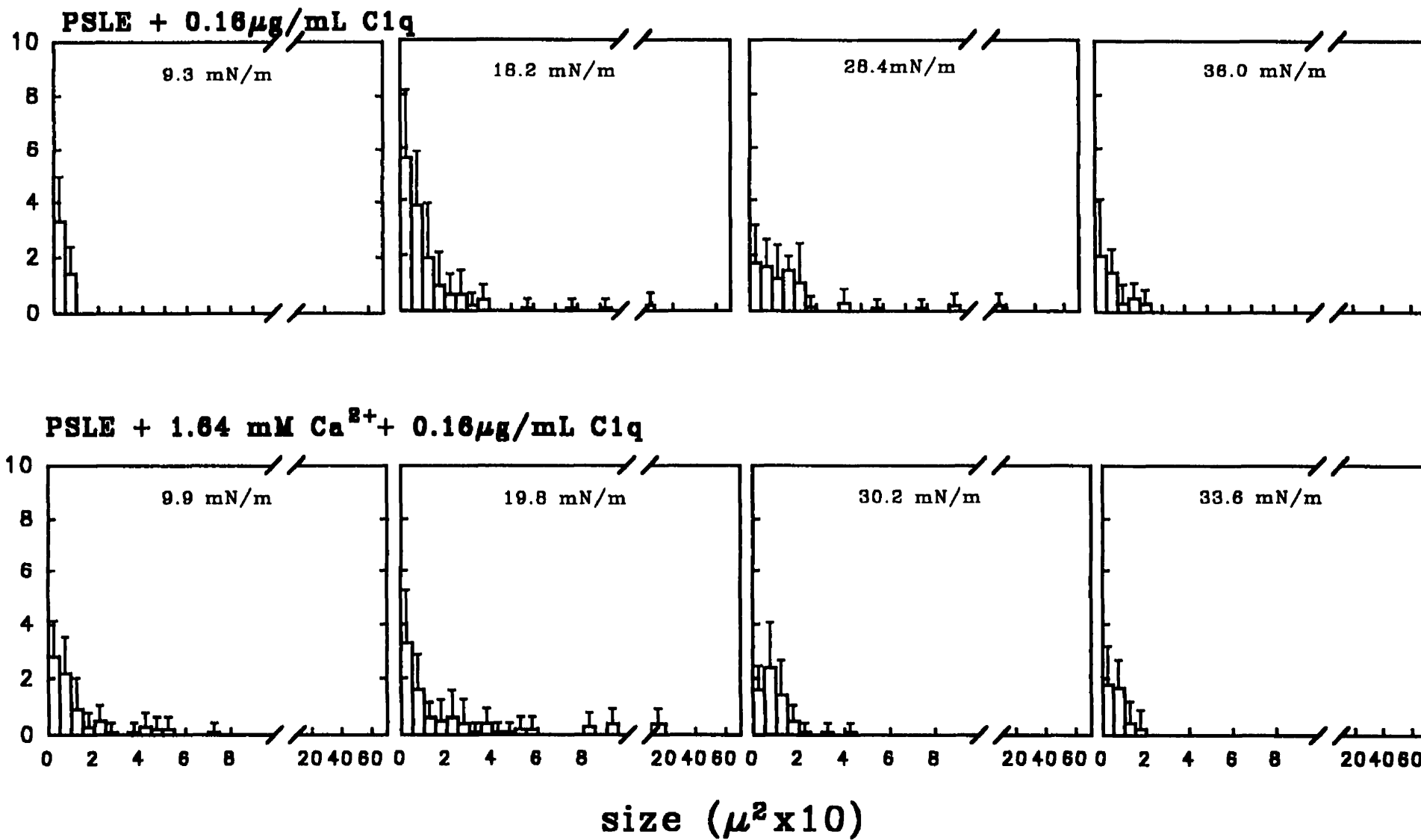
$\pi \sim 20$ mN/m

82

← →
25 μm

Figure 29. The frequency size distribution of PSLE films containing $0.16 \mu\text{g/mL}$ C1q in the absence and presence of 1.64 mM Ca^{2+} . At a particular π , the average number and size of dark domains was determined for each of the 10 frames. The surface pressure is indicated for each distribution shown. Areas $< 3 \mu\text{m}^2$ were not included in the data. Error bars indicate \pm one standard deviation for 10 frames analyzed at each π . Error bars not visualized are within the size limits of the symbol.

Number of domains



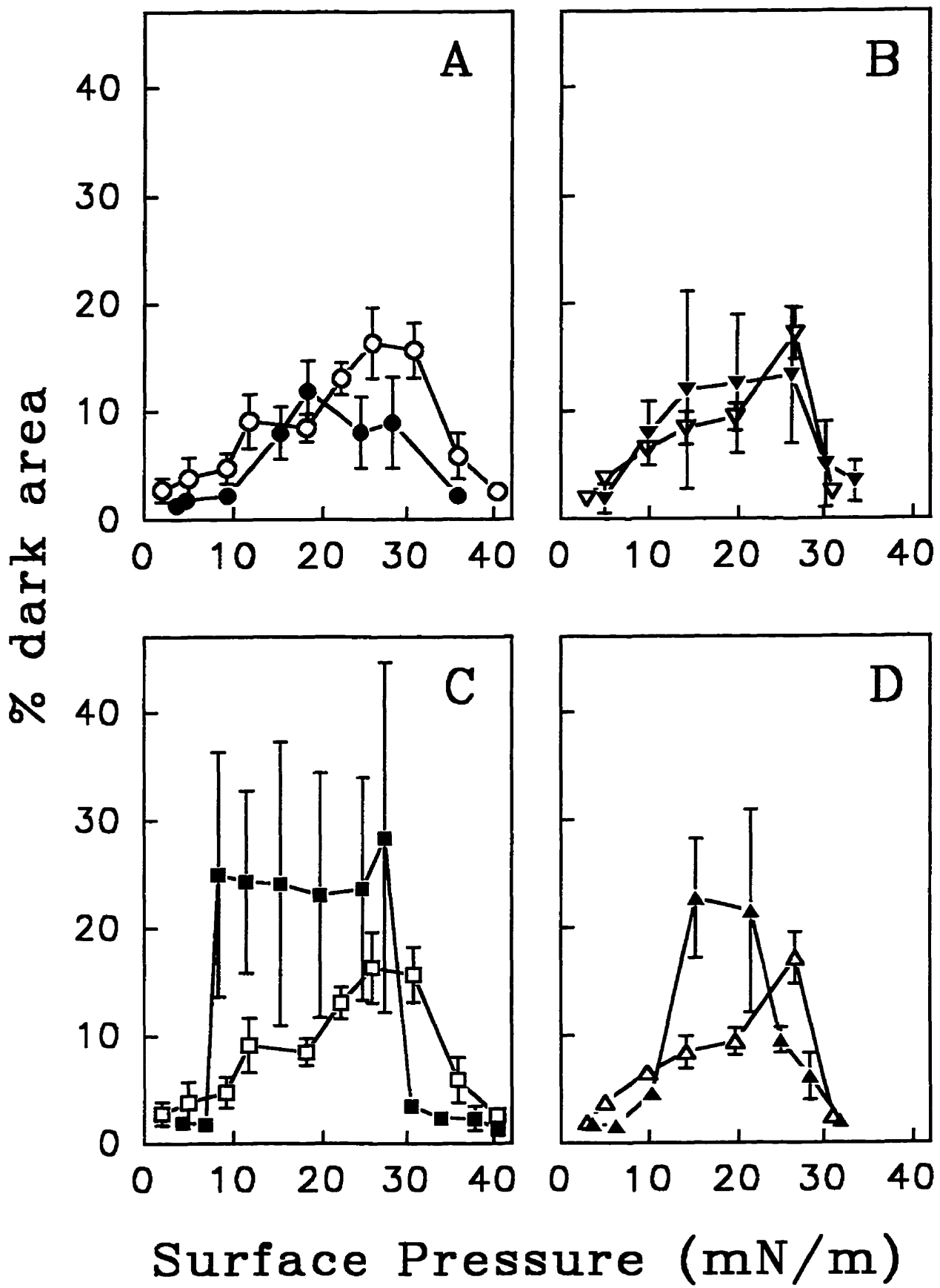
The %dark area of PSLE in the presence of 0.16 $\mu\text{g}/\text{mL}$ C1q or SP-A with or without the addition of 1.64 mM Ca^{2+} are compared in figure 30. The %dark area of PSLE containing 0.16 $\mu\text{g}/\text{mL}$ C1q in the absence (panel A) or presence of 1.64 mM Ca^{2+} (panel B) was decreased from that of PSLE films spread on subphases devoid of C1q. Yet, the %dark area of PSLE monolayers containing 0.16 $\mu\text{g}/\text{mL}$ SP-A in the absence (panel C) and presence of 1.64 mM Ca^{2+} (panel D) was increased from that of PSLE minus SP-A.

3.10 The Role of SP-A in PS Morphology

Electron micrographs (see figure 31) of rat pulmonary surfactant in the presence of 5 mM Ca^{2+} show the square lattice configuration that is a characteristic of tubular myelin. The dimensions of each square of the lattice was about 25 nm in width. Tubular myelin like structures are not observed in pulmonary surfactant that has been lavaged in the absence of Ca^{2+} (Benson et al., 1984).

The role of SP-A in tubular myelin formation was investigated by observing vesicle suspensions of PSLE (no SP-A present) + 5 mM Ca^{2+} by electron microscopy. Multilamellar bodies were observed, but the square lattice configuration typical of tubular myelin was absent (bottom, figure 32). Attempts at reconstituting tubular myelin-like structures from synthetic lipids (DPPC/POPG 7:3) and isolated surfactant proteins A and B in the presence of 5 mM Ca^{2+} were unsuccessful (top, figure 32). However, others have shown that tubular myelin can be synthesized in this manner (Williams et al., 1991; Suzuki et al., 1989).

Figure 30. The %dark area of A: PSLE monolayers (○) and PSLE containing 0.16 $\mu\text{g/mL}$ C1q (●), B: PSLE monolayers with 1.64 mM Ca^{2+} (▽) and PSLE with 1.64 mM Ca^{2+} and 0.16 $\mu\text{g/mL}$ C1q (▼), C: PSLE monolayers (□) and PSLE containing 0.16 $\mu\text{g/mL}$ SP-A (■), D: PSLE monolayers with 1.64 mM Ca^{2+} (△) and PSLE with 1.64 mM Ca^{2+} and 0.16 $\mu\text{g/mL}$ SP-A (▲). Error bars indicate \pm one standard deviation for 10 frames analyzed at each π . Error bars not visualized are within the size limits of the symbol.

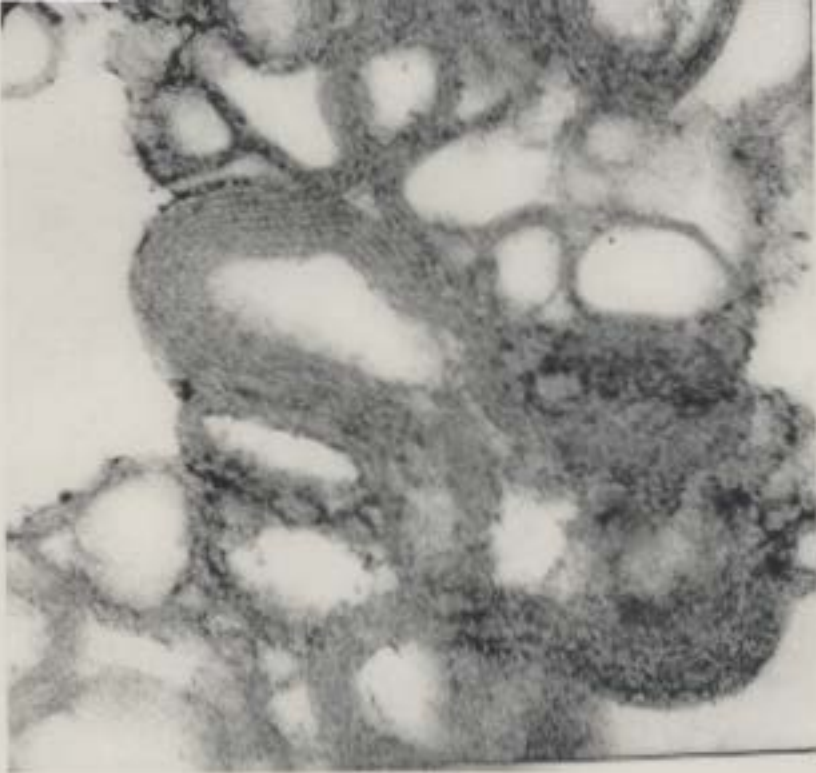




Tubular myelin mag. 11,760 X
(inset mag. 38,808 X)

Figure 31. Electron micrograph of rat pulmonary surfactant isolated in the presence of 5 mM Ca^{2+} . Magnification of micrograph is 11,760 X and the magnification of inset is 38,808 X.

Figure 32. Electron micrograph of PSLE + 5 mM Ca²⁺ vesicles (top) and vesicles of DPPC/POPG 7:3 + 5 wt% SP-A + 5 wt% SP-B + 5 mM Ca²⁺ (bottom). Vesicle preparations were performed by the detergent method (Williams et al., 1991). The magnification of the top and bottom micrographs are 10,300 and 58,000X respectively.



DPPC/POPG(7:3) + 5wt% SP-B + 5wt% SP-A + 5 mM Ca²⁺
mag. 58,000X



PSLE
mag. 10,300X

CHAPTER 4

DISCUSSION

This study focused on the effect of SP-A, a surfactant-associated protein, on pulmonary surfactant morphology and biophysical properties. Epifluorescent microscopy allowed us to directly observe the effects of SP-A on PSLE monolayer morphology, as well as its affect on the biophysical characteristics of the monolayer. Epifluorescence microscopy utilizes the solubility of fluorescent probes in particular phases of the monolayer. For example, the fluorescent lipid probe NBD-PC localizes in a fluid phase due to a bulky NBD group attached to the lipid acyl chain. At surface pressures greater than a few mN/m, any region which excludes this fluorescent probe is likely to be some form of condensed phase. The small amount of probe used in the monolayer does not affect lipid phase transition or surface texture characteristics (Ahlers et al., 1990). When examining lipid-protein interactions in monolayers, it is advantageous to use different fluorescent dyes to label either lipid or protein. For instance, in our study we used the fluorescent lipid NBD-PC and Texas-red labelled SP-A (TR-SP-A). The emission and excitation spectra of these dyes do not overlap, therefore both can be observed simultaneously by switching light filters.

4.1 PSLE Isotherms and the Effect of SP-A

The surface characteristics of PS have been studied extensively as it is directly applicable to the ability of the lung to expand and contract during respiration (Schürch et al., 1992; Wang et al., 1995; Yu and Possmayer, 1993). PSLE monolayers spread onto saline subphases do not experience a classical LE/LC phase transition as seen in monolayers of DPPC (Discher et al., 1996). A highly compressible region is observed at $\pi \sim 45$ mN/m, and it is possible that non-DPPC components are excluded from the monolayers surface at this pressure. At π beyond the compressibility region PSLE monolayers reached π of 70 mN/m. Our experiments were performed at room temperature, and extensive PL monolayer research has shown that only phases rich in DPPC can attain such high π at this temperature (Goerke and Gonzales, 1981; Hawco et al., 1981; Hildebran et al., 1979).

The addition of the water-soluble SP-A resulted in an expansion of the PSLE monolayer. The isothermal lift-off of the monolayers spread over protein was shifted ~ 20 Å²/phospholipid molecule to the right. The expanded state of the PSLE monolayer is indicative of SP-A association with the monolayer surface. It is possible that SP-A may be adsorbing to the air-saline interface, or altering PSLE lipid orientation at the monolayer surface (Heckl et al., 1985; Pérez-Gil et al., 1992; Ruano et al., 1998). Pressure-Area isotherms of PSLE spread over various concentrations of SP-A adopt a profile similar to that of PSLE in the absence of protein with increased π . This may be a consequence of the squeezing out of SP-A from the monolayer surface (Ruano et al., 1998; Taneva et al., 1995).

PSLE monolayers spread over subphases containing 5 mM Ca²⁺ were not significantly different from monolayers spread over subphases devoid of Ca²⁺. The addition of various concentrations of SP-A to the subphase expanded the monolayer at low π and compression resulted in a decrease of phospholipid molecular area indicative of protein exclusion from the surface (Ruano et al., 1998; Taneva et al., 1995). Ca²⁺ may enhance the ability of SP-A to mix with monolayer films containing PG (Taneva et al., 1995).

4.2 PSLE Surface Texture and Reorganization due to SP-A

The surface textures observed in monolayers of PSLE as visualized with the addition of NBD-PC indicate a phase partitioning at relatively low π . The observation of probe-excluded domains between π range 5-30 mN/m suggests that these domains represent a relatively dense, ordered phase. Yet the lack of phase transition over this π range in the isotherm suggests the possibility that the ordered phase might not be liquid-condensed (LC) normally viewed in monolayers of pure lipid such as DPPC (Discher et al., 1996; Nag et al., 1998). Others have noted that the amount of ordered, probe-excluding phase recorded in the calf lung PSLE monolayers corresponds to the amount of DPPC in this compound (Discher et al., 1996). It must be remembered that PSLE is a heterogenous mixture of lipid and hydrophobic lung proteins (SP-B and SP-C), and varying lipid and protein components may affect the apparent density of these "DPPC-rich" regions. At $\pi > 35$ mN/m, the dark domains decrease in size. This occurrence has been recorded in

PSLE monolayers visualized by brewster angle microscopy (BAM)(Discher et al., 1996), thus arguing against the possibility that unfavourable interactions with the fluorescent probe cause this change in monolayer surface texture. It has been suggested that high π may result in an increase in density of the molecules in the fluid phase (probe-rich region) and the density of the phase where the probe was localized acquires similar density as that of the probe-excluded region (Discher et al., 1996). As a consequence, the two phases are nearly indistinguishable with the fluorescent lipid probe. Observation of the PSLE monolayers using a higher magnification lens revealed an increase in the number of small dark domains at high π , but this increase did not account for the overall decrease in PSLE dark area recorded at the monolayer surface.

The presence of SP-A in the subphase altered PSLE phase organization in a concentration dependent manner. The presence of 0.13 $\mu\text{g/mL}$ SP-A did not change the general appearance of PSLE monolayer surface texture, yet 0.16 and 0.20 $\mu\text{g/mL}$ SP-A had a more substantial effect on monolayer organization. It might be proposed that this protein concentration dependent means of lipid-protein association may be consequence of SP-A self-association and aggregation. A threshold SP-A concentration may be necessary to initiate lipid aggregation and reorganization. However, half-maximal self-association and aggregation of porcine SP-A require at least 2.36 mM Ca^{2+} , and lipid aggregation is not dependent on Ca^{2+} concentration (Ruano et al., 1996). The overall size and relative amount of dark domains in PSLE monolayers spread over subphases containing 0.13 $\mu\text{g/mL}$ SP-A and in the absence of

Ca^{2+} were not significantly different than those of PSLE alone. The reorganization of dark domains in the presence of higher concentrations of SP-A (0.16 and 0.20 $\mu\text{g/mL}$) may be a consequence of specific interactions of SP-A with the ordered phase lipids, particularly DPPC (Casals et al., 1993; Akino and Kuroki, 1991) of the dark domains. The increase in dark phase in PSLE monolayers spread over subphases containing 0.16 and 0.20 $\mu\text{g/mL}$ SP-A suggests a possible lipid-protein interaction. As judged by eye, the intensity of the probe-excluded domains found in PSLE films was not as dark as those observed in the absence of protein in the subphase, suggesting some localization of lipid probe in these areas. SP-A might selectively bind and disrupt ordered phase lipid, thereby expanding the lipid molecules in this region. Thus the apparent increase in dark area reported in PSLE films spread over subphases containing 0.16 and 0.20 $\mu\text{g/mL}$ SP-A may be a consequence of expanding lipid molecular packing in the condensed phase, and not an increase in the total number of condensed phase lipids.

The use of fluorescently labelled SP-A enabled the direct visualization of the proteins association with lipids in PSLE monolayers. The location of the fluorescently labelled protein corresponds with the location of the dark domains observed when the fluorescent lipid probe was used as the reporter molecule. SP-A preferentially absorbs to, or near the surface of, the monolayer at the ordered phase regions. Recent studies involving DPPC monolayers spread over subphases containing SP-A have shown that the protein expands the area occupied by the monolayer. In addition, epifluorescent studies involving the interaction of SP-A with

monolayers of DPPC have shown that SP-A localizes at the LC/LE boundaries in those monolayers and decreases the size of the LC domains (Ruano et al., 1998). Some insight into specific protein interactions may be gained if one analyses the results obtained by Grainger and colleagues (1990) involving the interaction of phospholipase A₂ with monolayers of DPPC. Phospholipase A₂ hydrolysed monolayers of DPPC by specifically interacting with the LC/LE boundaries, and then unravelling the condensed domains. After a period of incubation, phospholipase A₂ was able to aggregate and form domains of pure protein at the film surface. However, in our study the apparent localization of fluorescent lipid probe in the previously dark regions as viewed by lipid probe fluorescence may suggest that the corresponding TR-SP-A fluorescent domains are not pure protein domains, but a mixture of ordered phase lipid and protein. In the case of pure DPPC monolayers, the increased order and density of the lipids in LC domains does not promote specific lipid-protein interaction with the domain interior, and this may explain the localization of SP-A at the boundaries of such domains. In monolayers of PSLE, the decreased order of lipids in the dark domain may allow the partial insertion of SP-A into the dark domain interior. The decrease in protein fluorescence at π beyond 30 mN/m offers evidence of the exclusion of SP-A from the film surface.

SP-A is soluble in its native octadecameric form at low ionic strength and physiological pH, but it aggregates and undergoes a slight conformational change at physiological concentrations of Ca²⁺ and saline solutions (Haagsman et al., 1990). At physiological pH and Ca²⁺ concentration, SP-A may aggregate near the ordered phase

lipids on the surface and the close proximity of the aggregated SP-A might disturb the orientation and density of the ordered phase lipids in these regions. Monolayer surface texture of PSLE films spread on subphases containing varying concentrations of SP-A and 5 mM Ca^{2+} are not significantly different from PSLE monolayers in the presence of 5 mM Ca^{2+} . However, isotherms of PSLE monolayers spread over subphases containing SP-A and 5 mM Ca^{2+} indicate that the protein is inserting into the monolayer, or absorbing close to the surface and perturbing lipid molecules. The appearance of the dark domains in monolayers of PSLE seem smaller in the presence of both SP-A and Ca^{2+} than in the presence of Ca^{2+} alone. This slight decrease in size of the dark domains may be a consequence of SP-A association with lipids at the ordered/fluid phase boundaries (Ruano et al., 1998). Aggregated SP-A may be too large to allow partial insertion and association with ordered phase lipids in the dark domain interior as observed in PSLE monolayers at lower Ca^{2+} concentrations.

Using fluorescently labelled SP-A, it was observed that in the presence of 5 mM Ca^{2+} , SP-A aggregated in the fluid phase and fluid/gel phase boundaries of the monolayer. The addition of 5 mM Ca^{2+} and varying concentrations of SP-A in the subphase caused a slight decrease in the total area of dark domains as visualized using a fluorescent lipid reporter molecule. The reduction of dark area implies an interaction between SP-A and ordered lipid at domain boundaries. The lipid at the ordered/fluid phase boundaries might be disrupted and fluidized due to the SP-A in the vicinity and this would account for the decrease in dark area recorded. The cation Ca^{2+} might localize in the area occupied by the anionic fluid-phase lipids, such as PG.

The PG content of PS is about 10 wt%, but the localization of PG in the fluid regions of the monolayer may increase the negatively charged environment of this phase. The ionic interaction between Ca^{2+} and PG would dissipate the charge of the fluid environment in the monolayer and allow the insertion of the acidic protein into the normally acidic fluid phase. An increase in fluorescence of the labelled protein in the fluid phase was observed at high π ($> 25 \text{ mN/m}$), but beyond 35 mN/m monolayer fields randomly showed fluorescent aggregates of protein consistent with the exclusion of the protein from the monolayer at higher π .

The presence of Ca^{2+} at a concentration of 1.64 mM is of interest for it best represents the hypophase environment that bathes the epithelial lining of the lung (Nielsen et al., 1981). Isotherms of PSLE spread on subphases containing 1.64 mM Ca^{2+} in the absence or presence of $0.16 \mu\text{g/mL}$ SP-A shared characteristics with PSLE isotherms observed in the presence or absence of 5 mM Ca^{2+} . PSLE monolayer surface textures in the absence of SP-A were not altered by the addition of Ca^{2+} to the subphase. However, the presence of SP-A and 1.64 mM Ca^{2+} showed monolayer surface texture characteristics observed in PSLE films spread over both 0 and 5 mM Ca^{2+} with SP-A. Previous studies have shown that the half-maximal self-association of porcine SP-A requires 2.36 mM Ca^{2+} (Ruano et al., 1996), hence at Ca^{2+} subphase concentrations of 1.64 mM there may not be a complete self-aggregation of the SP-A molecules. With subphases containing 1.64 mM Ca^{2+} , individual SP-A molecules may aggregate and reorganize lipid domains, while aggregated SP-A will localize in the fluid phase and at the fluid/gel phase boundaries.

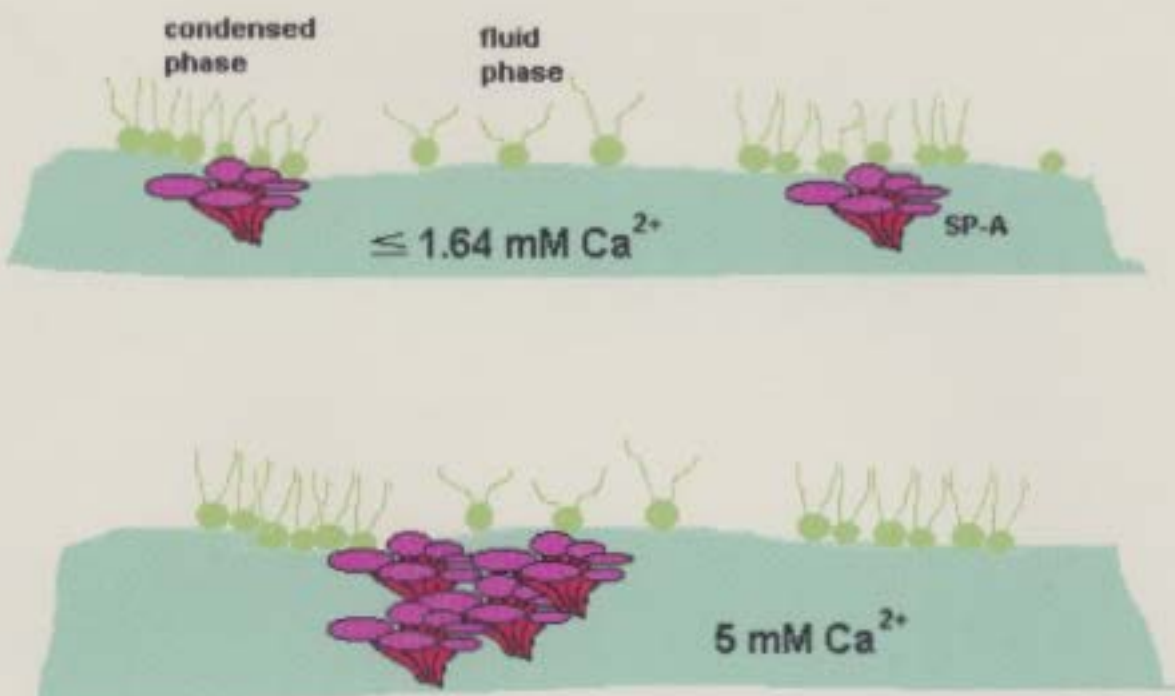


Figure 33. A schematic diagram of SP-A associations in monolayers of PSLE spread on subphases containing $\leq 1.64 \text{ mM}$ or $5 \text{ mM } \text{Ca}^{2+}$.

Figure 33 illustrates a potential mechanism for SP-A association with lipids in monolayers of PSLE spread over subphases containing either \leq 1.64 mM or 5 mM Ca^{2+} .

4.3 SP-A Oligomeric Structure and PS Interaction

The effect of SP-A tertiary structure on PSLE films was studied by comparing SP-A with its structural homolog, C1q. DPPC, a major lipid component of PSLE was used as a control to determine specific interactions of this protein with phospholipid. Isotherms of DPPC monolayers spread over subphases containing 0.16 $\mu\text{g/mL}$ C1q were slightly expanded, thus indicating an insertion of the protein at the monolayer surface. Images of DPPC monolayers spread over subphases containing the protein revealed large kidney-bean shaped domains of LC phase. Evidence of C1q at the monolayer surface was provided by visualization of disorganized aggregates amidst the LE phase. The LC domains of DPPC retained original size and shape, despite the inclusion of the protein into the subphase. This suggests that C1q was not disturbing the organization of the LC phase lipid molecules on the surface.

The effect of C1q on spread monolayers of PSLE was more pronounced. With the aide of a fluorescent lipid probe as a reporter molecule, dark domains were visualized which had different organization than PSLE dark domains in the absence of C1q. The reorganization of these domains imply that some association is occurring between the PSLE lipids and the C1q molecules at or near the surface of the film. The dark domains reorganized into a "loose network" not unlike that observed in

PSLE films spread over subphases containing 0.16 µg/mL SP-A. However, the total amount of dark area recorded at the monolayer surface was less than in the PSLE monolayers spread over subphases containing SP-A.

The flower-like oligomeric structure of SP-A may be important for lipid-protein interactions in monolayers of PSLE. It has been proposed that the neck region of SP-A monomers may be important for SP-A folding (Kuroki et al., 1994), and mutation studies have shown that this region is important for SP-A-lipid interactions (McCormack et al., 1994). The diminished interaction of mutant SP-A with PS lipid may be consequence of SP-A unfolding, providing an indication that the oligomeric structure of SP-A is responsible for an aspect of SP-A interaction with PS lipid. In this way, the oligomeric structure of C1q may be responsible for the lipid-protein interaction in films of PSLE.

4.4 Conclusions and Future Directions

SP-A, a large, hydrophobic surfactant associated protein, plays many roles in the normal functioning of pulmonary surfactant. This study focused on the morphological and biophysical contributions of SP-A in PS function. Previous biophysical studies have been inconclusive in their findings as to the exact role of SP-A in PS adsorption. We have proposed that SP-A may cause a reorganization of ordered phase domains at the air-saline interface. It might be implied that SP-A sorts PS material and stabilizes PS monolayers. Furthermore, SP-A may allow for the selective exclusion of non-DPPC components from the surface. The oligomeric

structure of SP-A may be partly responsible for the lipid recognition and subsequent interaction at the air-saline interface.

Future experiments utilizing recombinant mutants of SP-A may offer insights into the specific regions of this protein required for lipid-protein interactions at the air-saline interface. Furthermore, reconstitution of tubular myelin using these recombinant mutants might prove helpful in discerning the question of specific lipid-protein interactions.

References

- Ahlers, M., W. Müller, A. Reichert, H. Ringsdorf, and J. Venzmer. 1990. Specific interactions of proteins with functional lipid monolayers- ways of simulating biomembrane processes. *Angew. Chem. Int. Ed. Engl.* **29**:1269-1285.
- Albrecht, O., H. Gruler, and E. Sackmann. 1981. Pressure-composition phase diagrams of cholesterol/lecithin, cholesterol/phosphatidic acid, and lecithin/phosphatidic acid mixed monolayers: a langmuir film balance study. *J. Colloid Inter. Sci.* **79**:319-338.
- Beers, M. F., and A. B. Fisher. 1992. Surfactant protein C: a review of its unique properties and metabolism. *Am. J. Physiol.* **263**:L151-160
- Benson, B. J., M. C. Williams, K. Sueishi, J. Goerke, and T Sargeant. 1984. Role of calcium ions in the structure and function of pulmonary surfactant. *Biochim. Biophys. Acta* **793**:18-27.
- Bligh, E., and W. Dyer. 1959. A rapid method of total lipid extraction and purification. *Can. J. Biochem. Physiol.* **37**:911-917.

Cadenhead, D. A. 1985 Monomolecular films as biomembrane models. In *Structure and Properties of Cell Membranes*, Vol 3. G. Benga, editor. CRC Press. Boca Raton, FL. 21-62.

Cadenhead, D. A., F. Müller-Landau, and B. M. J. Kellner. 1980. In *Ordering in two Dimensions*. Elsevier North Holland, Inc. 73-81.

Casals, C., E. Miguel, and J. Perez-Gil. 1993. Tryptophan fluorescence study on the interaction of pulmonary surfactant protein A with phospholipid vesicles. *Biochem. J.* **296**:585-593.

Chung, J., S-H. Yu, J. A. Whitsett, P. G. R. Harding, and F. Possmayer. 1989. Effect of surfactant-associated protein A (SP-A) on the activity of lipid extract surfactant. *Biochim. Biophys. Acta* **1002**:348-358.

Discher, B. M., K. M. Maloney, W. R. Schief, Jr., D. W. Grainger, V. Vogel, and S. B. Hall. 1996. Lateral phase separation in interfacial films of pulmonary surfactant. *Biophys. J.* **71**:2583-2590.

Dobbs, L. G. 1989. Pulmonary surfactant. *Ann. Rev. Med.* **40**:431-446.

- Dobbs, L. G., J. R. Wright, S. Hawgood, R. Gonzales, K., Venstrom, and J. Nellenbogen. 1987. Pulmonary surfactant and its components inhibit secretion of phosphatidylcholine from cultured rat alveolar type II cells. *Proc. Natl. Acad. Sci. USA* **84**:1010-1014.
- Fleming, B. D., and K. M. W. Keough. 1988. Surface resspreading after collapse of monolayers containing major lipids of pulmonary surfactant. *Chem. Phys. Lipids* **49**:81-86.
- Froh, D., P. L. Ballard, M. C. Williams, J. Gonzales, J. Goerke, M. W. Odom, and L. W. Gonzales. 1990. Lamellar bodies of cultured human fetal lung: content of surfactant protein A (SP-A), surface film formation and structural transformation in vitro. *Biochim. Biophys. Acta* **1052**:78-89.
- Gaines, G. L. 1966. *In* Insoluble Monolayers at the Liquid-Gas Interface. Wiley Interscience. New York.
- Goerke, J., and J. Gonzales. 1981. Temperature dependence of dipalmitoyl phosphatidylcholine monolayer stability. *J. Appl. Physiol.: Respirat. Environ. Exercise Physiol.* **51**:1108-1114.

Grainger, D. W., A. Reichert, H. Ringsdorf, and C. Salesse. 1990. Hydrolytic action of phospholipase A₂ in monolayers in the phase transition region: direct observation of enzyme domain formation using fluorescence microscopy. *Biochim. Biophys. Acta* **1023**:365-379.

Haagsman, H. P., S. Hawgood, T. Sargeant, D. Buckley, R. T. White, K. Drickamer, and B. J. Benson. 1987. The major lung surfactant protein, SP 28-36, is a calcium-dependent, carbohydrate-binding protein. *J. Biol. Chem.* **262**:13877-13880.

Haagsman, H. P., R. T. White, J. Schilling, K. Lau, B. J. Benson, J. Golden, S. Hawgood, and J. A. Clements. 1989. Studies of the structure of lung surfactant protein SP-A. *Am J. Physiol.* **257**:L421-L429.

Haagsman, H. P., T. Sargeant, P. V. Hauschka, B. J. Benson, and S. Hawgood. 1990. Binding of calcium to SP-A, a surfactant-associated protein. *Biochemistry* **29**:8894-8900.

Hawco, M. J., P. J. Davis, K. P. Coolbear, and K. M. W. Keough. 1981. Exclusion of fluid lipid during compression of monolayers of mixtures of dipalmitoyl phosphatidylcholine with some other phosphatidylcholines. *Biochim. Biophys. Acta* **646**:185-197.

Hawgood, S. 1989. pulmonary surfactant apoproteins: a review of protein and genomic structure. *Am. J. Physiol.* **257**:L13-L22.

Heckl, W. M., B. N. Zaba, and H. Möhwald. 1987. Interactions of cytochromes *b₅* and *c* with phospholipid monolayers. *Biochim. Biophys. Acta* **903**:166-176.

Hildebran, J. N., J. Goerke, and J. A. Clements. 1979. Pulmonary surface film stability and composition. *J. Appl. Physiol.: Respirat. Environ. Exercise Physiol.* **47**: 604-611.

Jobe, A. H. 1993. Pulmonary surfactant therapy. *N. Eng. J. Med.* **328**:861-867.

Jobe, A. H., and M. Ikegami. 1987. Surfactant in the treatment of respiratory distress syndrome. *Am. Rev. Respir. Dis.* **136**:1256-1275.

Johansson, J., and T. Curstedt. 1997. Molecular structures and interactions of pulmonary surfactant components. *Eur. J. Biochem.* **244**:675-693.

Keough, K. M. W. 1992. Physical chemistry of pulmonary surfactant in terminal air spaces. In *Pulmonary Surfactant: from molecular biology to clinical practice*. B. Robertson, L. M. G. van Golde, and J. J. Batenburg, editors. Elsevier Science Publishers, Amsterdam. 109-164.

- Keough, K. M. W., G. Simatos, J. Pérez-Gil, K. Nag, L. A. Allwood, and M. R. Morrow. 1992. Pulmonary surfactant protein SP-C and phosphatidylcholines in bilayers and monolayers. *Thin Solid films* **210/211**:720-722.
- Keough, K. M. W., and N. Kariel. 1987. Differential scanning calorimetric studies of aqueous dispersions of phosphatidylcholines containing two polyenic chains. *Biochim. Biophys. Acta* **902**:11-18.
- King, R. J., D. Simon, and P. M. Horowitz. 1989. Aspects of secondary and quaternary structure of surfactant protein A from canine lung. *Biochim. Biophys. Acta* **1001**:294-301.
- Korfhagen, T. R., M. D. Bruno, G. F. Ross, K. M. Huelsman, M. Ikegami, A. H. Jobe, S. E. Wert, B. R. Stripp, R. E. Morris, S. W. Glasser, C. J. Bachurski, H. S. Iwamoto, and J. A. Whitsett. 1996. Altered surfactant function and structure in SP-A gene targeted mice. *Proc. Natl. Acad. Sci. USA* **93**:9594-9599.
- Kuroki, Y., and T. Akino. 1991. Pulmonary surfactant protein A (SP-A) specifically binds dipalmitoylphosphatidylcholine. *J. Biol. Chem.* **266**:3068-3073.

- Kuroki, Y., F. X. McCormack, Y. Ogasawara, R. J. Mason, and D. R. Voelker.
1994. Epitope mapping for monoclonal antibodies identifies functional domains
of pulmonary surfactant protein A that interact with lipids. *J. Biol. Chem.*
269:29793-29800.
- Kuroki, Y., and D. R. Voelker. 1994. Pulmonary surfactant proteins. *J. Biol. Chem.*
269:25943-25946.
- Laemmli, U. K. 1970. Cleavage of structural proteins during the assembly of the
head of bacteriophage T4. *Nature (London)* **277**:680-685.
- Lund-Katz, S., H. M. Laboda, L. R. McLean, and M. C. Phillips. 1988. Influence of
molecular packing and phospholipid type on rates of cholesterol exchange.
Biochemistry **27**:3416-3423.
- McCormack, F. X., Y. Kuroki, J. J. Stewart, R. J. Mason, and D. R. Voelker.
1994. Surfactant protein A amino acids Glu¹⁹⁵ and Arg¹⁹⁷ are essential for
receptor binding, phospholipid aggregation, regulation of secretion, and the
facilitated uptake of phospholipid by typeII cells. *J. Biol. Chem.* **269**:29801-
29807.

Meybloom, A., D. Maretzki, P. A. Stevens, and K. P. Hofmann. 1997. Reversible calcium-dependent interaction of liposomes with pulmonary surfactant protein *A. J. Biol. Chem.* **272**:14600-14605.

Möhwald, H. 1990. Phospholipid and phospholipid-protein monolayers at the air/water interface. *Annu. Rev. Phys. Chem.* **41**:441-476.

Morrow, M. R., J Pérez-Gil, G. Simatos, C. Boland, J. Stewart, D. Absolom, V. Sarin, and K. M. W. Keough. 1993. Pulmonary surfactant-associated protein SP-B has little effect on acyl chains in dipalmitoylphosphatidylcholine dispersions. *Biochemistry* **32**:4397-4402.

Nag, K., C. Boland, N. Rich, and K. M. W. Keough. 1990. Design and construction of an epifluorescence microscopic surface balance for the study of lipid monolayer phase transitions. *Rev. Sci. Instrum.* **61**:3425-3430.

Nag, K., C. Boland, N. Rich, and K. M. W. Keough. 1991. Epifluorescence microscopic observation of monolayers of dipalmitoylphosphatidylcholine: dependence of domain size on compression rates. *Biochim. Biophys. Acta* **1068**:157-160.

Nag, K., and K. M. W. Keough. 1993. Epifluorescence microscopic studies of monolayers containing mixtures of dioleoyl- and dipalmitoylphosphatidylcholine. *Biophys. J.* **65**:1019-1026.

Nag, K., J. Pérez-Gil, A. Cruz, and K. M. W. Keough. 1996. Fluorescently labelled pulmonary surfactant protein C in spread phospholipid monolayers. *Biophys. J.* **71**:246-256.

Nag, K., S. G. Taneva, J. Pérez-Gil, A. Cruz, and K. M. W. Keough. 1997. Combinations of fluorescently labelled pulmonary surfactant proteins SP-B and SP-C in phospholipid films. *Biophys. J.* **72**:2638-2650.

Nag, K., J. Pérez-Gil, M. L. F. Ruano, J. Stewart, C. Casals, and K. M. W. Keough. 1998. Phase transitions in films of lung surfactant at the air-water interface. *Biophys. J.* **74**

Netz, R. R., D. Andelman, and H. Orland. 1996. protein adsorption on lipid monolayers at their coexistence region. *J. Phys. II France* **6**:1023-1047.

Nielson, D. W. , J. Goerke, and J. A. Clements. 1981. Alveolar subphase pH in the lungs of anesthetized rabbits. *Proc. Natl. Acad. Sci. USA* **78**:7119-7123.

Oosterlaken-Dijksterhuis, M. A., M. van Eijk, B. L. Van Buel, L. M. Van Golde, and H. P. Haagsman. 1991. Surfactant protein composition of lamellar bodies isolated from rat lung. *Biochem. J.* **274**:115-119.

Phillips, M. C., and D. Chapman. 1968. Monolayer characteristics of saturated 1,2-diacylphosphatidylcholines (lecithins) and phosphatidylethanolamines at the air-water interface. *Biochim. Biophys. Acta* **163**:301-313.

Possmayer, F. 1988. A proposed nomenclature for pulmonary surfactant-associated proteins. *Am. Rev. Respir. Dis.* **138**:990-998.

Ruano, M. L. F., E. Miguel, J. Pérez-Gil, and C. Casals. 1996. Comparison of lipid aggregation and self-aggregation activities of pulmonary surfactant-associated protein A. *Biochem. J.* **313**:683-689.

Ruano, M. L. F., K. Nag, L-A. Worthman, C. Casals, J. Pérez-Gil, and K. M. W. Keough. 1998. Differential partitioning of pulmonary surfactant protein SP-A into regions of monolayers of dipalmitoylphosphatidylcholine (DPPC) and DPPC/dipalmitoylphosphatidylglycerol. *Biophys. J.* **74**:1101-1109.

- Ryan, R. M., R. E. Morris, W. R. Rice, G. Ciraolo, and J. W. Whitsett. 1989. Binding and uptake of pulmonary surfactant protein (SP-A) by pulmonary type II epithelial cells. *J. Histochem. Cytochem.* 37:429-440.
- Schürch, S., F. Possmayer, S. Cheng, and A. Cockshutt. 1992. Pulmonary SP-A enhances adsorption and appears to induce surface sorting of lipid extract surfactant. *Am. J. Physiol.* 263:L210-L218.
- Slotte, J. P., and P. Mattjus. 1995. Visualization of lateral phases in cholesterol and phosphatidylcholine monolayers at the air/water interface- a comparative study with two different reporter molecules. *Biochim. Biophys. Acta* 1254:22-29.
- Stratton, C. J. 1978. The ultrastructure of multilamellar bodies and surfactant in the human lung. *Cell Tiss. Res.* 193:219-229.
- Suzuki, Y., Y. Fujita, and K. Kogishi. 1989. Reconstitution of tubular myelin from synthetic lipids and protein associated with pig pulmonary surfactant. *Am. Rev. Respir. Dis.* 140:75-81.
- Tanева, S. G., and K. M. W. Keough. 1994a. Dynamic surface properties of pulmonary surfactant proteins SP-B and SP-C and their mixtures with dipalmitoylphosphatidyl choline. *Biochemistry* 33:14660-14670.

Tanева, S. G., and K. M. W. Keough. 1994b. Pulmonary surfactant proteins SP-B and SP-C in spread monolayers at the air-water interface I: monolayers of pulmonary surfactant protein SP-B and phospholipids. *Biophys. J.* **66**:1137-1148.

Tanева, S., T. McEachren, J. Stewart, and K. M. W. Keough. 1995. Pulmonary surfactant protein SP-A with phospholipids in spread monolayers at the air-water interface. *Biochemistry* **34**:10279-10289.

Tenner, A. J. , S. L. Robinson, J. Borchelt, and J. R. Wright. 1989. Human pulmonary surfactant protein (SP-A), a protein structurally homologous to C1q, can enhance FcR- and CR1- mediated phagocytosis. *J. Biol. Chem.* **264**:13923-13928.

Udenfriend, S., S. Stein, P. Bohlen, W. Dairman, W. Loimgruks, and M. Weigle. 1972. Fluorescamine: a reagent for assay of amino acids, peptides and primary amines in the picomole range. *Science (Wash. DC)* **178**:871-872.

Vandenbussche, G., A. Clerc, T. Curstedt, J. Johansson, and H. Jornvall. 1992. Structure and orientation of the surfactant-associated protein C in a lipid bilayer. *Eur. J. Biochem.* **203**:201-209.

von Tscharner, V., and H. M. McConnell. 1981. An alternative view of phospholipid phase behaviour at the air-water interface. *Biophys. J.* **36**:409-419.

Voss, T., H. Eistetter, K. P. Schäfer, and J. Engel. 1988. Macromolecular organization of natural and recombinant lung surfactant protein SP 28-36: structural homology with the complement factor C1q. *J. Mol. Biol.* **201**:219-227.

Wang, Z., S. B. Hall, and R. H. Notter. 1995. Dynamic surface activity of films of lung surfactant phospholipids, hydrophobic proteins, and neutral lipids. *J. Lipid Res.* **36**:1283-1293.

Wang, Z., S. B. Hall, and R. H. Notter. 1996. Roles of different hydrophobic constituents in the adsorption of pulmonary surfactant. *J. Lipid Res.* **37**:790-798.

Weis, R. M., and H. M. McConnell. 1985. Cholesterol stabilizes the crystal-liquid interface in phospholipid monolayers. *J. Phys. Chem.* **89**:4453-4459.

Williams, M. C. 1992. Morphological aspects of the surfactant system. In Pulmonary Surfactant: from molecular biology to clinical practice. B. Robertson, L. M. G. van Golde, and J. J. Batenburg, editors. Elsevier Science Publishers, Amsterdam. 87-107.

Williams, M.C., S. Hawgood, and R. L. Hamilton. 1991. Changes in lipid structure produced by surfactant proteins SP-A, SP-B, and SP-C. *Am. J. Respir. Cell Mol. Biol.* **5**:41-50.

Wright, J. R., and J. A. Clements. 1987. Metabolism and turnover of lung surfactant. *Am. Rev. Respir. Dis.* **135**:426-444.

Wright, J. R., R. E. Wager, S. Hawgood, L. Dobbs, and J. A. Clements. 1987. Surfactant apoprotein Mr=26,000-36,000 enhances uptake of liposomes by type II cells. *J. Biol. Chem.* **262**:2888-2894.

Wright, J. R., J.D. Borchelt, and S. Hawgood. 1989. lung surfactant apoprotein SP-A (26-36 kDa) binds with high affinity to isolated alveolar type II cells. *Proc. Natl. Acad. Sci. USA* **86**:5410-5414.

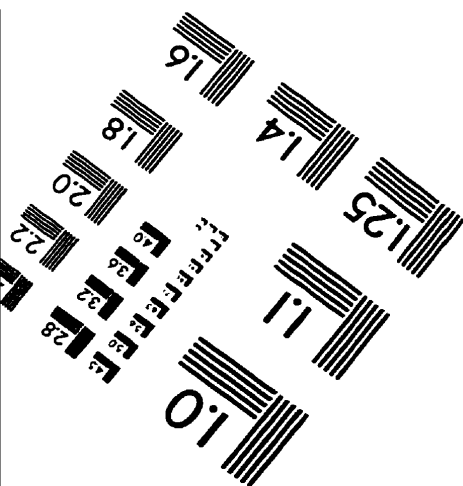
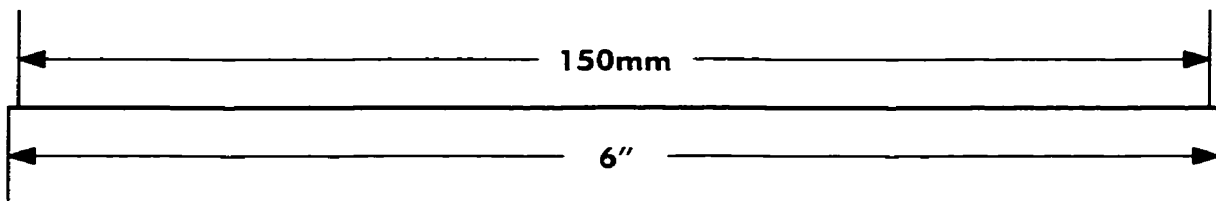
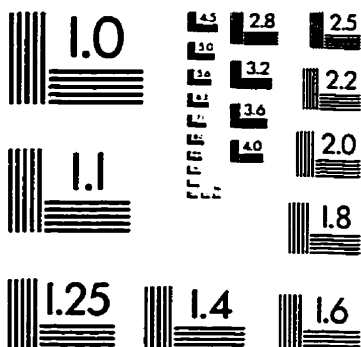
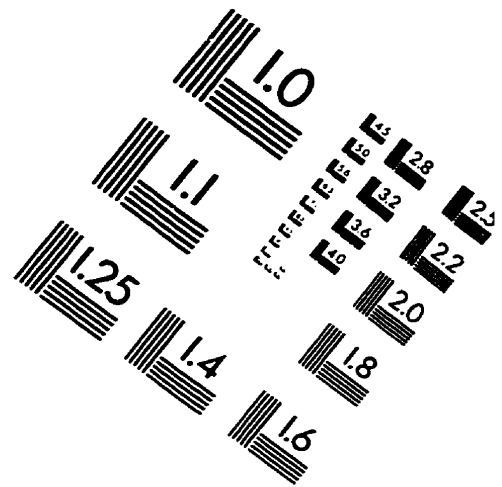
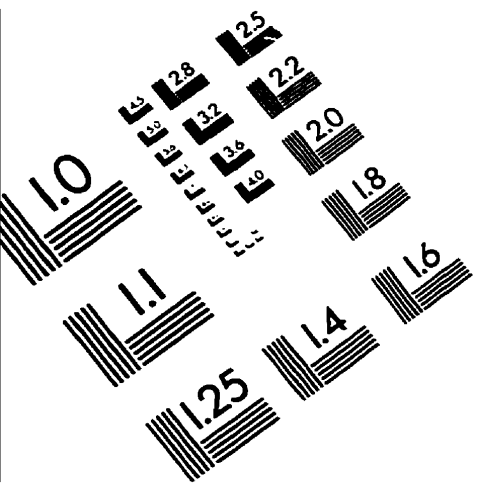
Wright, J. R. 1997. Immunomodulatory functions of surfactant. *Physiolog. Rev.* **77**:931-962.

Young, S. L., J. R. Wright, and J. A. Clements. 1989. Cellular uptake and processing of surfactant lipids and apoprotein SP-A by rat lung. *J. Appl. Physiol.* **66**:1336-1342.

Yu, S-H., and F. Possmayer. 1993. Adsorption, compression and stability of surface films from natural, lipid extract and reconstituted pulmonary surfactant. *Biochim. Biophys. Acta* **1167**:264-271.

Yu, S-H., and F. Possmayer. 1996. Effect of pulmonary surfactant protein A and neutral lipid on accretion and organization of dipalmitoylphosphatidylcholine in surface films. *J. Lipid Res.* **37**:1278-1288.

IMAGE EVALUATION TEST TARGET (QA-3)



APPLIED IMAGE, Inc.
1653 East Main Street
Rochester, NY 14609 USA
Phone: 716/482-0300
Fax: 716/288-5989

© 1993, Applied Image, Inc., All Rights Reserved

